24572

Canpolar Inc.

Proj. #157

INVESTIGATION OF REMOTE OIL THICKNESS MEASUREMENT

Submitted to

Esso Resources Canada Limited
3535 Research Road N.W.
Calgary, Alberta T2L 2K8

Submitted by

Canpolar Inc.
265 Rimrock Road, Unit 4
Downsview, Ontario M3J 3C6

Final Report - June 1990

Canpolar Inc. Project 1089

TABLE OF CONTENTS

1. INTRODUCTION

In late 1988 Canpolar Inc. was contracted (through its affiliate, Intera Technologies Ltd.) by Esso Resources Canada Limited to conduct further feasibility investigation into several techniques for remote measurement of the thickness of oil on water. The work followed a study by Canpolar (Reimer and Rossiter, 1987) which suggested two new approaches for oil thickness measurement: laser ultrasonics (electromagnetic thermoelastic emission) and microwave spectroscopy. In discussions with Esso, a third approach was suggested, thermal diffusion. In the work reported here only the laser ultrasonics and optothermal techniques were investigated. Microwave techniques are being covered under a separate contract to the University of Calgary.

Most of the work reported here was performed at the Industrial Materials Research Institute (IMRI) of the National Research Council of Canada, Boucherville, Quebec. This Institute has both specialized personnel and unique facilities for these investigations. Canpolar's role was largely one of project management, co-ordination, technical review and evaluation.

This report is therefore a brief summary of the work, the conclusions arrived at by the project team, and Canpolar's recommendations. Detailed technical discussion is given in the IMRI reports appended.

2. TECHNICAL DISCUSSION

2.1 Laser Ultrasonics

The technique is based on the stimulation of an acoustic wave at the air-oil interface by a strong laser pulse. The acoustic signal travels through the oil and is reflected at the oil-water boundary and detected at some delay time at the oil-air boundary where it can be detected by a sensitive interferometer. The work performed (Appendix 1) was to confirm the initial estimates of the feasibility of this approach outlined in Reimer and Rossiter (1987) and, if successful, to plan follow-on work.

The work did confirm the ability of this approach to measure the thickness of oil on water. Experimental measurements using both heterodyne and Fabry-Perot detectors were used at a range of 1 m from Norman Wells crude oil in a beaker. A CO_2 TEA laser with a 100 ns pulse was used as the source. Oil thicknesses from 0.6 to 32 mm were investigated. The results were very encouraging in that consistent thickness estimates could be achieved, with high signal-to-noise ratios. Experiments on the angle of illumination showed that both the Fabry-Perot and heterodyne detectors were very sensitive to this parameter. The Fabry-Perot approach was relatively insensitive to small waves (made by blowing air over the oil), but the heterodyne system was unable to detect the return echo under these conditions.

Although the resolution of oil thickness using this approach is very high, since it depends only on the ability to resolve the return signal in time, typically a few ns, the accuracy of thickness measurement depends on knowledge of acoustic velocity in the oil. For an unknown oil this might be $\pm 25\%$, but for a known oil would be much less.

Because of the high dependence on angle, care will be required in the design to allow detection when the oil/ocean surface is perpendicular to the detecting laser. Also autofocus and focus tracking will likely be required.

Successful tests were made with the Fabry-Perot detector at a range of 15 m and the source laser at 2 m. The source laser could not be placed much further from the oil, but it is believed that this limitation can be overcome with appropriate lenses. Effects of fog, rain, bright sunshine, etc. are not yet known. Tests are suggested to assess these factors.

An interesting idea which emerged out of the work was the possibility of estimating the viscosity of the oil by evaluating the ultrasonic dispersion suffered by the acoustic pulse. Viscosity estimates would be of substantial interest for oilspill countermeasures.

2.2 Optothermal Techniques

It had been suggested that measurement of the rate of diffusion of a thermal pulse set up on an oil layer might be related to its thickness. A theoretical estimate by IMRI suggested that this might be feasible, since the thermal contrast at the oil-water boundary would appear to be sufficient. Further theoretical calculations were made, and it was determined that the observation period required for even a thin layer (< 1 mm) was on the order of several seconds. Some experimental measurements were made on oil layers 0.3 to 1.2 mm thick, which tended to confirm the theory. It appears that there are a number of complicating factors, especially convection, which indicate that this approach will not give a diagnostic thickness measurement.

A second approach was also investigated, called thermally-stimulated spectroscopy. The oil is irradiated at a wavelength which essentially penetrates and heats the full thickness of the oil layer but not the underlying water. Then the oil layer is "probed" at two or more wavelengths which have differing absorption lengths. The ratio of the responses is indicative of the oil thickness.

Some initial tests were completed to evaluate this concept. Although the results were encouraging, they were hampered by lack of appropriate equipment for a thorough evaluation. Further tests are suggested.

2.3 Comparative Analysis

A comparison of the two approaches is given in Table 1. Several points emerge.

The laser ultrasonics has demonstrated its ability to measure oil thickness in the laboratory; hence it clearly warrants further investigation. The optothermal approach still requires conclusive demonstration, but this may be possible with relatively little effort. However, until further testing (laboratory and perhaps airborne) is complete, the technical risk associated with both approaches is still fairly high.

It is likely that the two approaches are complementary in the sense that the optothermal would be best for thin oil (< 1 mm thick), whereas the laser ultrasonics is only effective for oil > 1 mm thick. A better defined functional requirement will be needed to determine whether the cost of both systems would be warranted.

Although less advanced than the laser ultrasonics work, the optothermal approach appears to warrant further investigation because, if successful, it could be implemented with smaller and far less complex equipment than the ultrasonics.

Measurement accuracy would likely be comparable, but resolution would likely be lower. It is not known whether other significant parameters, such as viscosity, could be estimated.

Work is still needed to assess how either approach would be affected by environmental factors, such as rain, fog, snow, waves, sun, etc. Some effort to estimate these effects could likely made before full field testing.

Table 1 Comparison of Oil Thickness Technologies

Paramater	Laser Ultrasonics	Thermal Spectroscopy
Oil type	All	Most
Oil thickness	>1 mm	<1 mm
Accuracy	±25% (unknown oil)	±10%?
Resolution	<1%	±10%?
Spot size	Cm^2	Cm^2
Other parameters	Viscosity?	?
Technical complexity	High	Medium
Technical risk	Medium-high	High
Development cost	>$1m	$250K?
Cost per unit	$300K?	$100K?
Aircraft restrictions	Flying hight <20m?	?
size estimate	0.5-1.0m^3	0.2-0.5m^3
weight estimate	250-500 kg?	<200 kg?
weather constraints	Precipitation?, fog	Precipitation?, fog
waves	Probably OK	?

3. IMPLEMENTATION FACTORS

3.1 Market Assessment

Although a quantitative market assessment was not undertaken, we estimate that the world market for such a device, if available, might be 8 to 10 units worldwide over 5 to 10 years. Likely locations for such a device, which would not be used greatly except in spill situations, might be one unit per continent, plus several in Europe and one on each coast of North America.
At a selling price of $250,000 to $500,000 per unit, the market size would be $2 to 5 million. Since development costs are likely to be at least $1 million, this device will not be developed with commercial risk capital. Therefore, development costs will have to be borne by agencies with operational requirements for this type of equipment.

3.2 Development Team

Several different types of skills will be required to carry the development through to implementation, including research and development personnel and facilities, equipment manufacturer, aircraft instrumentation specialists, and experimental test groups. IMRI clearly has the expertise to undertake the research needed and have unique optics facilities. The firm of Ultra Optec are already commercializing some of IMRI's technologies and have expressed interest in doing the same for this development.

Several Canadian firms have aircraft equipment capability, including Barringer Research, Intera Technologies, MPB, CAL, etc. One of these should be selected to be involved in the project well before airborne trials begin.

It may be appropriate to have a field experimental group involved to co-ordinate the various activities from research to development. Canpolar has taken on this task in other field and laboratory projects, and would be prepared to take on this project if required.

It appears that the key skills to complete this project are available in Canada. Funding will be required and may come from a combination of Canadian and American sources. Development should be phased so that go/no-go decisions can be made at key milestones until the technical uncertainties described above are reduced or eliminated.

4. CONCLUSIONS AND RECOMMENDATIONS

4.1 Conclusions

The project team (see Table 2) met at IMRI on March 9, 1990 to review the project and plan the next stage. The following conclusions were reached:

1. Laser ultrasonics appears able to measure oil thickness remotely and further development work should be undertaken.

2. Thermal diffusion is not a practical approach and should not be pursued.

3. Thermally-stimulated spectroscopy shows promise and further laboratory tests should be undertaken to confirm the analytical work.

4. The funds required for development would likely be available from Canadian-U.S. joint projects.

5. IMRI would put together a proposal for Esso which would be circulated to appropriate agencies.

6. The overall development plan would be:
   - summer 1990 - further extended laboratory tests at IMRI;
   - fall 1990 - minimal local airborne tests using government aircraft;
   - winter 1991 - start prototype fabrication.

4.2 Recommendations

Based on the results described above, the following recommendations are offered:

1. The laser ultrasonics and thermally-induced spectroscopy should both be investigated further in the laboratory, leading to field trials when technical feasibility has been demonstrated. The cost of field trials could be substantially reduced by use of tank test facilities to evaluate response due to waves, sun, altitude, etc.

2. These techniques should be compared to other oil thickness measurement approaches (such as microwave spectroscopy) being pursued elsewhere before a substantial prototype fabrication task is begun.

3. The cost-benefits of various measurement approaches should be assessed in the light of operational functional requirements. For example, the benefits of measuring the thickness of thinner vs thicker oils, measurement accuracy required, importance of other information (such as viscosity) will need to be specified before meaningful comparisons of several technologies can be made.

4. A multi-disciplinary project team (including aircraft equipment specialists) should be involved in the project in order to carry the implementation through to commercial devices smoothly. Participants who will not have an active role until later in the development process should still be involved to bring their expertise to the planning stages.

Table 2 Attendees of March 9, 1990 Review Meeting Held at IMRI

Jean-Daniel Aussel	NRCC-IMRI Boucherville, Quebec	514-641-2280
Paul Bouchard	Ultra Optec Bourcherville, Quebec	514-449-2096
Jean Bussière	Section Head Instrumentation & Sensors NRCC-IMRI Boucherville, Quebec	514-641-2280
Paolo Cielo	NRCC-IMRI Boucherville, Quebec	514-641-2280
Gérard Durou	Ultra Optec Bourcherville, Quebec	514-449-2096
Merv Fingas	Environment Canada Ottawa, Ontario	613-998-9022
Ron Goodman	Esso Calgary, Alberta	403-284-7489
Larry Hannon	Dept. of Interior Mineral Management Service Herndon, VA	703-787-1558
Ivan Lissauer	United States Coast Guard R & D Center Groton, CT	203-441-2742
Jean-Pierre Monchalin	NRCC-IMRI Boucherville, Quebec	514-641-2280
James Rossiter	Canpolar Inc. 265 Rimrock Rd., #4 Downsview, Ontario M3J 3C6	416-635-5484
Edward Tennyson	Mineral Management Service 381 Elden Street Herndon, VA 22070	703-787-1560

5. REFERENCE

Reimer, E.M., Rossiter, J.R., 1987. Measurement of oil thickness on water from aircraft: A. Active microwave spectroscopy; B. Electromagnetic thermoelastic emission. Environmental Studies Research Funds Report No. 078. Ottawa, viii + 82 p.

Appendix 1

Laser-Ultrasonic Measurement of

Oil Thickness on Water From

Aircraft Feasibility Study

LASER-ULTRASONIC MEASUREMENT OF OIL THICKNESS ON WATER FROM AIRCRAFT FEASIBILITY STUDY

Jean-Daniel Aussel and Jean-Pierre Monchalin
Industrial Materials Research Institute
National Research Council Canada
75 de Mortagne Blvd, Boucherville (Quebec)
J4B 6Y4 Canada

March 1990

TABLE OF CONTENTS

ABSTRACT

This report describes laboratory measurements of the thickness of an oil layer floating on a water substrate using laser-ultrasonics. Ultrasonic waves are generated at the surface of the oil in the thermoelastic regime with a pulsed CO_2 laser and detected with either a Helium-Neon laser coupled to a heterodyne displacement interferometer, or a Nd:Yag laser coupled to a Fabry-Pérot velocity interferometer. The thickness of the oil layer is calculated from the time delay between the ultrasonic surface pulse and the ultrasonic echo reflected by the oil-water interface. This time delay is precisely measured by a crosscorrelation method, which has a high precision even with low signal-to-noise ratio data. Measurements were performed with oil thickness ranging from 0.6 mm to 32 mm, using Norman Wells crude oil floating on tap water. Oil thickness above 1 mm was successfully measured by the crosscorrelation method. Below 1 mm, the ultrasonic interface echo was not observed, because, at least in part, of the very large step-like surface deformation and the too-slow recovery of the interferometer. The accuracy is in general essentially limited by the knowledge of the ultrasonic velocity of oil.

To estimate the effect of the waves or of the motion of the aircraft on the technique, measurements were performed while blowing air over the oil and agitating the beaker. Good results were obtained with the Fabry-Pérot system, which was provided with large 15 cm input lens aperture and the thickness variations due to the perturbations were easily monitored in real-time on an oscilloscope. The signal-to-noise ratio of the ultrasonic signals was quite constant for angles of incidence of the receiving laser beam with the normal to the oil surface in the range $\pm$ 1.4°, the input lens of the interferometer being 1.5 m away of the oil surface. On the other hand, the heterodyne interferometer was very sensitive to the perturbations, and it was difficult to monitor the oil thickness in real-time on the oscilloscope. Indeed, the signal-to-noise ratio of the ultrasonic signals rapidly decreased with increasing angle of incidence of the receiving beam with the normal to the oil surface in the range $\pm$ 0.4°.

Some measurements were successfully performed with the Fabry-Pérot velocity interferometer 15 meters away from the oil surface, the CO_2 laser being shot 2 meters away from the oil surface. When the CO_2 laser was located at 15 m, the ultrasonic echo was not observed because the energy density was too low for adequate generation.

This report includes several recommendations concerning the design of a prototype system, the tests to be conducted at a pilot facility and several additional tasks. In particular, it is recommended that the prototype include a CO_2 laser, a YAG system similar to the one used and a Fabry-Pérot receiving interferometer. Among the additional tasks, the effect of waves, wind, rain, fog should be assessed with a simple experimental setup which measures back-scattered light. It is thought that additional computer modelling of the generation and detection processes is needed, in particular in order to find the best Fabry-Pérot mirror configuration. It is also recommended to perform several studies in the laboratory which could allow the determination of parameters important to the oil slick spreading or to allow the measurement of thinner oil layers. The cost of a prototype is also estimated.

1. LASER-ULTRASONIC THICKNESS MEASUREMENT

In the first section of this chapter we briefly present the principles of laser-generation of ultrasound, and wave propagation in an oil layer on an infinite water substrate. In the second section we outline the two methods of laser-detection of ultrasonic waves used in the experimental section, i.e., heterodyne displacement interferometry and velocity interferometry. The signal processing procedure to measure the oil thickness is given in the third section and finally the diffraction correction on the time delay are calculated in the last section.

1.1 Laser-generation and propagation of ultrasound

At low power density, below the vaporization threshold, a laser pulse incident on a material generates acoustic waves by thermal expansion (thermoelastic effect)[1]. The amplitude and the time dependence of the generated ultrasonic pulse depends upon the optical, thermal and acoustic parameters of the material, and upon the laser pulse time variation. The theoretical ultrasonic wave generated in a composite material, such as an oil layer on a water substrate, can be calculated by resolution of the coupled equations of thermal conductivity and motion[2]. In practice in this case heat diffusion is negligible and the depth of the heated zone is given by the optical penetration $1/\alpha$ (typically 100 μm at CO_2 wavelengths in oil, see Table I). For oil layers thicker than the optical penetration depth generation takes place only in oil and can be understood qualitatively as sketched in Figure 1 a-b.

Figure 1a shows a buried uniformly heated layer which expands in both directions. At a given observation point inside the medium, one observes the arrival of a positive pressure variation (compressive stress), then a negative pressure variation (tensile stress) delayed by the propagation time τ through the layer (for 100 μm layer, τ - 77 ns). The time variation of each of the pressure changes correspond to the integral of the laser pulse. It then results in a unipolar bell-shaped time variation for the pressure. Because of the linear relationship between pressure and strain, the strain follows the same variation. Since we are in the case of a plane wave variation, i.e. pressure, strain, velocity and displacement are fonction of $z - ct$ and $\partial/\partial z = -c\,\partial/\partial t$, the particule velocity follows the same variation as well (c is the velocity of propagation). Displacement is obtained by integrating velocity and has consequently a step-like variation.

When the layer is at the surface, which is the case here, the stress at an observation point is the sum of a direct and a delayed reflected pressure pulses (inverted because of the free boundary). It then results a bipolar variation of the pressure. Strain and particule velocity follow the same variation. Displacement is obtained by integration and has therefore a unipolar bell-shape. This corresponds to the variation of the ultrasonic displacement signal which is observed at the oil surface after reflection by the oil-water interface. It should be noted that the initial surface displacement is simply the integral of the laser pulse and has therefore a step-like variation (fig. 1-c). In general, there is no simple relationship between an ultrasonic echo and the surface deformation. In the case where the propagation time τ through the heated layer is much smaller than the pulse duration, the ultrasonic displacement echo follows in good approximation the laser pulse variation and the derivative of the initial surface deformation. In this case, proper gauging of the layer thickness can be obtained by cross-correlating the ultrasonic echo with the derivative of the surface deformation.

Additional insight can be obtained from the papers of Gournay[3] and Bushnell and McCloskey[4]. The phenomenon can be viewed as the generation of pressure waves by the thermal expansion of many elemental layers. Each layer gives pressure waves which propagate in both directions and which reach the observation point at a well defined later time, given by the distance between the layer and the observation point divided by c. The wave which is reflected by the free surface is inverted. Fig. 2a illustrates this explanation for instantaneous energy deposition and exponential absorption (absorption length = $1/\alpha$). The displacement is deduced from the pressure by integration. Figure 2b shows the pressure and displacement pulses in the case of finite laser pulse duration. These results are deduced from the ones of fig. 2a by convolution with the laser pulse. As noted above, when $\tau \ll$ laser pulse duration, the ultrasonic displacement follows the laser pulse variation and cross correlation with the derivative of the initial surface displacement is then a perfectly appropriate procedure.

However, we are not in this simple case, since τ is of the order of the pulse length duration. A computer program based on the solution of the coupled equations (neglecting heat diffusion) was used to predict the various variations. (The results of ref. 3 and 4 could have been used as well for layers thicker than $1/\alpha$, the program is more general and allows absorption in the substrate). The results are shown in figs. 3 and 4 using the parameters of the Table I and a pulse length duration of 100 ns

(assuming a gaussian shape). It is observed in Fig. 4 that the ultrasonic pulse has in good approximation the same variation as the derivative of the surface deformation.

Once the ultrasonic pulse has been produced in the oil medium by thermoelasticity, it is then reflected by the interface oil-water towards the oil surface where it can be detected. It should be noted that a large fraction of the acoustic energy is transmitted into the water, since the acoustic impedances of oil and water are very close. The acoustic reflection coefficient (for the pressure) is given by:

$$R = (\rho_{water}\, c_{water} - \rho_{oil}\, c_{oil}) / (\rho_{water}\, c_{water} + \rho_{oil}\, c_{oil}) = 0.18 \qquad (1)$$

where ρ is the density and c is the ultrasonic velocity. The first and second echoes reflected by the interface oil-water will thus have an amplitude 15 dB and 30 dB respectively below the surface pulse amplitude. Therefore in practice the second echo may be barely seen so a cross correlation between echos may be difficult. Therefore, in order to measure the thickness of oil, crosscorrelation of the first echo with the surface initial displacement derivative appears to be the best approach.

Acoustic attenuation also decreases the amplitude of the interface echo. This attenuation is difficult to estimate a priori, since it is strongly dependent on the type of oil[5]. It has a f^2 general variation, f being the ultrasonic frequency, but the absolute attenuation ranges from 0.03 to 35 dB/m at 1MHz depending on the type of oil.

1.2 Laser-detection of ultrasound

Concerning the optical detection of ultrasound, two methods based on optical interferometry have been used[6]. Both permit measurement of the ultrasonic motion along the line of sight, i.e. the normal motion when the probe beam is sent perpendicularly to the surface.

The first method, called optical heterodyning[7], consists in making the wave scattered by the surface interfere with a reference wave directly derived from the laser, and is sketched in figure 5. Such a technique is sensitive to optical speckle and the best sensitivity is obtained when one speckle is effectively detected. This means that the mean speckle size on the focusing lens has to be about the size of the incoming beam and that this beam should be focused onto the surface. Therefore, this technique generally permits measurement of the ultrasonic displacement over a small spot, which in the MHz range can be considered as giving point-like detection.

The second detection method, called velocity interferometry or time-delay interferometry[8], is based on the Doppler frequency shift produced by the surface motion and its demodulation by a confocal Fabry-Pérot interferometer having a filter-like response (see figure 6). This technique is primarily sensitive to the velocity of the surface and is therefore very insensitive to low frequencies. The filter-like response is obtained by giving a path delay between the interfering waves within the interferometer. Unlike optical heterodyning, this technique permits collection of many speckles and allows a large detecting spot (several mm and even more).

Experiments on oil thickness measurements have been performed with both a heterodyne displacement interferometer[7] and a confocal Fabry-Pérot[8] velocity interferometer. The detecting laser beam is superimposed with the generating laser beam on the surface of the oil. The time delay is measured by crosscorrelation of the derivative of the surface displacement pulse with the ultrasonic pulse reflected at the oil-water interface.

1.3 Time delay measurement by crosscorrelation

The procedure we have used is based on the crosscorrelation of consecutive pulses[9] and is illustrated in figure 7 with data taken with the heterodyne interferometer on a 6.4 mm thick oil layer on water. To measure the time delay due to ultrasonic propagation in the oil layer, the initial surface displacement and the echo reflected by the interface are first identified. To eliminate the low frequency component of the signal, we process the first and second derivative of the ultrasonic displacement. The experimental displacement and the corresponding derivatives are shown in Fig. 7-a. Two portions of the data curves, one including the surface pulse and the other the interface echo are then selected. The interface echo is selected in the data of the first derivative in a window of length $T = 5\ \mu s$ starting at time $t_1 = 10\ \mu s$. The surface pulse is selected in the data of the second derivative, since its waveform corresponds approximatively to the derivative of the interface echo waveform, in a window of same length starting at time $t_2 = 0\ \mu s$. Both data portions are then normalized to the same energy and their mean value is set to zero (dc offset elimination). Normalized and mean value corrected data portions are shown in figure 7-b and 7-c. The result of crosscorrelation of the two data portions is given in figure 7-d. The coarse delay between the two windows is $T_c = t_2 - t_1 = 10\ \mu s$. The maximum of the crosscorrelation gives the fine delay $T_f = 0.161\ \mu s$. The round trip time t_{2x} corresponding to the propagation time of the longitudinal pulse over two layer thickness is therefore :

$$t_{2x} = T_c - T_f = 9.839\ \mu s \qquad (2)$$

which gives an oil thickness x = 6.395 mm with a theoretical oil velocity of 1300 m/s. This procedure does not require the knowledge of the initial time and the determination of the exact waveforms of the ultrasonic echoes. It uses the whole shape of the signals, and therefore diminishes the effect of local uncorrelated noise: in spite of low signal-noise ratio, the maximum can be precisely measured.

Additionally, the ultrasonic phase velocity dispersion can be measured from frequency analysis of the crosscorrelation between surface pulse and interface echo. The phase of the Fourrier transform of this crosscorrelation signal gives the phase velocity as a function of frequency[10]. Figure 8 shows the ultrasonic phase velocity of the Norman Well's oil measured from the experimental data of figure 7. It is observed that the dispersion is lower than 1 % in the frequency range 1 to 9 MHz. Such dispersion is related to viscosity which is an important parameter for oil slick spreading. Such data indicates that it may be possible to get some information on oil viscosity but, in order to fully clarify this aspect, further studies would be needed, since other phenomena may contribute to ultrasonic dispersion..

The precision of the time delay measurement by crosscorrelation can be readily evaluated by differentiating the formula x = c t relating the oil thickness x to the ultrasonic velocity c of the oil and the propagation time t :

$$\delta x/x = \delta c/c + \delta t/t \qquad (3)$$

where δt is the uncertainty on the time measurement and δc is the error on the ultrasonic velocity of oil. Sampling time limitations are eliminated by using an interpolation algorithm around the maximum of crosscorrelation. The time uncertainty δt is therefore only caused by the finite signal-to-noise ratio, frequency bandwidth and measurement time. The error, or more precisely the standard deviation δt, of a time delay measurement by crosscorrelation is given by[9]:

$$\delta t = \sqrt{3/8\pi^2 T}\ \sqrt{(1 + 2\,SNR)/SNR^2}\ 1/\sqrt{f_2^3 - f_1^3} \qquad (4)$$

where T is the duration of each selected echo, SNR is the signal-to-noise ratio, and f_1, f_2 are the lower and upper frequencies of the detection system bandwidth. In the case of the data of figure 7, we have T = 5 µs, f_1 = 1 MHz, f_2 = 10 MHz, and SNR = 20 dB,

hence giving an error $\delta t \sim 1$ ns. To enhance the precision, either the signal-to-noise ratio or the time duration T should be increased.

1.4 Correction of the ultrasonic diffraction

Finally, as it is done for conventional ultrasonics[11], the measured phase velocity must be corrected for the effects of diffraction. Ultrasonic diffraction is caused by the finite size of the source and the finite size of the receiver and is known to bring a frequency dependent time bias on the time delay measurement[11].

With the heterodyne interferometer, the detecting laser beam is focused on the surface of the oil to a small spot of the order of 100 μm. The interferometer can thus be considered as a point-like detector in the MHz frequency range. For a point-like detector, the correction which must be applied to the measured time delay can be estimated by[9]:

$$\delta t/t = a^2/16x^2 \qquad (5)$$

where a is the radius of the generating laser spot, and x the thickness of the sample. For the example of figure 7, the generating spot radius is a = 2 mm and equation (5) gives a correction of -0.6 % or -0.060 μs, hence a calculated thickness of 6.356 mm.

With the Fabry-Pérot velocity interferometer, the detecting laser spot is approximately the same size as the generating laser spot, on the order of a few millimeters. In the megahertz frequency range, the plane wave approximation can thus be made[12], i.e. the dimensions of the source and receiver are larger than the ultrasonic wavelength, and the diffraction corrections are negligible.

1.5 Accuracy of the thickness measurement

As seen in the previous sections, the precision on the time delay is of the order of a few nanoseconds and the effect of the diffraction is of the order of a few percent. Equation (3) shows that the accuracy of the measurement is also limited by the error in the ultrasonic velocity. Since the ultrasonic velocity of various oils may vary between 950 m/s to 1500 m/s [5], the thickness estimate will be accurate to about ± 25% if the properties of the oil are completely unknown.

2 MEASUREMENTS WITH THE HETERODYNE INTERFEROMETER

2.1 Experimental set-up

The experimental set-up is sketched in figure 9. The generating laser is a pulsed TEA CO_2 laser (model PRF 150G of Laser Science) operating at 10.6 μm wavelength and giving typically 60 mJ energy per pulse with a pulse duration of ~ 100 ns (plus a weak longer tail). The laser beam is free-expanding and gives at the surface of the oil a spot of ~ 4 mm diameter. The receiving laser is a continuous HeNe laser of 0.634 μm wavelength and 5 mW power, and is coupled to a heterodyne displacement interferometer[7] (model OP-35-O of Ultra-Optec). The input lens of the interferometer has a 25 mm (~ 1 cm diameter effectively used) diameter and is 1 m away of the oil surface. The receiving laser beam is focused onto the surface of the oil to a near-diffraction limited spot of diameter of the order of 100 μm, approximately centered on top of the generating laser spot. The reflection of the receiving laser beam by the surface of the oil is specular, since the surface is smooth and mirror-like. The light reflectivity of the oil at 0.634 μm has been measured and is equal to ≈ 4 %. Seven different samples with oil thickness ranging from 0.6 to 32 mm were studied during the experimental phase of December '88 at IMRI. The precision on the oil thickness is limited to 5 % by the scales of the beakers. All measurements reported in section 2.2 were performed within 3 hours to limit the effect of evaporation of the volatile components of oil.

2.2 Oil thickness measurement

Figure 10 shows the ultrasonic waveforms detected at the surface of the oil with the experimental set-up of figure 9. These experimental waveforms are in good qualitative agreement with the theoretical waveform of figure 3. The signal-to-noise ratio is 6 dB for single shot data and 20 dB for averaged data, hence giving a typical time delay error of 3 ns and 1 ns, respectively. The signal-to-noise ratio is evaluated from the signal spectrum by taking the ratio of the peak spectral compoment of the signal to the noise average level (as shown below in fig. 22b). Since the interferometer has a finite bandwidth, ranging from 500 KHz to 35 MHz, the low frequencies are filtered, resulting in a large low frequency oscillation instead of the continuous step of figure 3. The interface echo is clearly seen on oil thickness above 2.3 mm. On the other hand the interface echo is not apparent on the 0.6 mm thickness sample and is lost in the surface pulse. The crosscorrelation procedure described in

section 1 was applied to the data of figure 10, and the results are shown in figure 11, which shows the variation of the time delay measured by laser-ultrasonics versus the oil thickness. The signal-to-noise ratio is such that the time error is small and the points of both single shot and averaged data are superimposed. The horizontal error bars correspond to the error on the thickness, which has been estimated from the volume of oil added to a beaker of known diameter. The precision in the added volumes is ± 5%, hence a precision in the thickness of ± 5%. Linear fits were performed on the data of figure 11, and the regression lines are plotted in the same graph.

2.3 Estimation of the effect of the waves

To estimate the effect of the waves and of the motion of the aircraft, measurements were performed with the same set-up while blowing air over the oil with a fan and agitating a beaker of 20 cm diameter. This procedure produced a low frequency motion of the surface, and the reflection of the receiving laser beam was always specular. It is not clear however if this corresponds to the real case of oil on sea water, but it is suspected that the surface of the oil will be a good approximation of a mirror, due to the viscosity of the oil and the low temperature of the sea. It was impossible with the surface perturbations to monitor the interface echo on the screen of the oscilloscope with a 50 Hz pulse repetition frequency of the generating laser. The motion of the oil modified the angle of the receiving laser beam with the surface, hence sending the receiving laser beam outside the effective input aperture of the interferometer.

The effect of the angle of incidence of the receiving laser beam with the normal to the surface of the oil on the signal-to-noise ratio was estimated, and the results are shown in figure 12. It is clear that the signal-to-noise ratio gradually decreases with increasing tilt, down to zero at ± 0.45°. It should be noted that the signal stays constant up to ± 0.3° because the interferometric system used has a gain-controlled circuit which maintains constant the fringe amplitude at the offset frequency (Bragg frequency) . Beyond 0.3° angle, the signal decreases as well, because the fringe amplitude becomes out-of-range of the gain-controlled circuit. Since the beam is focused onto the surface, the effect of the tilt is to translate the return beam in front of the detector until it does not overlap anymore with the reference beam, as sketched in fig. 13a. 0.3° or 5×10^{-3} rd between the incident laser beam and the normal to the surface gives an offset of the reflected beam on the front lens of $2 \times 5\ 10^{-3} \times 1000 \sim 10$ mm for a distance of 1 m. This value corresponds to the size of incident beam on the

front lens, which is the effective receiving aperture of the receiver. The theoretical variation of the decrease of the signal-to-noise is plotted in fig. 13b. It can be easily shown that this variation is proportional to $(2/\pi)(\theta - \sin\theta\cos\theta)$ where $\cos\theta = \delta/a$, δ being here the offset and a the beam diameter. Note that the slope of this function is equal to $-4/\pi$ when $\delta = 0$ and 0 when $\delta = a$. This theoretical variation is in qualitative agreement with the data of fig. 12. Quantitative verification was not possible because the noise in this data originated partially from the limitation introduced by 8-bits sampling.

2.4 Quantitative measurement of the initial surface displacement and of the ultrasonic echos

The same experiments were performed again in December 1989 and January 1990 at IMRI in order to evaluate quantitatively the displacements produced by a given energy density of the CO_2 laser. The results are shown in fig. 14 a-b and show that the surface displacement δ can be very large and that a phase shift $4\pi\delta/\lambda$ larger than $\pi/2$ can be obtained easily (λ is the optical wavelength). For these measurements, the latest version of the heterodyne probe OP-35-O of Ultra-Optec set at a low frequency cut-off of 10 KHz was used. The output of this probe is proportional to $\sin 4\pi\delta/\lambda$ and reaches a maximum equal to ~ 1.9 v when $\sin 4\pi\delta/\lambda = 1$. When $\sin 4\pi\delta/\lambda = 1$, which was found to occur for energies between 10 and 26 mJ, the sensitivity to an additional small displacement (e.g. ultrasonic) is zero. The polarity of the signal corresponding to ultrasonic displacement should change sign when the energy goes through this signal saturation limit and this is verified by comparing fig. 14a and fig. 14b. Calibration of the probe can also be deduced from these measurements. The probe responsivity is therefore equal to $1900\ 4\pi/\lambda$ (mV/Å) or 3.77 mV/Å and the calibration factor is equal to 0.27 Å/mV. This value is different from the value 0.45 Å/mV deduced from the measurement with a RF spectrum analyser of the ratio of the sidebands to the central carrier when continuous ultrasonic excitation is applied. At this time, the reason of this discrepancy is unclear.

Quantitative displacements for a given energy density follow from the data of fig. 14 and the determination of the beam size. The beam diameter 2w was evaluated to ~ 6 mm at half maximum power. Assuming a gaussian shape, the total energy of the pulse E is related by the energy density at center Q_o by:

$$E = Q_o \pi w^2 / \ln 2 \qquad (6)$$

In the case of fig. 14b, the energy used is ~ 26 mJ, which gives an energy density of ~ 0.064 J/cm^2 at center. The phase shift being ~π, the displacement is then ~ $\lambda/4$ = 0.16 μm, which corresponds to ~ 2.5 μm/(J/cm^2). The theoretical surface displacement can be readily evaluated by calculating the expansion of a heated layer dz at depth z below the surface,

$$d\delta = \beta\, dz \left(\frac{h(z)\, dz}{\rho\, C_p\, dz} \right) \tag{7}$$

where the factor between brackets represents the temperature increase of the layer. β, ρ, C_p are the linear coefficient of thermal expansion, the density and the specific heat, respectively. h represents the heat source term. After integration through depth it follows

$$\delta = \beta\, \frac{Q\,(1-R)}{\rho\, C_p} \tag{8}$$

where Q is the energy density and R the optical reflection coefficient. Using the values of Table 1, we find δ ~ 1.2 μm/(J/cm^2), which is in reasonable agreement with the measured value.

Concerning the ultrasonic displacement observed at the surface after reflection by the interface water-oil, it is observed to be much smaller than the initial surface elevation by ~ 56 x 0.45 / ($\lambda/4$) ~ 1.6% the initial surface displacement (taking a calibration factor of the probe equal to 0.45). Theory[4] indicates that the maximum displacement of the travelling wave is 3 $a\beta Q(1-R)/\rho C_p$ where a is a factor which depends upon the ratio of the pulse duration to propagation time through the penetration depth (in our case ~ 100/77 = 1.3 according to Table 1). According to fig. 4 of ref. 4, a ~ 0.23 in this case. Therefore, the maximum displacement of the ultrasonic travelling wave propagating through oil is about the same as the initial surface elevation. The small ultrasonic displacement observed at the surface is caused by the weak interface reflection which appears consequently much weaker than the one calculated from the data of Table 1 and also, possibly, by some ultrasonic absorption.

Finally, these experiments show that in order to avoid a possible black-out of sensitivity, such a probe should be configurated with a low frequency cut-off adjusted to a sufficiently high value, in order to have fast recovery. A value of a few MHz is

desirable in order to probe layers below 1 mm (1 mm gives a separation between initial pulse and interface echo of ~ 1.5 μs).

Other data collected at the same time as the one of figure 14 a-b seems also to show that the oil surface deformation does not increase linearly with energy density but this does not appear conclusive and this point will require additional experiments to be made completely clear.

3. MEASUREMENTS WITH THE FABRY-PÉROT INTERFEROMETER

3.1 Experimental set-up

The experimental set-up is sketched in figure 15. The generating laser is the same pulsed CO_2 laser of section 2, focused at the surface of the oil to a spot estimated to 4 mm in diameter (6 mm measured in December 1989). The receiving laser is a pulsed Nd:YAG laser of 1.06 μm wavelength, and is coupled to a confocal Fabry-Pérot velocity interferometer described in reference 8. The input lens of the interferometer has a 15 cm diameter and is 1.5 m away of the oil surface. Because of the low reflectivity of oil and of the various losses along the optical path only 1.25 mW was received by the detector. The reflectivity of the oil at 1.06 μm was measured to be 4.5 %, which is almost the same value as the reflectivity measured for the HeNe wavelength. The receiving laser beam is focused onto the surface of the oil to a diameter estimated to 6 mm (4 mm measured in December 1989), on top of the generating laser spot. Six of the seven different samples of section 2 were used, but the thicknesses were different since some of the oil had evaporated. In the beaker corresponding to the previous 32 mm thickness, only 150 ml of oil was left instead of the initial 200 ml. The oil thicknesses were calculated using this evaporation rate, and ranged between 0.7 to 28 mm.

3.2 Oil thickness measurement

Figure 16 a-b shows the ultrasonic waveforms detected at the surface of the oil with the experimental set-up of figure 15. The signal-to-noise ratio is 10 dB for the single shot data, hence giving a typical time error of 2.5 ns. The interface echo is clearly seen for oil thickness above 2 mm. On the other hand the interface echo is not apparent on the 0.7 mm thickness sample and is lost in the surface pulse. The crosscorrelation procedure described in section 1 was applied to the data of figure 16, and the results are shown in Figure 17. As for the heterodyne interferometer, the signal-to-noise ratio be such that the time error is small, the points of both single shot and averaged data are superimposed. The horizontal error bars correspond to the error on the thickness, estimated to ± 10 % since the exact rate of evaporation has been measured on the scale of a beaker. Linear fits were performed on the data of figure 17, and the regression lines are plotted on the same graph.

3.3 Estimation of the effect of the waves

To estimate the effect of the waves and of the motion of the aircraft, measurements were performed with the same set-up while blowing air over the oil with a fan and agitating a beaker of 20 cm diameter. Unlike with the heterodyne interferometer, it was possible to monitor in real-time the interface echo on the screen of the oscilloscope with a 50 Hz p.r.f. of the generating and receiving lasers. The signal-to-noise ratio allowed monitoring the variations of the thickness of the oil due to agitation. The effect of the angle of incidence of the receiving laser beam with the normal to the surface of the oil on the signal-to-noise ratio was studied, and the results are shown in figure 18. The signal and the signal-to-noise ratio does not vary too much in the range ± 1.4°, i.e., as long as the specular reflection from the oil is inside the input lens. The cut-off angle predicted by the size of the input lens and the distance is ~ 7.5/(2 x 150) = 0.025 rd ~ 1.4°. The theoretical variation of the signal-to-noise with tilt angle is in this case square-like and is plotted in figure 19. The variation expected from an heterodyne detecting probe having the same aperture is plotted also for comparison. This theoretical variation is in qualitative agreement with the data of figure 18. Quantitative verification was not possible because the noise in these data was dominated by digitization.

3.4 Measurements 15 meters away from the sample

To study the effect of the distance on the technique, measurements were performed with the confocal Fabry-Pérot interferometer with the receiving unit located 15 meters away from the sample. Due to a lack of appropriate infrared lenses, the CO_2 laser was not superimposed with the receiving laser, but was shot at angle 2 meters away of the oil surface. The experimental set-up is sketched in figure 20 and the corresponding waveforms are shown in figure 21. The signal-to-noise ratio of the data is a little lower than for the 1.5 m remote configuration and is equal to 6 dB. This set-up was more sensitive to the orientation of the receiving laser beam with the surface, and as with the heterodyne interferometer, it was impossible to monitor in real-time on an oscilloscope the thickness of the oil while agitating the surface.

A final experiment was performed with the generating and receiving laser beam colinear, and 15 meters away of the oil surface. The signal-to-noise ratio was thus too low to detect the interface pulse. Since no optical components were available to focus the CO_2 laser, the generating spot had a 25 mm diameter on the oil surface, with an

energy per pulse of 36 mJ. The energy density of the generating laser is thus approximately 65 times lower than with the experimental set-up of figure 15, which gives a signal-to-noise ratio 36 dB lower. This problem can be overcome by a suitable 2 lens optical combination which will project a 6 mm beam waist at 15m.

3.5 Received power and signal-to-noise

Additional data were taken in November and December 1989 with complete recording of all power, signal and noise levels. A layer of oil 5 mm thick was used. The conditions of one experiment were the following:

CO_2 laser:	power 57 mJ, spot diameter ~ 6 mm
YAG receiving laser:	adjusted to give 11 mW average power onto the oil which corresponds at 50 Hz prf and with 60 µs long pulses to ~ 4W peak.
Detector YAG 100 of EGG:	received power ~ 5 mW peak.

The power loss is accounted by the surface reflectivity (~ 4.5%), by the loss of one polarization because of fiber coupling and of the use of a polarizing cube in front of the Fabry-Pérot (~ 50%), by the transmission of the Fabry-Pérot when properly stabilized (~ 25%) and by the losses introduced by the fiber and various optical surfaces (transmission ~ 22%).

The results of this experiment are shown in figure 22 a-b. Figure 22a shows the recorded signal (a 1 MHz high pass filter was used), figure 22b displays the spectra of the signal within the window 5 - 12 µs which comprises the first echo. From this spectra, we deduce a signal-to-noise ratio of ~ 35 db. It should be noted that even better results would be obtained by reducing the losses with better coatings and reducing the number of optical elements. A gain of ~ 3 in signal-to-noise is then possible in the case where the only losses originate from the surfaces and the Fabry-Pérot. It should also be noted that the power used (~ 4 W peak) can be obtained with a single amplification stage YAG system instead of the two-stages KW system which was used and which was strongly attenuated to perform these experiments.

4. CONCLUSIONS AND RECOMMENDATIONS

4.1 Conclusions

The main general conclusion which follows from this work is that the thickness of an oil layer on top of water can be measured by a laser-ultrasonic technique, at least if this layer is thicker than 1 mm. The accuracy appears essentially dependent on the knowledge of ultrasonic velocity of oil. For layers thinner than 1 mm, the ultrasonic echo is lost within the surface pulse or in the dead response interval of the interferometer (see recommendation, below). It is however possible to certify that the layer is less than 1 mm by observing the surface pulse and the noise level. Generally, it will be known beforehand that the echo has to be above a certain fraction of the surface pulse. If the signal-to-noise is sufficient and if no echo is observed, it would be then possible to conclude with confidence that the oil thickness is below this threshold value. Measurement with a system mounted in an aircraft is judged feasible, but several tests would have to be conducted first, especially to evaluate the true effect of waves and wind on the oil surface and the effect of other environmental factors (rain, fog, ...).

4.2 Recommendations on the design of a prototype system

This system is intended to be used for tests at a pilot facility, such as the one existing in Alberta and for experimentation from an aircraft. We list below the various elements of such a system with justifications of the choice which has been made. The system will include:

- a single optical breadboard

  all the lasers and optical hardware will be mounted on this breadboard.

- a generating laser

a CO_2 TEA laser, like the one used, appears to be a proper choice. A pulse duration shorter than the one used (100 ns) will allow the improvement of depth resolution and the measurement of thinner layers. Other solid state lasers may also be considered (see below 4.3.3). The laser will fire when enough scattered light from the detecting laser is received.

- detecting laser:

A Nd-YAG system operating at 1.06 μm is the best choice, since there is no concern for eye-safe operation and since it is a well developed technology. It is recommended to build a system like the one at IMRI and like the unit sold by Ultra-Optec. One amplification stage should be enough, except if future tests reveal stronger scattering from the oil surface in some field conditions. Two alternatives are to be considered regarding the repetition rate, a high repetition system (100 or 200 Hz) which will allow to catch a signal from time to time or a single shot system which will be fired when a sufficient light level is received from a continuous probe laser. This probe laser can be the stable mini-YAG, which is amplified and is part of the detecting laser. Calculations show that a laser power of a few mW should be sufficient for this purpose.

Such a single shot system is very attractive from the point of view of energy consumption but it may not work properly since a flashlamp Nd-YAG amplifier requires ~ 200 μs before reaching its maximum gain. During this time the wave motion may be sufficiently strong to displace the return beam so it misses the entrance aperture. It should also be noted that the aircraft motion will cause the probing zone on the surface to be displaced (a velocity of 100 Km/h gives a displacement of 6 cm during 200 μs), so it can be located on a sufficiently different slope when the measurement is taken. This point could only be clarified after some study of the effect of the waves and of the aircraft motion (see below, follow-up work 4.3.1).

- detecting interferometer.

The choice is between an heterodyne and a confocal Fabry-Pérot system. Both are roughly equivalent from the point of view of complexity and have about the same sensitivity for mirror-like surfaces. (see ref. 6). We have also seen that the sensitivity to surface orientation is roughly the same for the same effective aperture (although the variations versus tilt angle are not identical). Both require in practice a single frequency laser with good frequency stability. For both, means have been devised to minimize the effect of intensity fluctuations. The confocal Fabry-Pérot performance can be affected by a strong background source such as the sun. This effect would have to be assessed and can be minimized by absorbing and interference filters. It can obviously occur only on a sunny day and at a well defined direction of observation and therefore does not appear as a severe limitation. On the other hand, an heterodyne system is sensitive to the optical phase (i.e. it is speckle sensitive) and its performance

is strongly affected by factors which affects the phase, such as surface roughness or surface profile variations over the probed area, wind by the modification of the refracting index and light fog or mist (part of the light received would have been scattered in the forward direction). This drawback does not occur with the time-delay type confocal Fabry-Pérot, which can demodulate all the light received within a given étendue (throughput). The confocal Fabry-Pérot system is therefore the proper choice for this application. A spot of 6 mm diameter and a receiving aperture of 25 cm separated by 25 m corresponds to an étendue of 2.2 10^{-3} mm^2 sr, which is easily fulfilled by a fairly short unit (length < 15 cm).

- launching and collecting optics.

The generating laser (CO_2) spot should be sufficiently small in order to provide adequate energy density. A spot of 6 mm diameter at 10.6 µm and 25 m distance requires a lens size of ~ 5 cm. The detecting YAG spot should match the generating spot and therefore require smaller size optics. Detection requires as large collecting optics as is possible. Figure 23 shows a recommended design using a mirror telescope with a diameter which could be in practice in the order of 25 - 30 cm. An airborne system will probably need an autofocus system for optimum illumination of the confocal Fabry-Pérot for any height. The CO_2 beam will use most of the area of the mirror to minimize center clipping and may also need some focus tracking. Focus adjustments can be omitted for the test at the pilot facility.

- signal detector, digital acquisition system and processing software

The acquisition system can be conviently a PC mounted board and the software UDASP (Ultrasonic Digital Acquisition and Signal Processing) developed by IMRI and Ultra-Optec and now commercialized by Ultra-Optec. This software runs on the micro-computer sufficiently fast to be used during the initial test phase. It is also likely that this could be sufficient even for the first prototype, since useful data will be produced at low rate because of the effect of the waves. If more rapid processing is needed, it is likely that some developments now being performed for the application to material inspection would be readily applicable.

4.3 Recommendations on the follow-up work

4.3.1 Assessment of the effect of waves, wind, rain and fog

Since the detection is phase insensitive by the use of a confocal Fabry-Pérot system, the effect of waves, wind, rain and fog can be assessed by measuring the amount of light received through the collecting aperture. The experimental setup is rather simple and is sketched in Figure 24. The laser used will be a mini-YAG continuous laser (40 mW). A large area detector can be used, thus allowing the use of a large area Fresnel lens instead of a mirror. Tests should be conducted at the pilot facility and at sea from an aircraft. At sea, more likely, one could probe only the free water surface (reflectivity ~ 2%), but by combining with the results obtained at the pilot facility, one should be able to predict fairly well the effect of waves, wind, rain and fog on the performance of the system. Particular attention will be paid to the change of collected light occurring on average during a time interval of 200 μs. It also seems likely that some information can be derived on the matter from existing LIDAR data.

4.3.2 Modeling and Fabry-Pérot configuration

It will be useful to choose a Fabry-Pérot mirror configuration which minimizes the dead detection interval, i.e. a system which recovers rapidly to the giant surface elevation and has a strong rejection of low frequencies. A system operating in reflection[13] with a non-transmitting second mirror seems to be a better choice than the system operating in transmission used for the measurements described in this report, since its response versus ultrasonic frequencies has a zero slope at zero frequency. However, this will have to be proven by a computer model, which will allow to calculate the response in the time domaine of the interferometer to the giant surface displacement step and to the weak ultrasonic displacement superimposed upon it. Therefore it is proposed to write a PC run software which will calculate the surface motion using a more realistic laser pulse shape than the Gaussian one used so far and then the response of the interferometer.

4.3.3 Search for another generating laser

It will be worth to study absorption of various oils at the wavelengths of several solid state lasers which have recently been developed or are in development (erbium-YAG, holmium-YAG, ...). If it turns out that the absorption length of one of these lasers is suitable, this laser may represent an attractive alternative to the CO_2 laser which

requires compressed gases to operate. The computer model will help to make a final choice.

4.3.4 Building and testing a prototype

A prototype, as described above, and which will take into account the information obtained from tasks 4.3.1, 4.3.2, 4.3.3, should be built and then tested at a pilot facility and from an aircraft. The cost of the necessary hardware and of the effort is roughly evaluated in Appendix A.

4.3.5 Other studies

The purpose of these additional studies will be to find out if additional information can be obtained from the technique, especially if parameters important to oil slick spreading can be estimated. Among those, it will be worth to study further ultrasonic dispersion and its relation to viscosity. The variation of the surface deformation versus incident energy density deserves also further studies. It will also worth to give some thought to the generation of surface waves, since their dispersion can give various informations, including surface tension, viscosity and the thickness of a thin layer[14, 15]. The low frequencies involved with these waves may however make the implementation difficult.

APPENDIX A

Prototype building and testing.

Duration: ~ 18 months

Manpower:	
2 research engineers at 100 K/year	300 K
additional technical assistance	200 K
IMRI (J.-P. Monchalin, consultant) 4 weeks	14 K
	514 K
Hardware: (assume use of hardware ot task 1)	
CO2 laser	70 K
YAG receiving laser (provided by Ultra-Optec)	90 K
Fabry-Pérot assembly	15 K
Optical Breadboard	10 K
Launching and receiving optics (includes some consulting costs for optical design).	40 K
Miscellaneous optics and mechanical hardware	55 K
PC computer, acquisition board and software	20 K
	300 K
TOTAL:	814 K

REFERENCES

1 **D.A.Hutchins**, *Mechanisms of pulsed photoacoustic generation*, Can. J. Phys., vol. 64 (1986) pp.1247-1264

2 **R.M.White**, *Generation of elastic waves by transient surface heating*, J. Appl. Phys. vol. 34 (1963) pp.3559-3567

3 **L.S. Gournay**, *Conversion of electromagnetic to acoustic energy by surface heating*, J. Acoust. Soc. Am., vol. 40, (1966), pp. 1322-1330.

4. **J.C. Bushnell and D.J.McCloskey**, *Thermoelastic stress production in solids*, J. Appl. Phys., vol. 39, (1968), pp. 5541-5546.

5 **E.M.Reimer, J.R.Rossiter**, *Measurement of oil thickness on water from aircraft A: Active microwave spectroscopy, B: Electromagnetic Thermoelastic emission*, Environmental Studies Research Funds Report No.078, Ottawa, Ontario, Canada (1987) viii + 82p.

6 **J.-P.Monchalin**, *Optical detection of ultrasound*, IEEE transactions on Ultrasonics, Ferroelectrics and Frequency Control, vol.UFFC-33 No.5 (1986) pp.485-499

7 **J.-P.Monchalin, R.Heon, N.Muzak**, *Evaluation of ultrasonic inspection procedures by field mapping with an optical probe*, Canadian Metallurgical Quaterly, vol.25 No.3 (1986) pp.247-252

8 **J.-P.Monchalin, R.Heon**, *Laser ultrasonic generation and optical detection with a confocal Fabry-Pérot interferometer*, Materials Evaluation vol. 44 (1986) pp.1231-1237

9 **J.-D.Aussel, J.-P.Monchalin**, *Precision laser-ultrasonics velocity measurement and elastic constant determination*, Ultrasonics, vol. 27, 1989, pp. 165-177.

10 **J.-D.Aussel, J.-P.Monchalin**, *Study of surface acoustic wave dispersion using laser-ultrasonics and application to thickness measurement*, Review of Progress in Quantitative NDE, Ed. by D.O.Thompson and D.E.Chimenti, Plenum Publishing Corp., 1989, vol. 8A, pp. 535-542.

11 **E.P.Papadakis**, *Ultrasonic diffraction loss and phase change for broadband pulses*, J. Acoust. Soc. Am., vol.52 (1972) pp.847-849

12 **J.-D.Aussel, J.-P.Monchalin**, *Measurement of ultrasound attenuation by laser-ultrasonics*, J. Appl. Phys., vol. 65, 1989, pp. 2918-2922.

13. **J.-P. Monchalin, R. Héon, P. Bouchard, C. Padioleau**, *Broadband optical detection of ultrasound by optical sideband stripping with a confocal Fabry-Pérot*, Appl. Phys. Lett, vol. 55, 1989, pp. 1612-1614.

14. **J. Hartikainen, J. Jaarinen and M. Luukkala**, *Deformation of a liquid surface by laser heating: laser-beam self-focusing and generation of capillary waves*, Can. J. Phys. Vol. 64, 1986, pp. 1341-1344.

15. **E.H. Lucassen-Reynders and J. Lucassen**, *Properties of capillary waves*, Adv. Colloid Interface Sci., vol. 2, 1969, pp. 347-395.

TABLE I

Optical, thermal and acoustic properties of oil and water (from Reimer and Rossiter[5], except optical reflectivity of oil measured in this work and optical reflectivity of water from The Infrared Handbook, W.L. Wolfe and G.J. Zissis ed., Office of Naval Research, Dept. of the Navy, Washington, DC, 1978, chap. 3.7.5).

	OIL	SEA-WATER	TAP WATER
Sound velocity c (m/s)	1300.	1500.	1500.
Thermal linear expansion coefficient β ($°C^{-1}$)	1.0×10^{-4}	4.1×10^{-5}	6.9×10^{-5}
Specific heat C_p (cal/Kg °C)	250.	1000.	1000.
Density ρ (Kg/m^3)	800.	1000.	1000.
Optical penetration depth $1/\alpha$ at 10.6 μm (μm)	100	10	10
Optical reflectivity R at 0.6328 and 1.06 μm	4.5%	2%	2%

FIGURE CAPTIONS

Figure 1 - Thermoelastic generation of ultrasound. a) Ultrasonic pulses generated by a buried heated layer; b) Ultrasonic pulses generated by a heated layer at the surface; c) Initial surface displacement corresponding to case b.

Figure 2 - Thermoelastic generation of ultrasound. a) Instantaneous energy deposition; b) Finite laser pulse duration.

Figure 3 - Theoretical laser-generated ultrasonic displacement and velocity of the surface of an oil layer on a water substrate. The generating laser pulse is gaussian with duration of 100 ns and the optical penetration is 100 μm (10.6 μm wavelength). The oil thickness is 3.2 mm and larger than the optical penetration length.

Figure 4 - Comparison of the ultrasonic displacement pulse with the derivative of the initial surface displacement (theoretical data as in figure 3).

Figure 5 - Schematic of an optical ultrasonic receiver based on optical heterodyning[7]. The reference wave is frequency offset with a Bragg acousto-optic cell. The ultrasonic signal then appears as a phase modulation of the fringe signal at the offset frequency. This frequency is 40 MHz for the Ultra-Optec probe OP-35.O we have used.

Figure 6 - Schematic of an optical ultrasonic receiver based on velocity or time-delay interferometry. The insert explains the principle of demodulation[8].

Figure 7 - Crosscorrelation measurement of the time delay in the oil layer. Heterodyne interferometer.

a - Surface displacements with first and second derivatives

b - Normalized and mean value corrected initial surface pulse, selected on the second derivative, starting at time 0 μs.

c - Normalized and mean value corrected interface echo, selected on the first derivative, starting at time 10 μs.

d - Crosscorrelation of the two data portions in b and c.

Figure 8 - Ultrasonic phase velocity dispersion of Norman Well's crude oil deduced from the data of figure 7.

Figure 9 - Experimental set-up with heterodyne displacement detection. The receiving laser is a continuous HeNe laser. The generating laser is a pulsed CO_2 laser.

Figure 10 - Ultrasonic waveforms detected at the surface of the oil with the heterodyne interferometer. a - single shot measurements; b - averaged 90 shots

Figure 11 - Measured time delay versus oil thickness for the heterodyne interferometer data.

Figure 12 - Effect of the variation of the angle of incidence of the receiving laser beam with respect to the normal to the surface (heterodyne interferometer configuration).

Figure 13 - Effect of surface orientating on heterodyne detection; a) sketch of the displacement of the return beam with respect to the incoming beam; b) variation of the signal-to-noise with tilt, theoretical and experimental.

Figure 14 - Measurement with an heterodyne displacement interferometer which operates with a low frequency cut-off equal to 10 KHz. a) CO_2 laser energy = 10 mJ; b) CO_2 laser energy = 26 mJ.

Figure 15 - Experimental set-up with the confocal Fabry-Pérot velocity interferometer. The generating laser is a pulsed CO_2 laser. The receiving laser is a pulsed Nd:YAG laser. The generating and receiving beams are superimposed.

Figure 16 - Ultrasonic waveforms detected at the surface of the oil with the 1.5 meter remote Fabry-Pérot configuration.
a - single shot measurements
b - averaged data

Figure 17 - Measured time delay versus oil thickness with the 1.5 meter remote Fabry-Pérot configuration.

Figure 18 - Effect of the variation of the angle of incidence of the receiving laser beam with the normal to the surface on the signal-to-noise ratio (1.5 meter remote Fabry-Pérot configuration).

Figure 19 - Effect of surface orientation on the signal-to-noise ratio obtained with the confocal Fabry-Pérot receiver (theoretical). The variation given by an heterodyne probe with the same effective entrance aperture is sketched in dash line.

Figure 20 - Experimental setup used for 15 meters remote laser-ultrasonics oil thickness measurements.

Figure 21 - Ultrasonic waveforms detected with the Fabry-Pérot 15 meters away of the oil surface.

Figure 22 - Signal observed with the Fabry-Pérot system and ~ 4W peak incident on a 5 mm thick oil layer. a) signal (through a 1 MHz-high pass filter) b) spectra of the signal portion between 5 to 12 µs in db (spectra unit is mV/MHz).

Figure 23 - Launching and collecting optics of the prototype.

Figure 24 - Experimental configuration to evaluate the effect of waves, wind and fog.

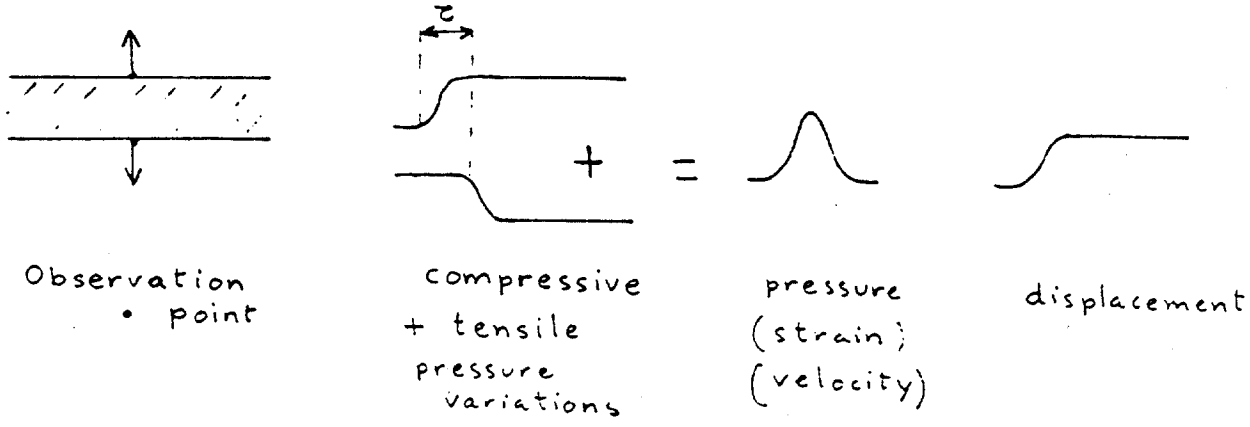

a. Buried heated layer

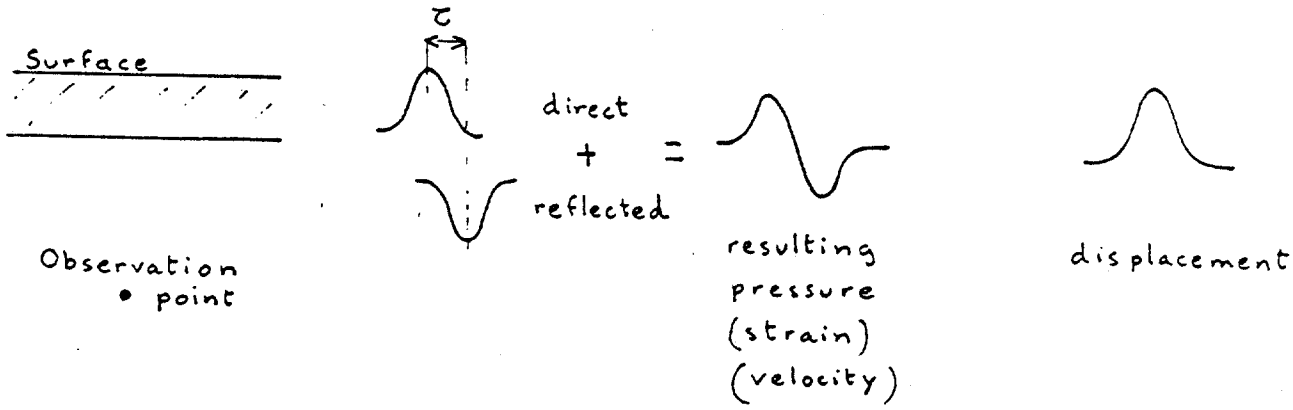

b. Heated layer at the surface

c. Initial surface displacement

Figure 1

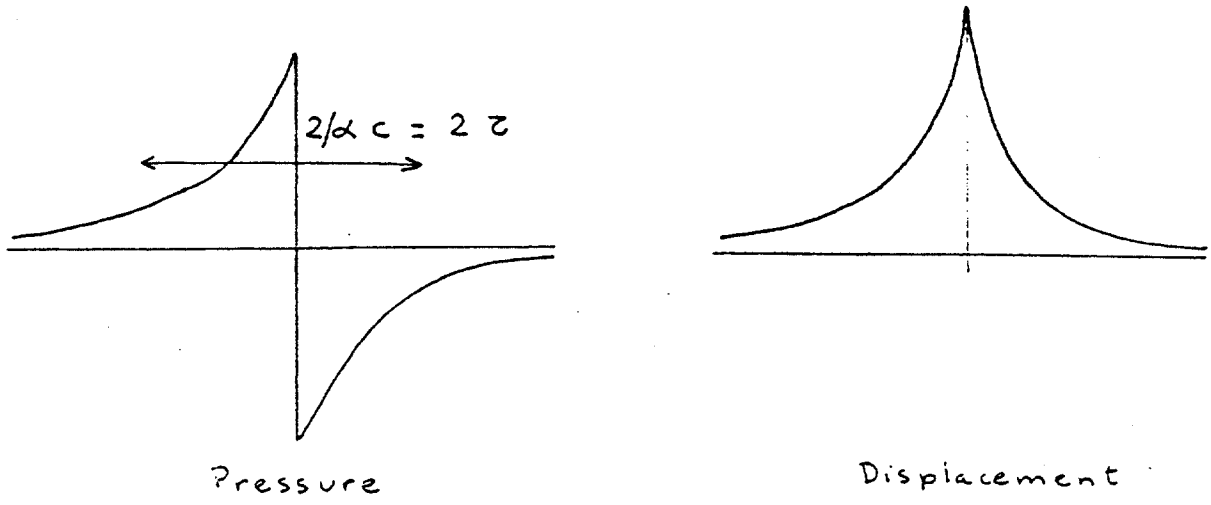

a. Instantaneous energy deposition

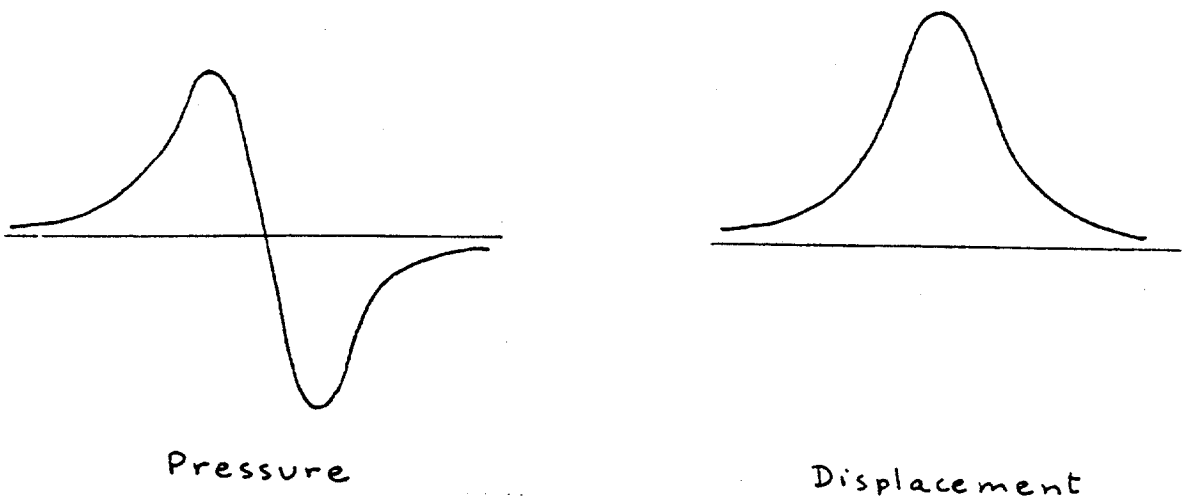

b. Finite laser pulse duration

Figure 2

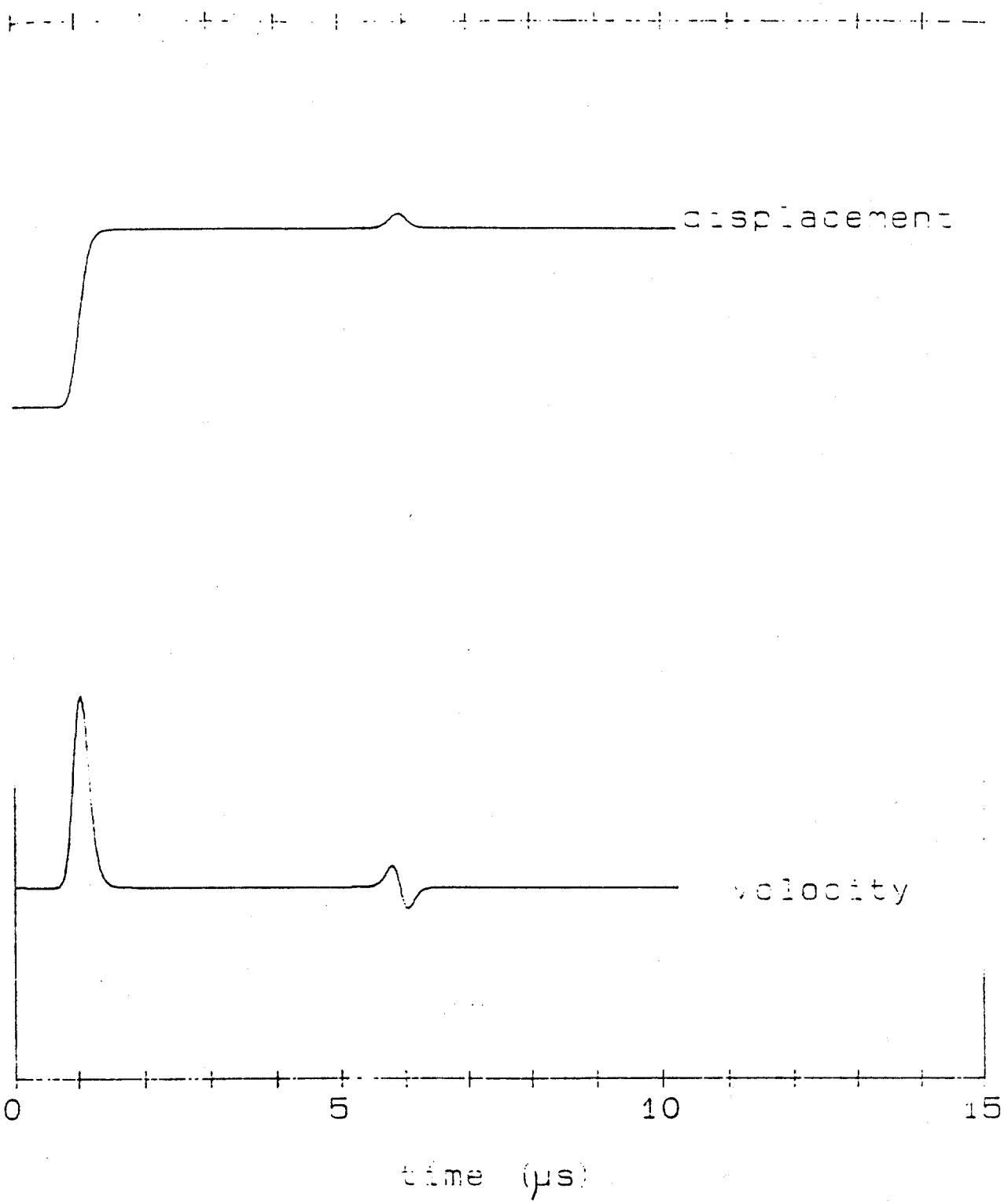

Figure 3

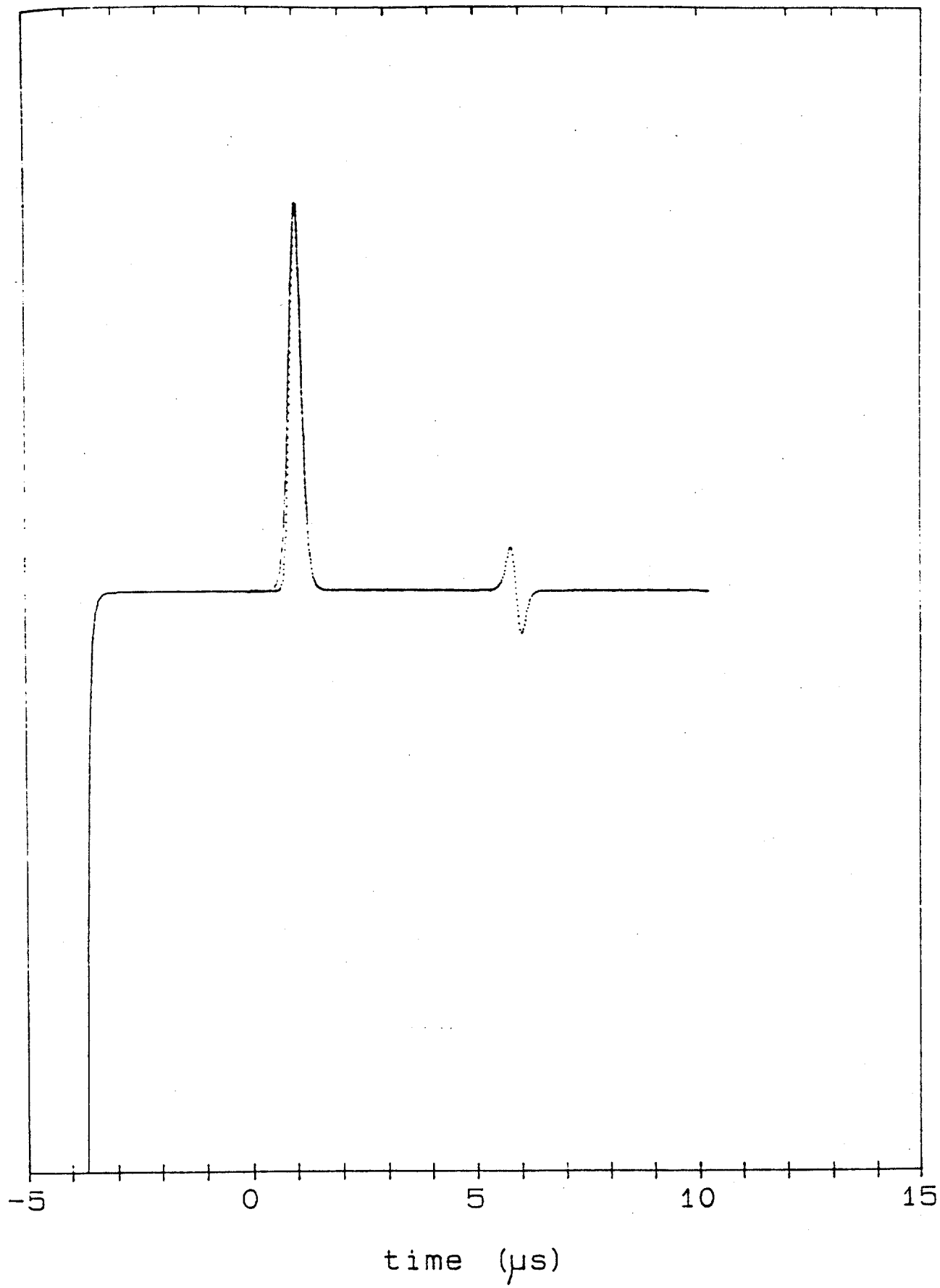

Figure 4

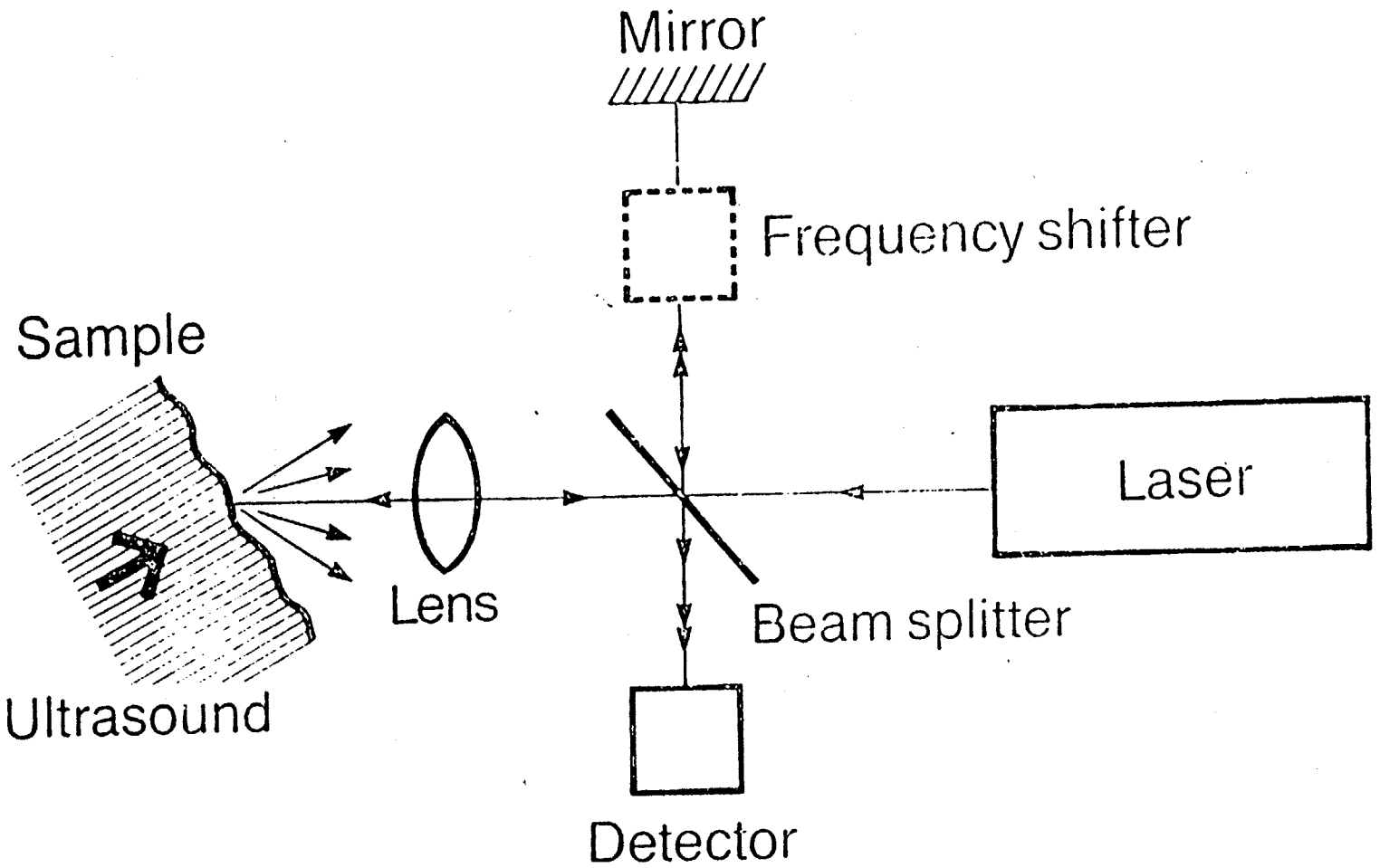
Mirror
Frequency shifter
Sample
Laser
Lens
Beam splitter
Ultrasound
Detector

Figure 5

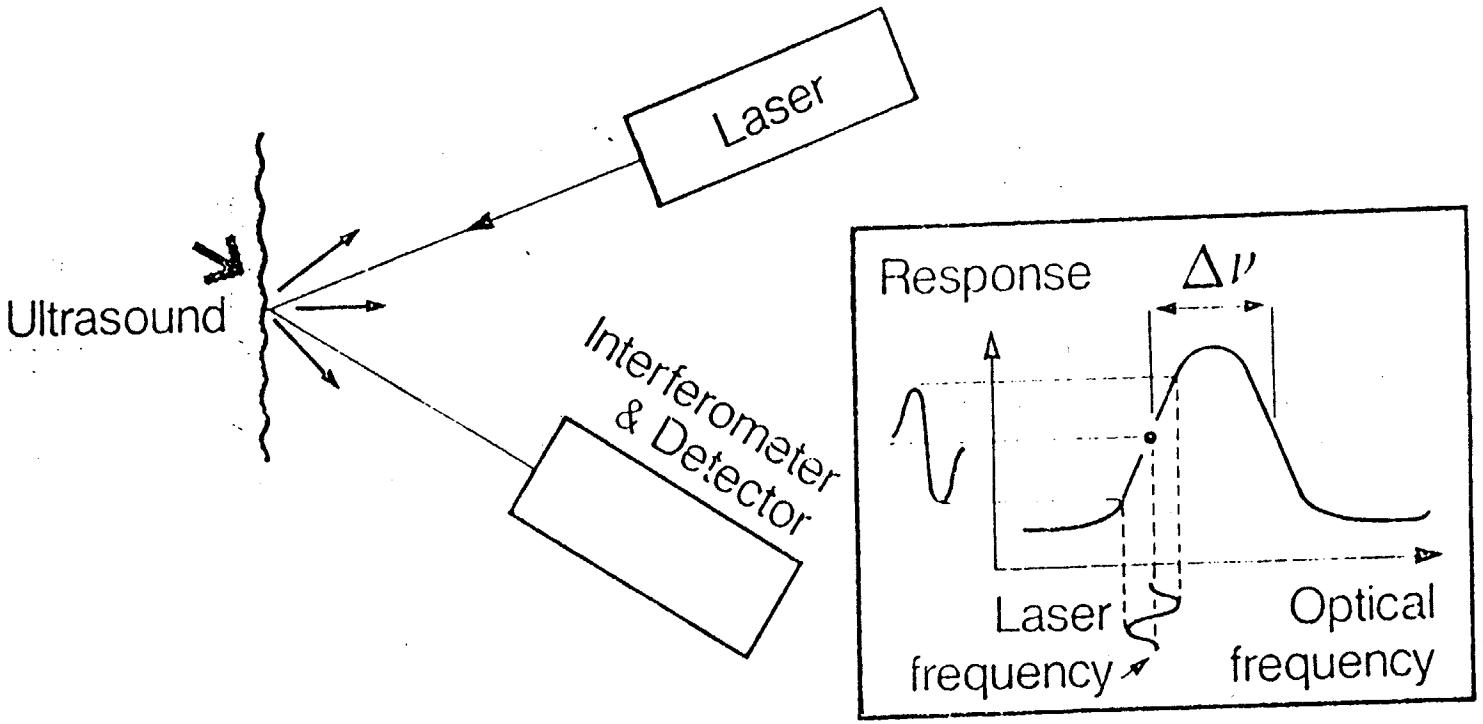
Laser
Ultrasound
Interferometer
& Detector
Response
Δν
Laser
frequency
Optical
frequency

Figure 6

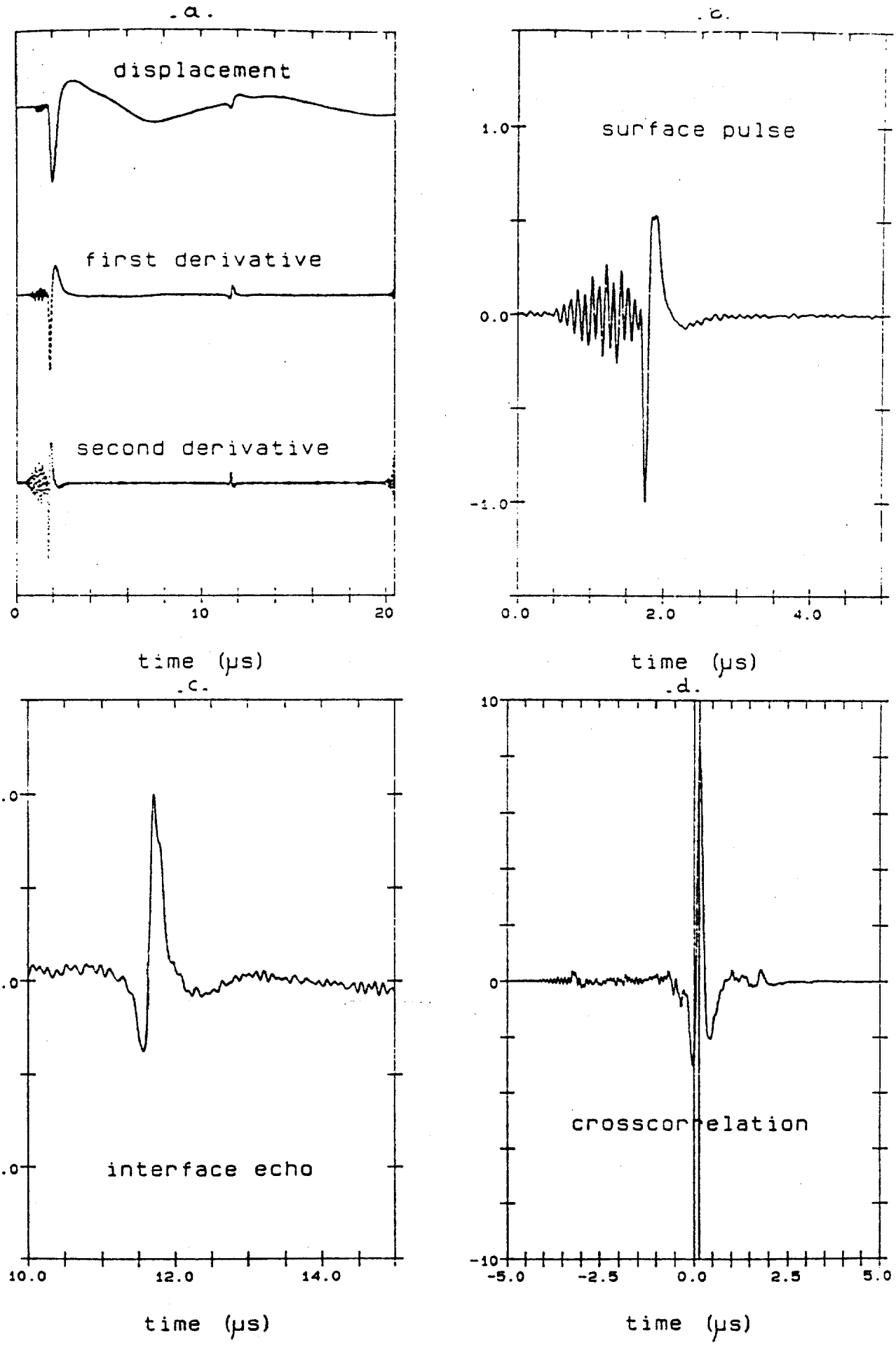
.a.
displacement
first derivative
second derivative
0
10
20
time (μs)
.b.
1.0
surface pulse
0.0
-1.0
0.0
2.0
4.0
time (μs)
.c.
1.0
0.0
-1.0
interface echo
10.0
12.0
14.0
time (μs)
.d.
10
0
-10
crosscorrelation
-5.0
-2.5
0.0
2.5
5.0
time (μs)

Figure 7

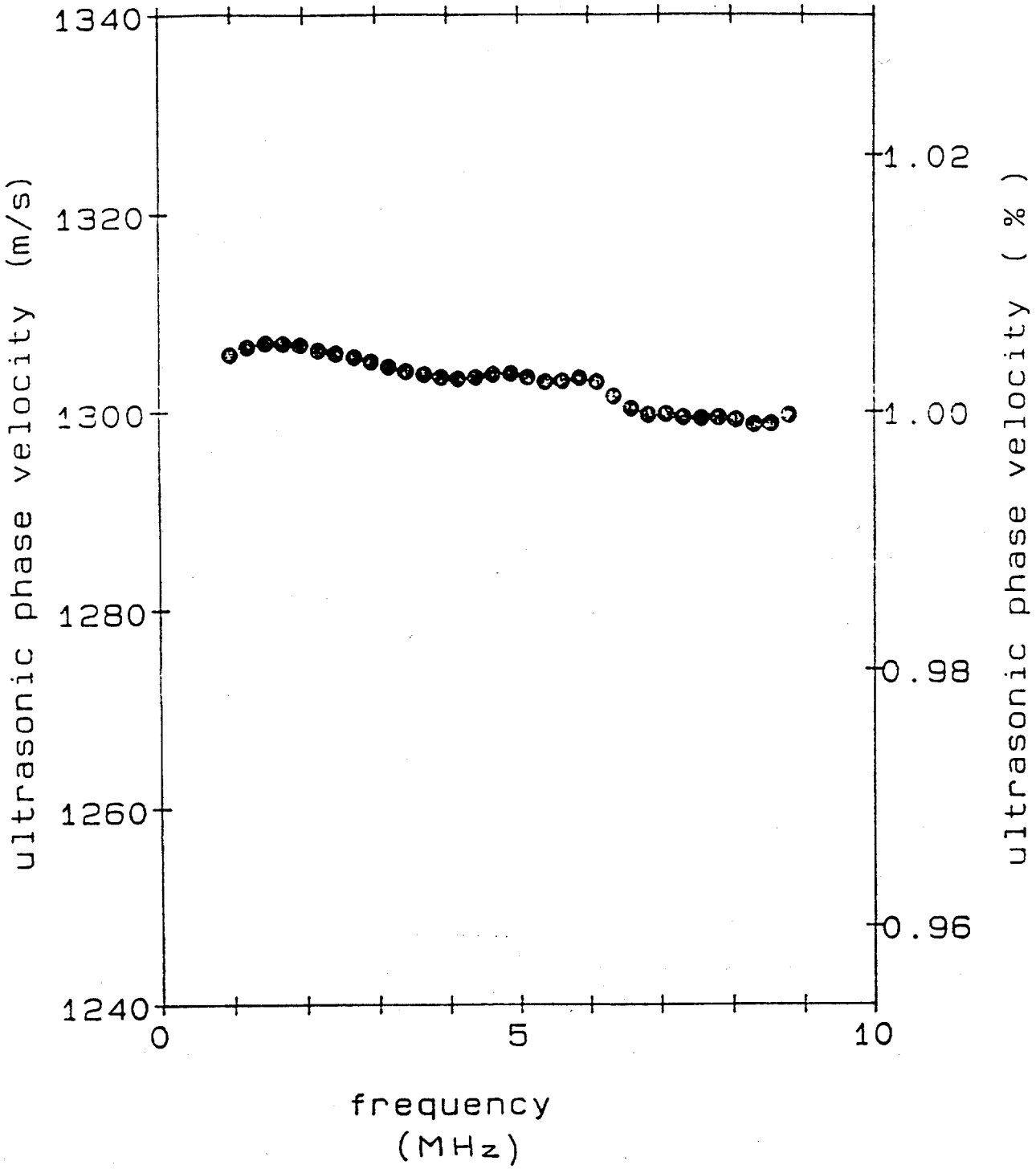
1340
1320
1300
1280
1260
1240
ultrasonic phase velocity (m/s)
1.02
1.00
0.98
0.96
ultrasonic phase velocity (%)
0
5
10
frequency
(MHz)

Figure 8

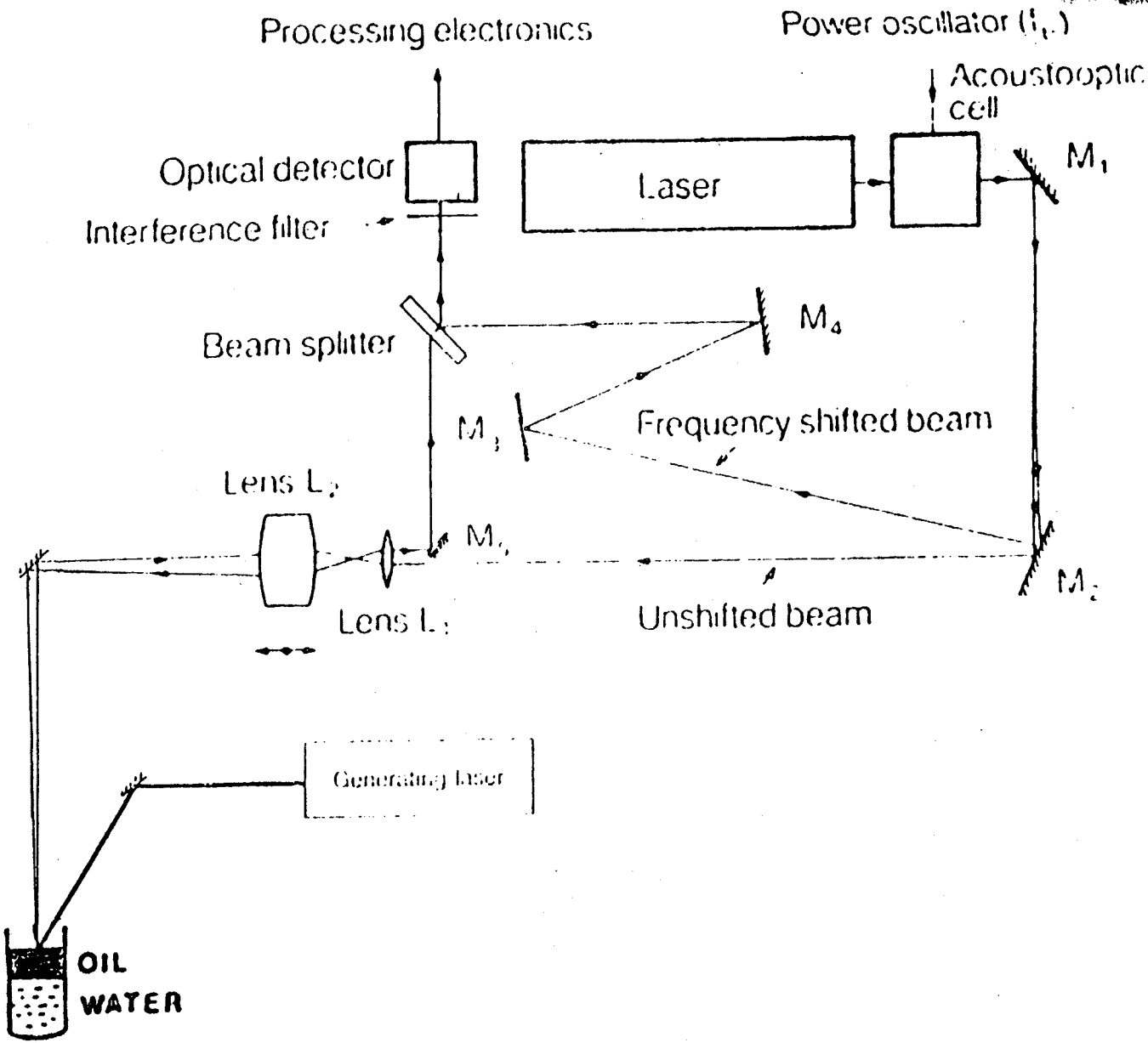
Processing electronics
Power oscillator
Acoustooptic cell
Optical detector
Laser
M_1
Interference filter
Beam splitter
M_4
M_3
Frequency shifted beam
Lens L_2
M_2
M_2
Lens L_1
Unshifted beam
Generating laser
OIL
WATER

Figure 9

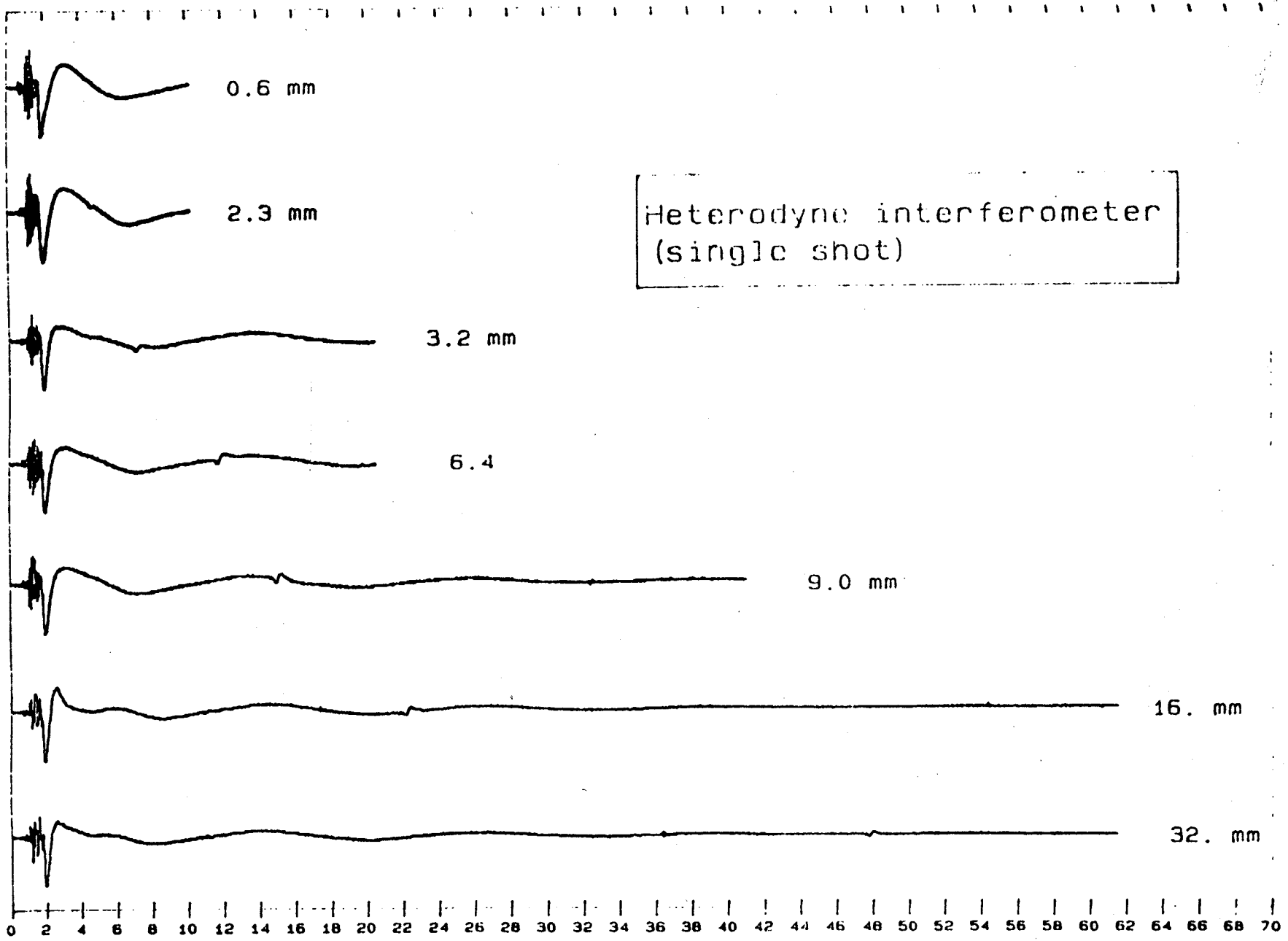
0.6 mm
2.3 mm
Heterodyne interferometer
(single shot)
3.2 mm
6.4
9.0 mm
16. mm
32. mm
0 2 4 6 8 10 12 14 16 18 20 22 24 26 28 30 32 34 36 38 40 42 44 46 48 50 52 54 56 58 60 62 64 66 68 70
time (μs)

Figure 10.a.

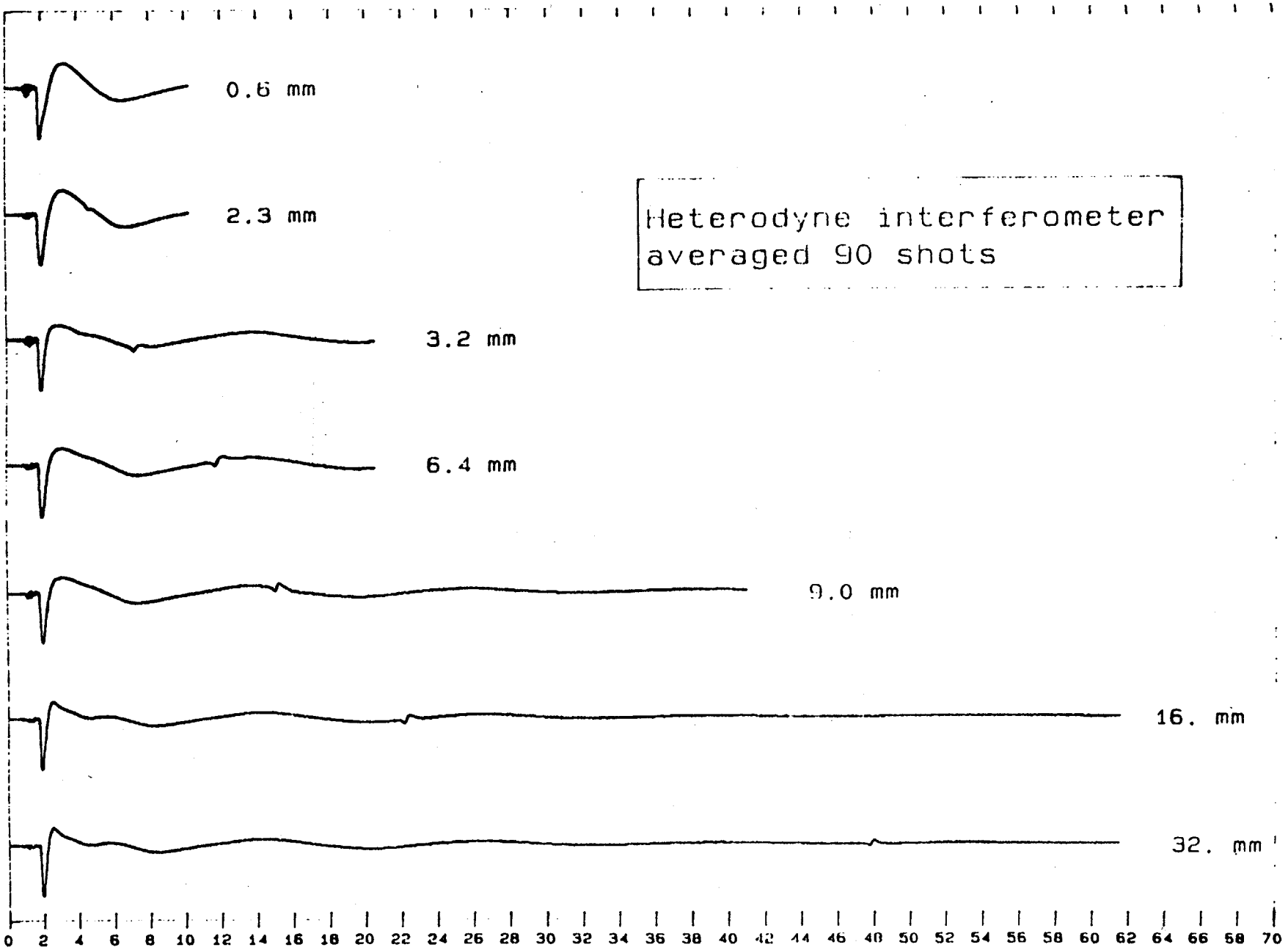
0.6 mm
2.3 mm
3.2 mm
6.4 mm
9.0 mm
16. mm
32. mm
Heterodyne interferometer
averaged 90 shots
0 2 4 6 8 10 12 14 16 18 20 22 24 26 28 30 32 34 36 38 40 42 44 46 48 50 52 54 56 58 60 62 64 66 68 70
time (μs)

Figure 10.b.

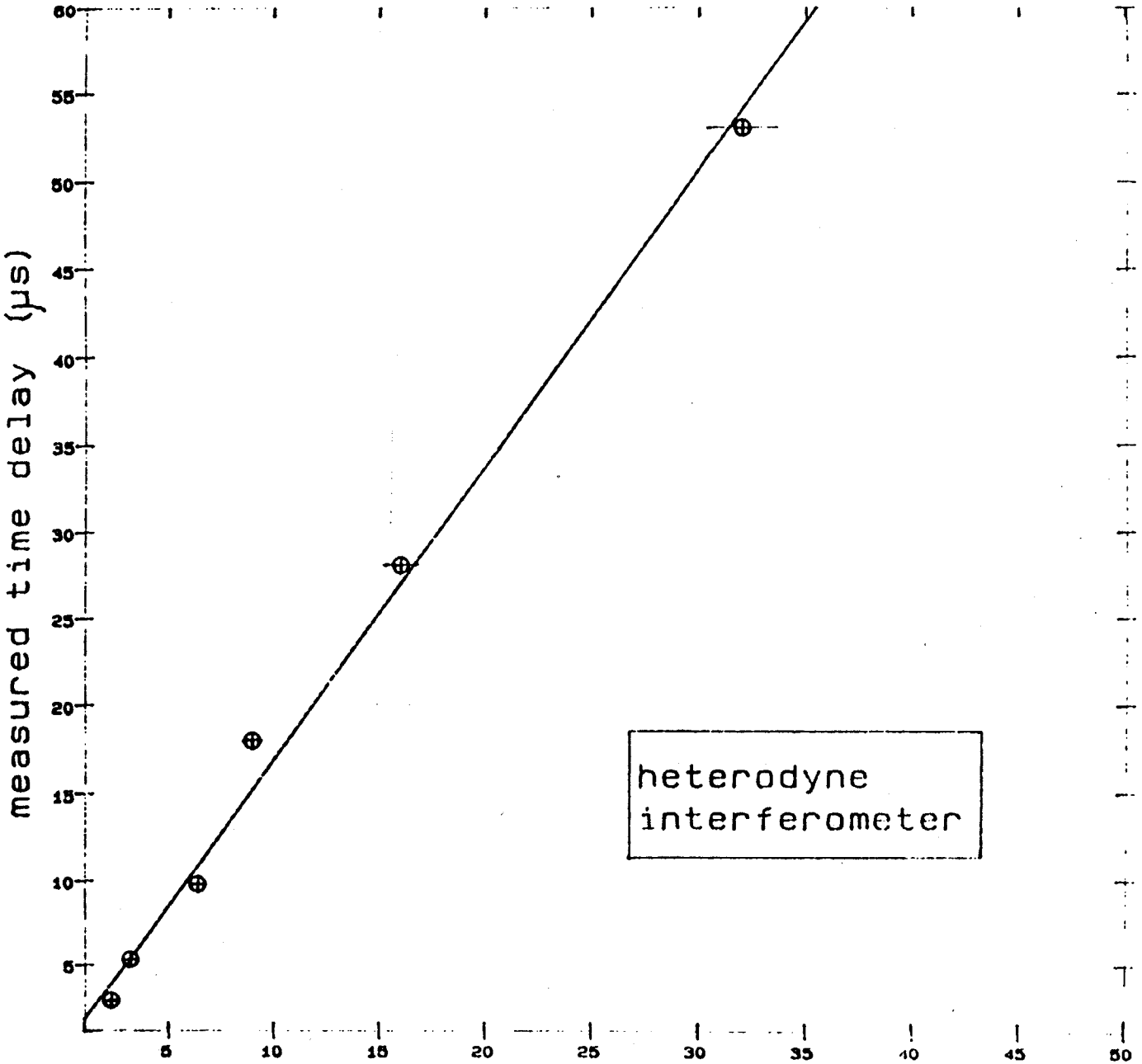
measured time delay (μs)
oil thickness (mm)
heterodyne
interferometer
O averaged data
+ single shot data
1.690997*X
1.691117*X

Figure 11

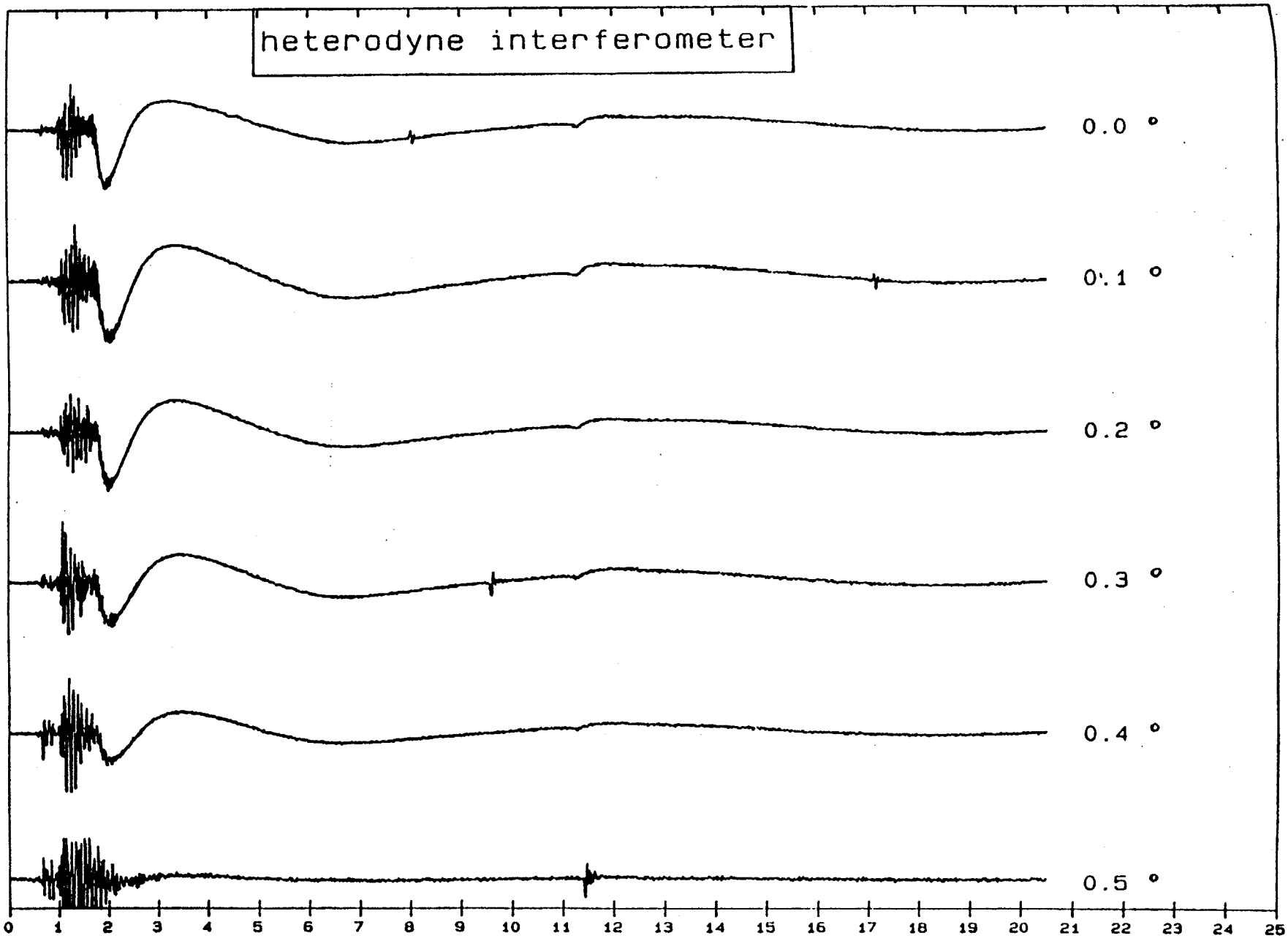
heterodyne interferometer
0.0 °
0.1 °
0.2 °
0.3 °
0.4 °
0.5 °
0 1 2 3 4 5 6 7 8 9 10 11 12 13 14 15 16 17 18 19 20 21 22 23 24 25
time (μs)

Figure 12

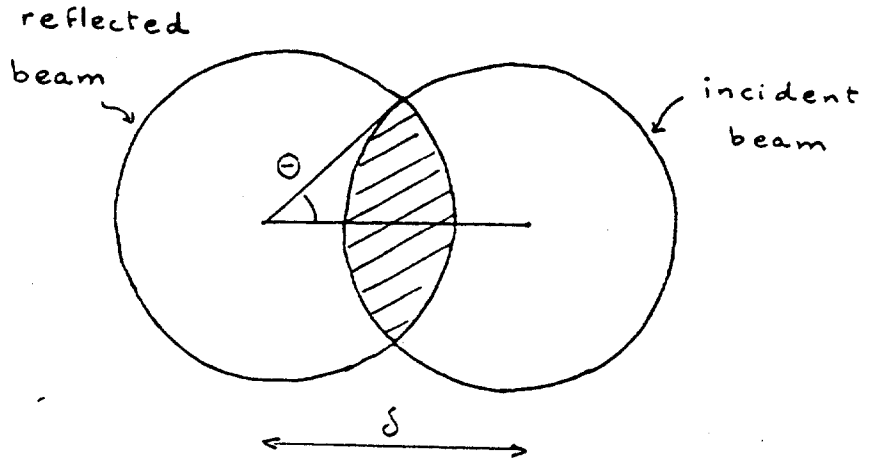
reflected
beam
incident
beam
Θ
δ

-a-

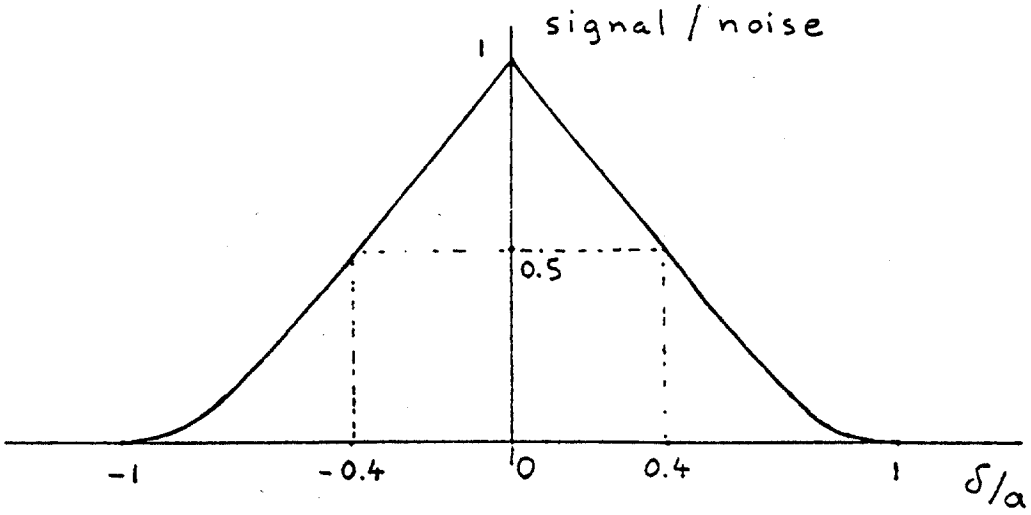
signal / noise
1
0.5
-1
-0.4
0
0.4
1
δ/a

-b-

Figure 13

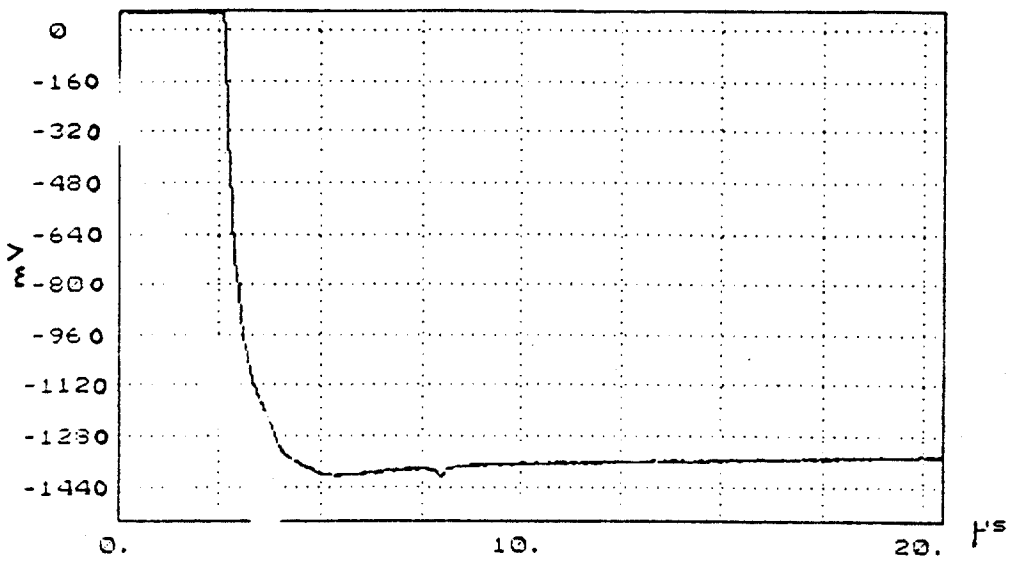
0
-160
-320
-480
-640
-800
-960
-1120
-1280
-1440
V
0.
10.
20.
μs

-a-

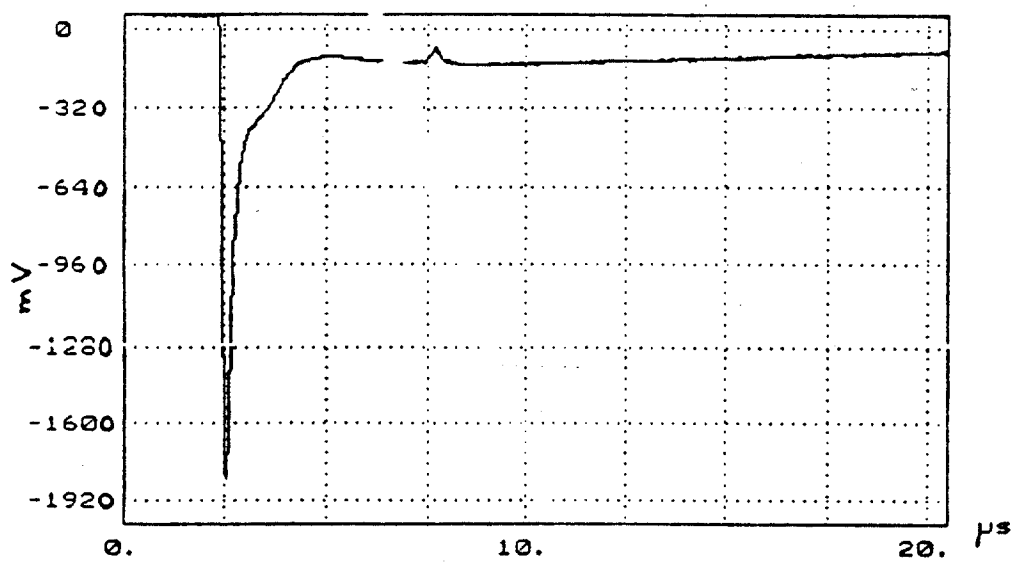
0
-320
-640
-960
-1280
-1600
-1920
V
0.
10.
20.
μs

-b-

Figure 14

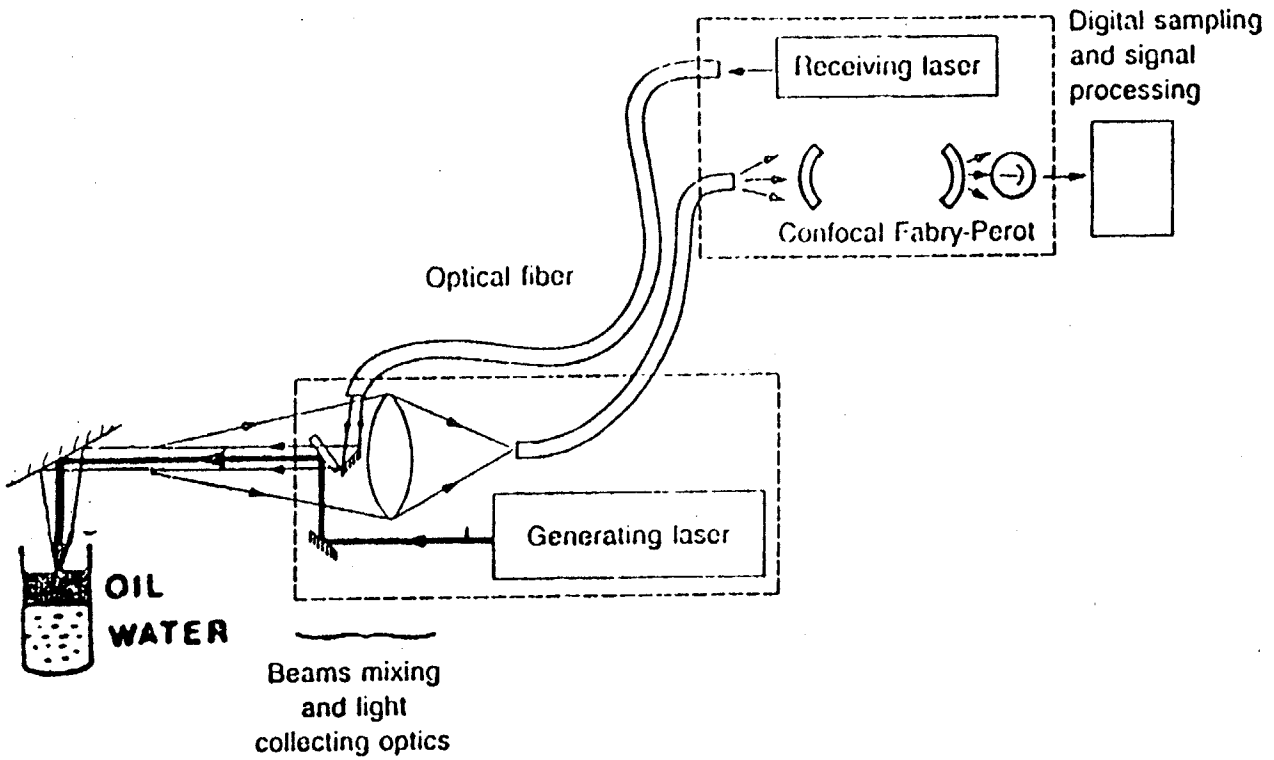
Digital sampling
and signal
processing
Receiving laser
Confocal Fabry-Perot
Optical fiber
Generating laser
OIL
WATER
Beams mixing
and light
collecting optics

Figure 15

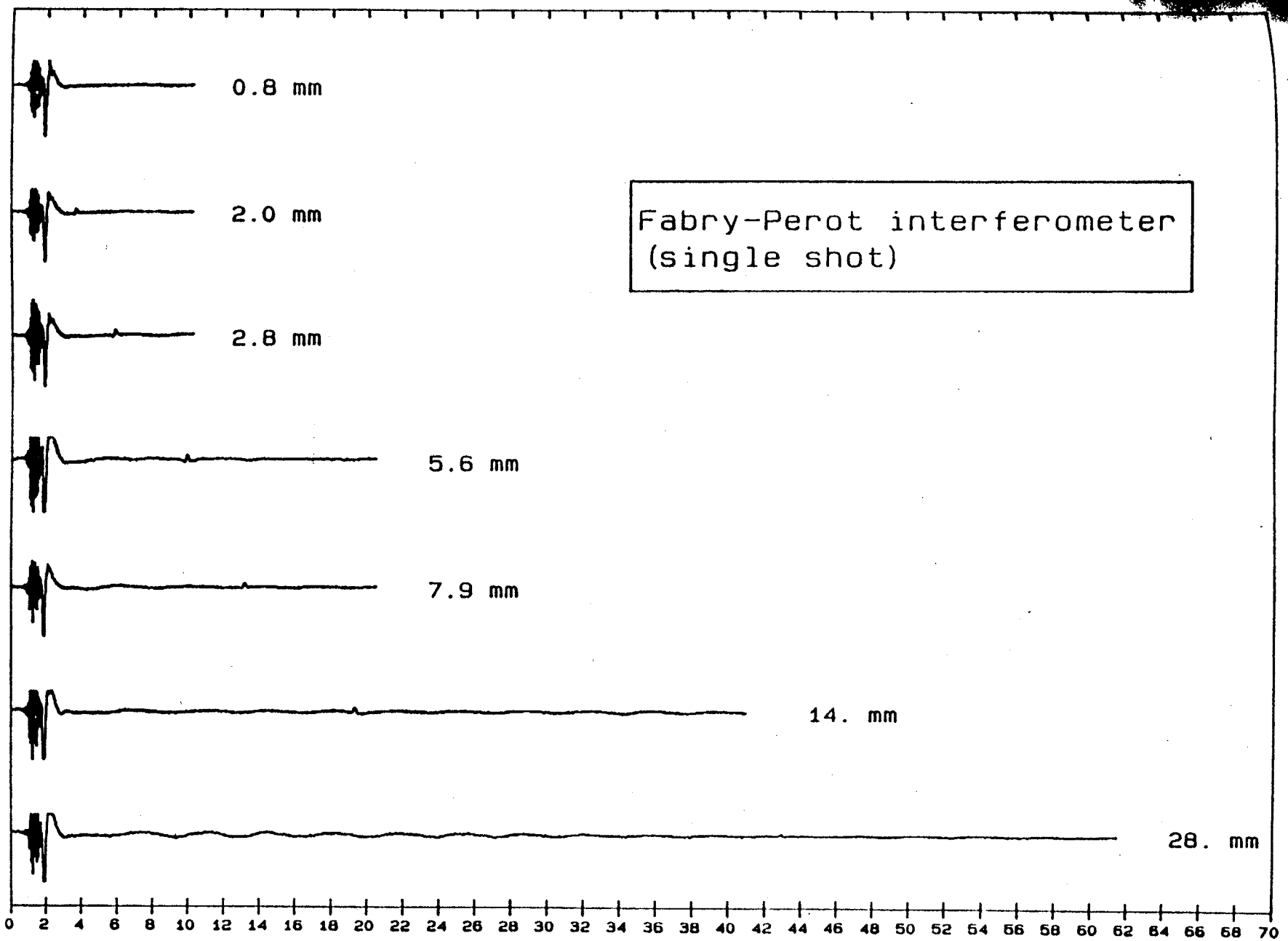
0.8 mm
2.0 mm
2.8 mm
5.6 mm
7.9 mm
14. mm
28. mm
Fabry-Perot interferometer
(single shot)
0 2 4 6 8 10 12 14 16 18 20 22 24 26 28 30 32 34 36 38 40 42 44 46 48 50 52 54 56 58 60 62 64 66 68 70
time (μs)

Figure 16.a.

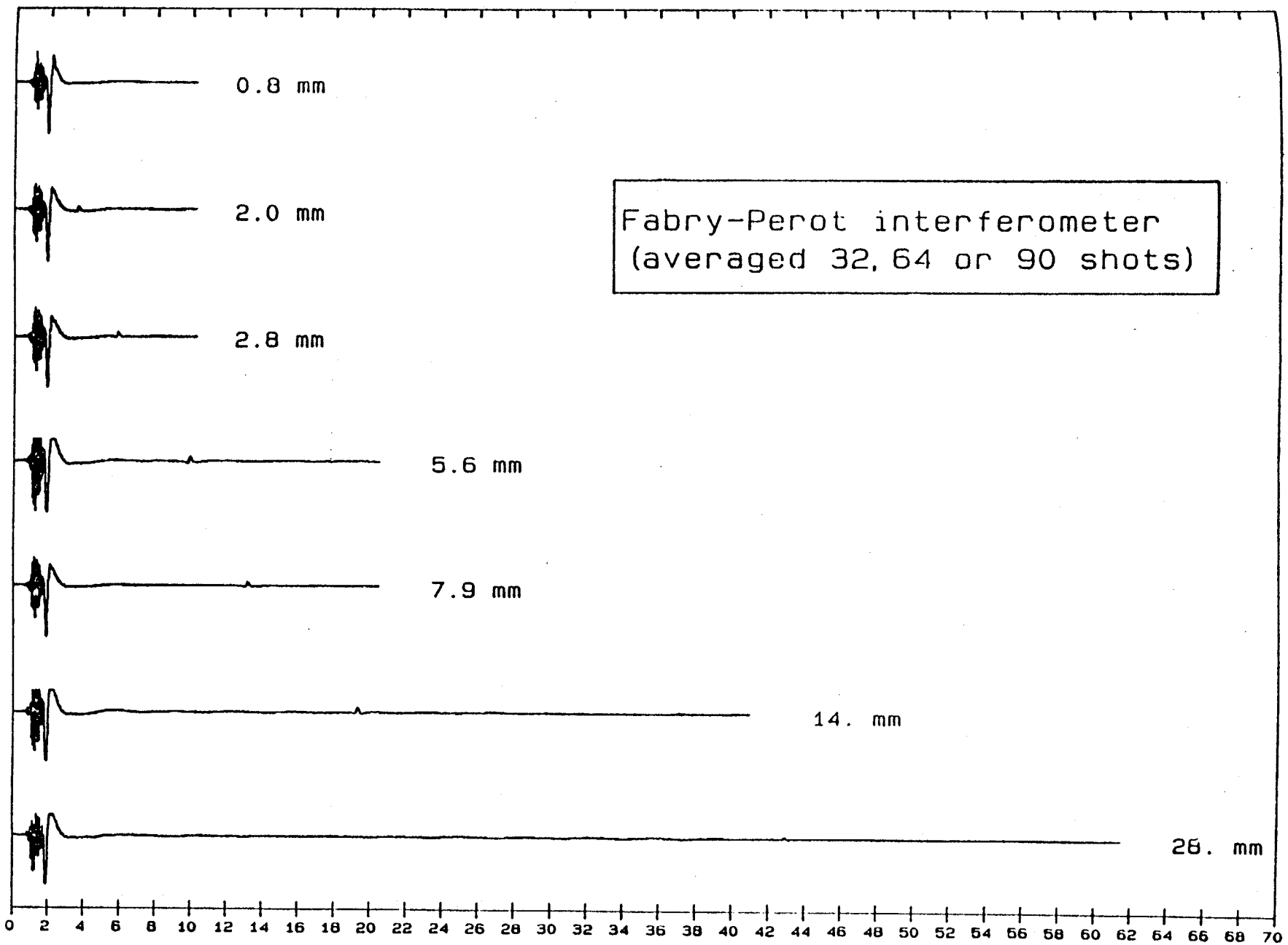
0.8 mm
2.0 mm
2.8 mm
5.6 mm
7.9 mm
14. mm
28. mm
Fabry-Perot interferometer
(averaged 32, 64 or 90 shots)
0 2 4 6 8 10 12 14 16 18 20 22 24 26 28 30 32 34 36 38 40 42 44 46 48 50 52 54 56 58 60 62 64 66 68 70
time (μs)

Figure 16.b.

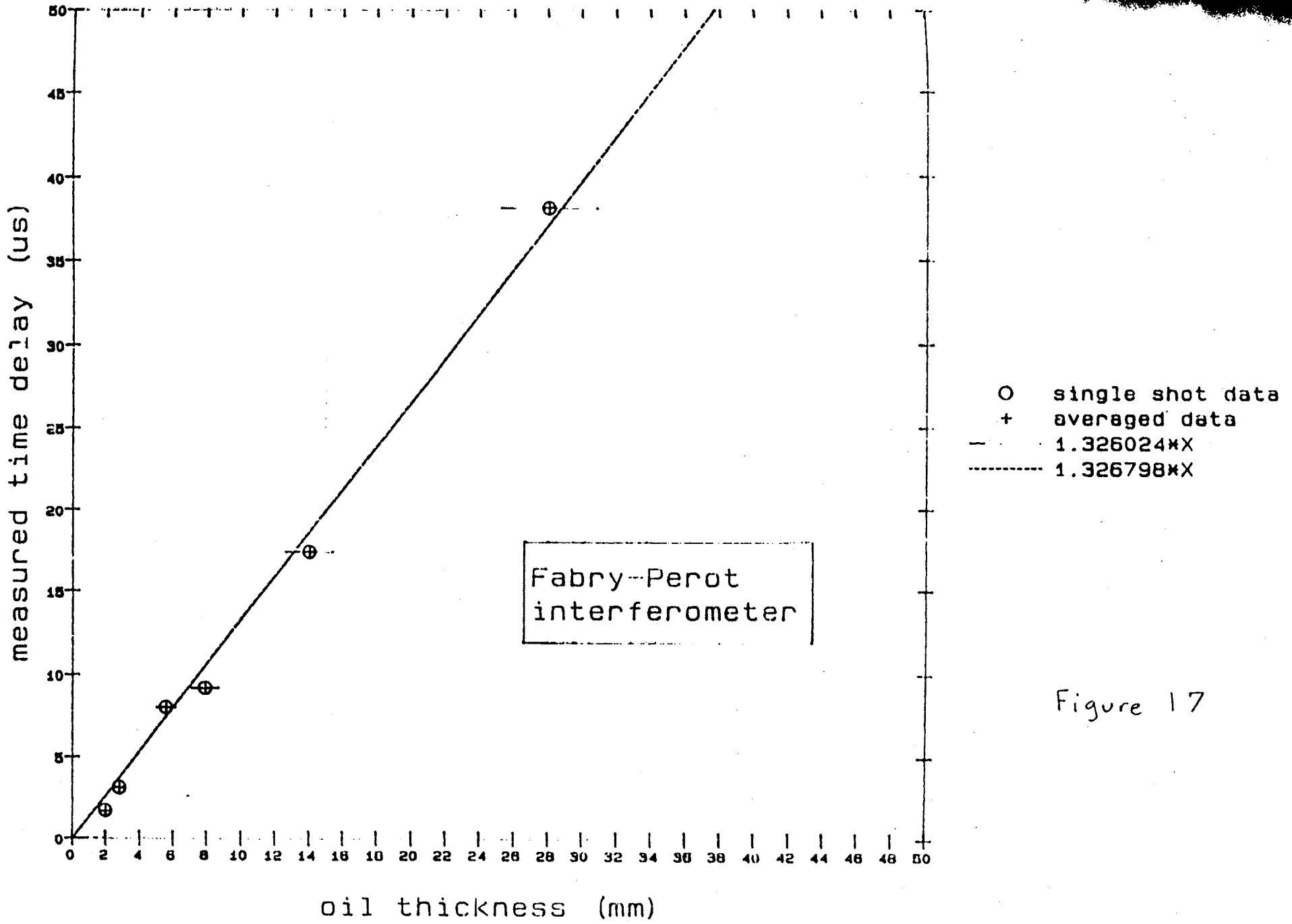
measured time delay (us)
oil thickness (mm)
0
5
10
15
20
25
30
35
40
45
50
0 2 4 6 8 10 12 14 16 18 20 22 24 26 28 30 32 34 36 38 40 42 44 46 48 50
Fabry-Perot
interferometer
O single shot data
+ averaged data
1.326024*X
1.326798*X

Figure 17

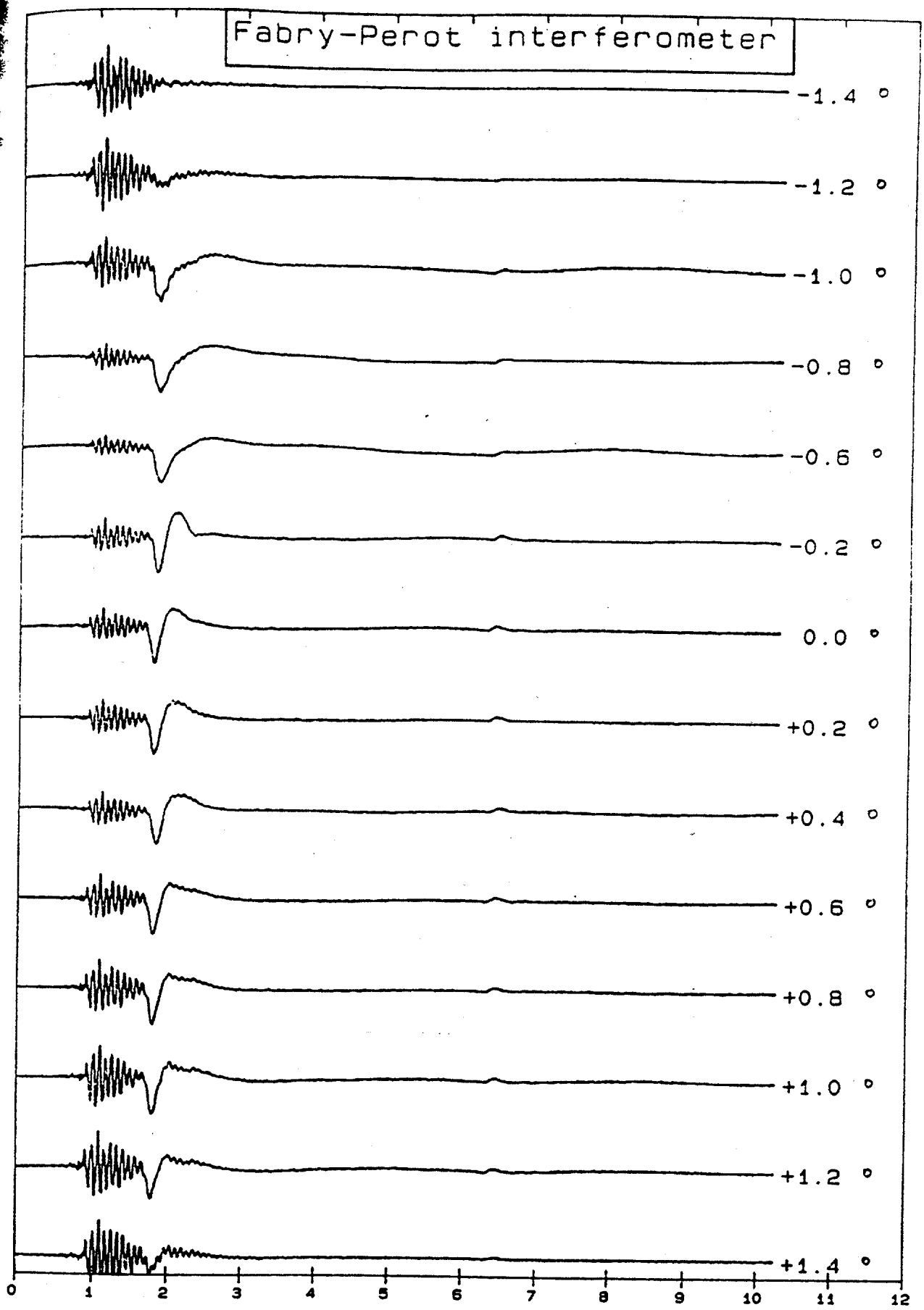
Fabry-Perot interferometer
-1.4 °
-1.2 °
-1.0 °
-0.8 °
-0.6 °
-0.2 °
0.0 °
+0.2 °
+0.4 °
+0.6 °
+0.8 °
+1.0 °
+1.2 °
+1.4 °
0
1
2
3
4
5
6
7
8
9
10
11
12
time (μs)

Figure 18

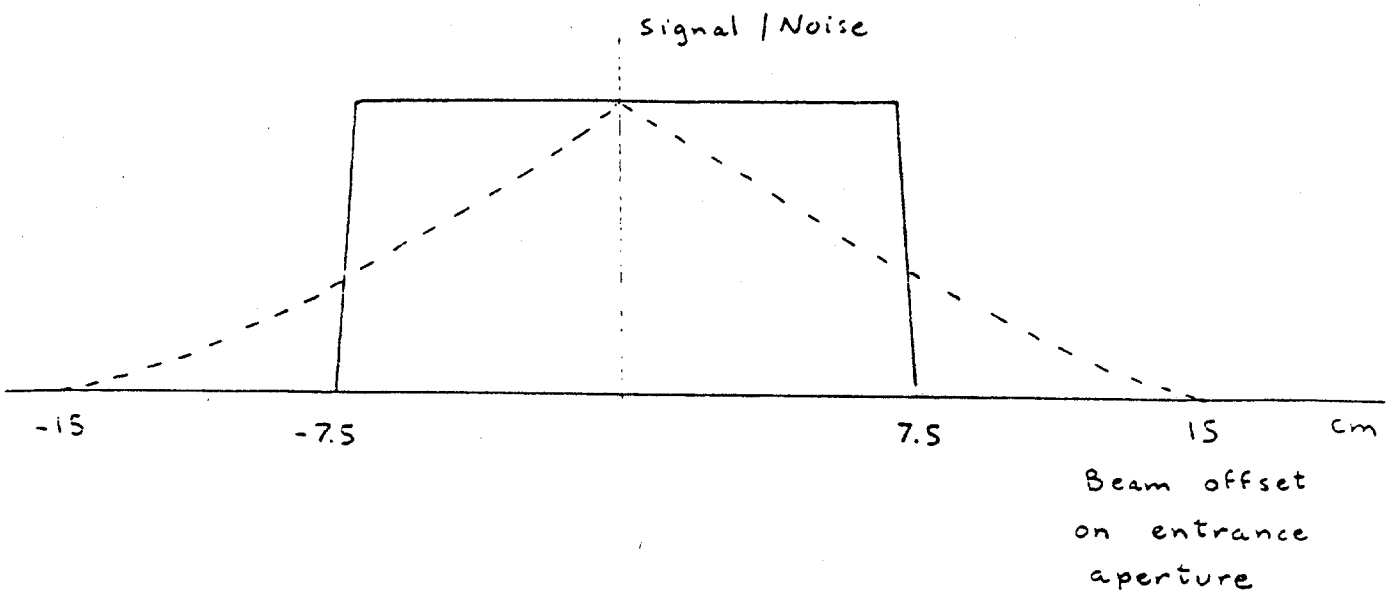

Figure 19

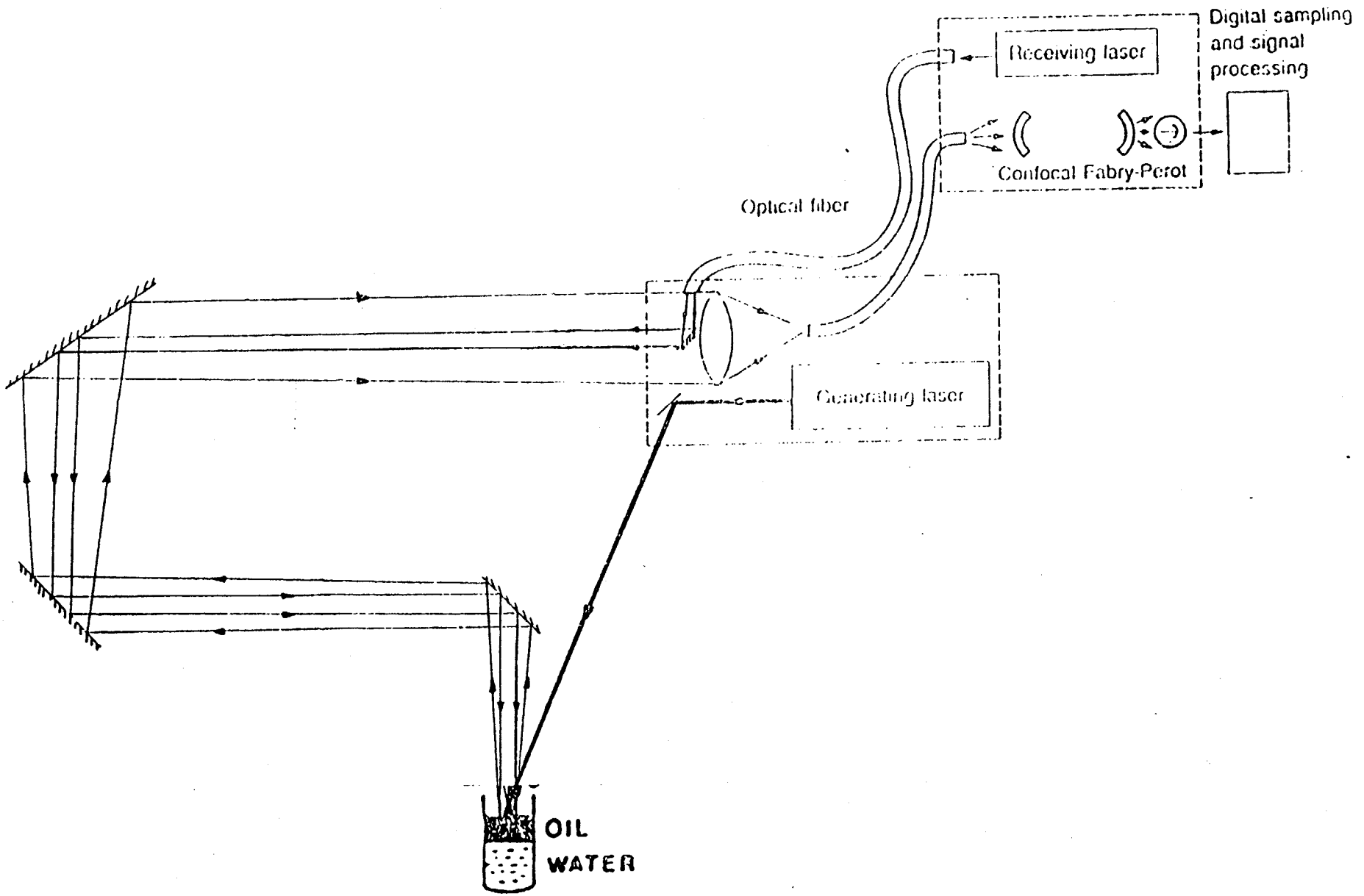
Digital sampling
and signal
processing
Receiving laser
Confocal Fabry-Perot
Optical fiber
Generating laser
OIL
WATER

Figure 20

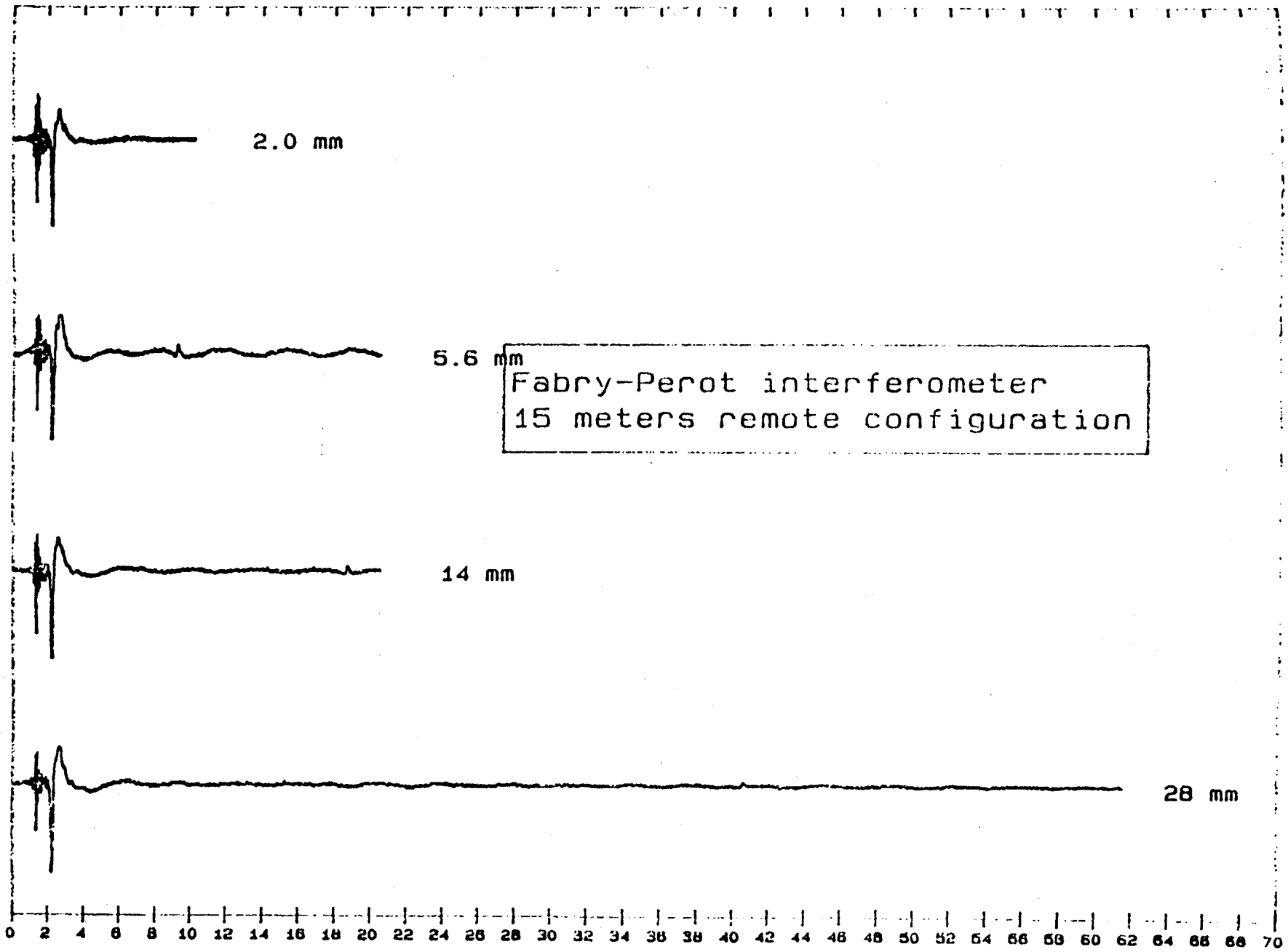
2.0 mm
5.6 mm
Fabry-Perot interferometer
15 meters remote configuration
14 mm
28 mm
0 2 4 6 8 10 12 14 16 18 20 22 24 26 28 30 32 34 36 38 40 42 44 46 48 50 52 54 56 58 60 62 64 66 68 70
time (μs)

Figure 21

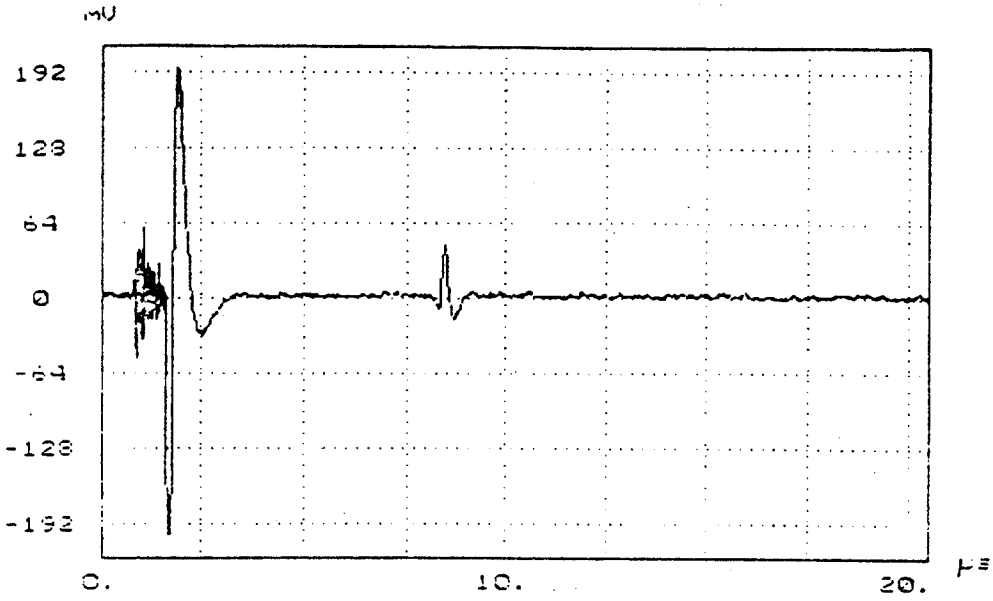
mV
192
128
64
0
-64
-128
-192
0.
10.
20.
μs

.a.

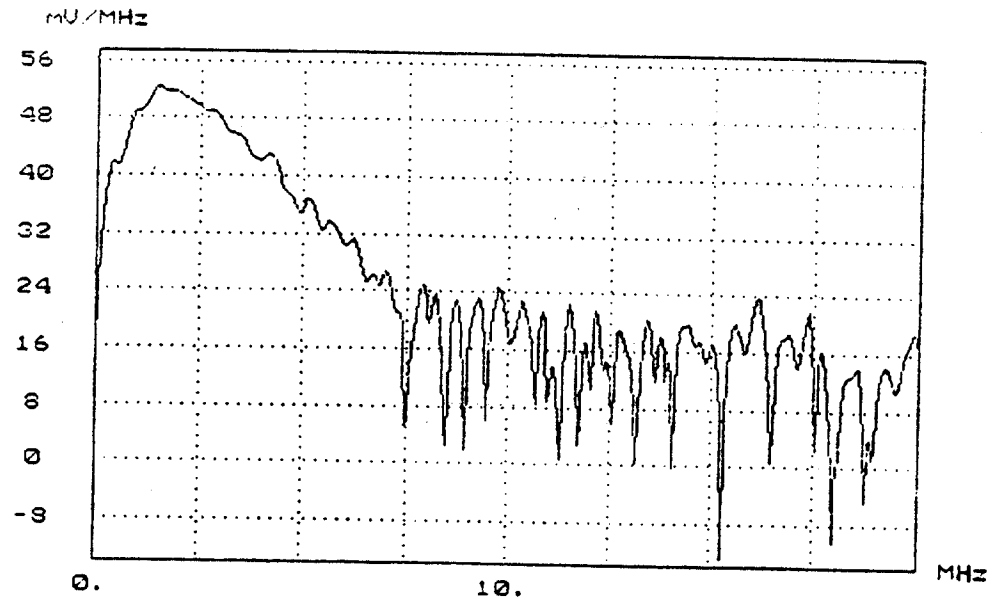
mV/MHz
56
48
40
32
24
16
8
0
-8
0.
10.
MHz

.b.

Figure 22

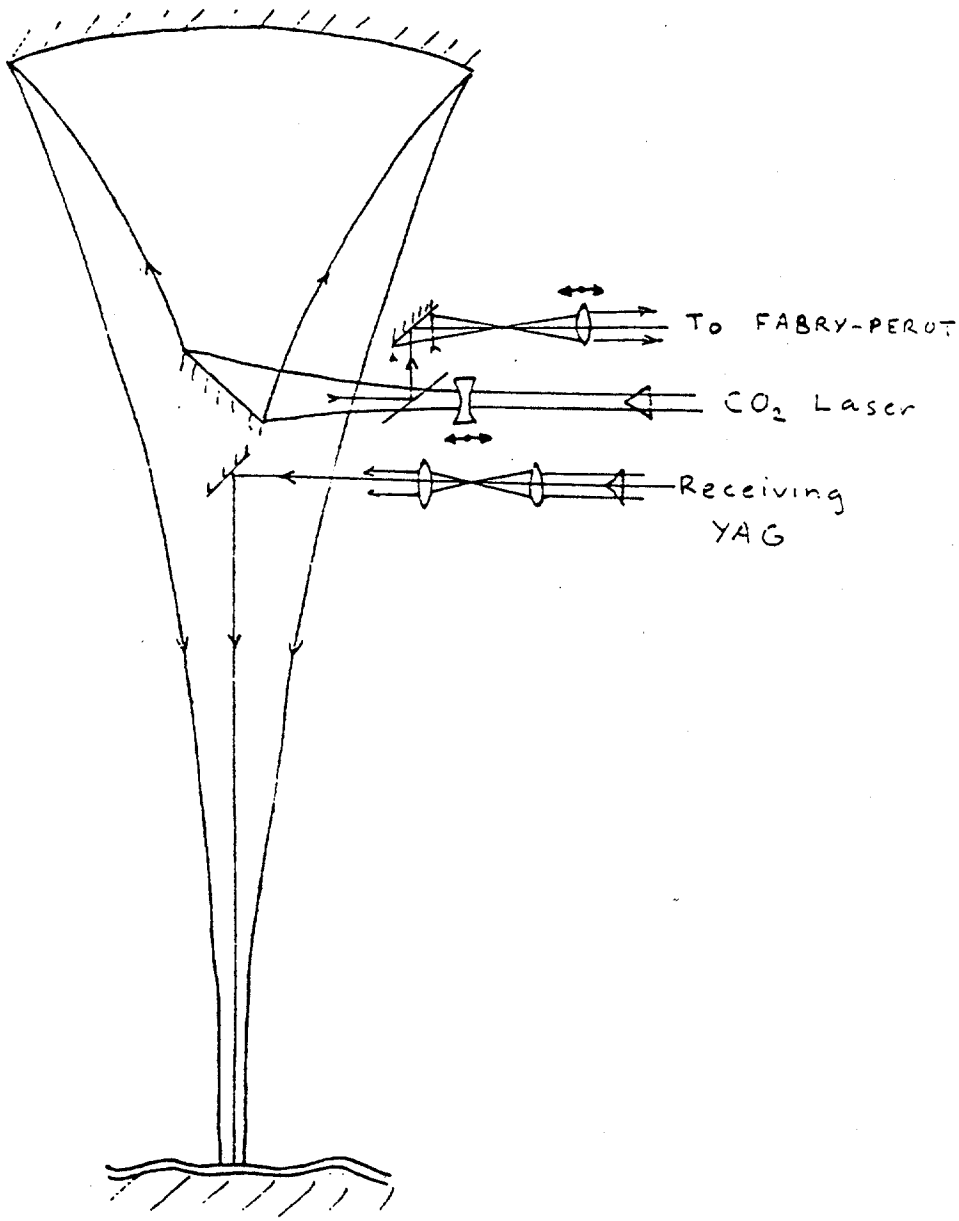

Figure 23

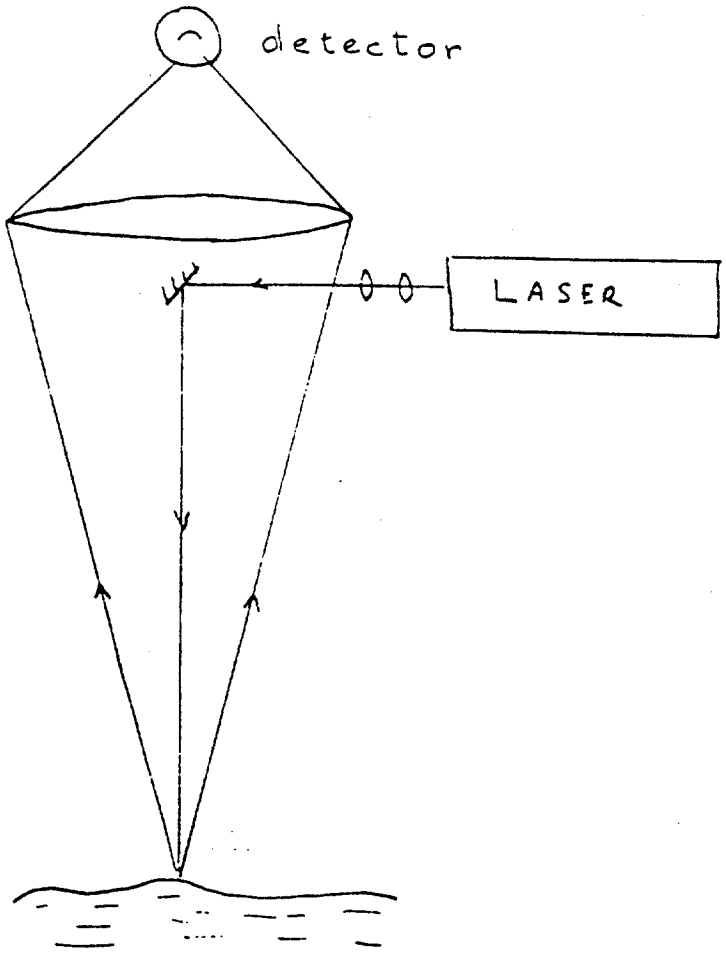

Figure 24

Appendix 2

Laboratory Evaluation of Optothermal

Techniques for Remote Oil Thickness

Monitoring Applications

Report IGM-RT89-404-07-C

CONFIDENTIAL
October 1989

Laboratory evaluation of optothermal techniques for remote oil thickness monitoring applications

By J.C. Krapez and P. Cielo
National Research Council Canada
Industrial Materials Research Institute
75 De Mortagne Blvd.
Boucherville, Québec J4B 6Y4

Distribution: J. Bussière
J. Martel
J.R. Rossiter (Canpolar)

SUMMARY

A theoretical and experimental investigation is presented on the suitability of optothermal techniques for oil spill monitoring applications. Two approaches are taken into consideration for a remote evaluation of the oil film thickness on water.

The first approach is based on transient heating of the oil film and monitoring of the thermal propagation through the oil-water medium by an infrared surface temperature detector. A correlation between the oil film thickness and the shape of the temperature-vs-time curve is established by theoretical modelling and partially confirmed by our experimental results. However, the length of the required observation time, several tens of seconds to follow the thermal propagation through a 1 mm-thick film, introduced substantial convectional perturbations to the experimental data, even in a quiet laboratory environment. This resulted in poor signal repetitivity and reliability.

The second approach, thermally stimulated spectroscopy, may be implemented with observation times much shorter than the thermal propagation time through the film. A theoretical model shows that films of light oil may be probed up to 1 mm of thickness by this method if a YAG laser is used for the thermal stimulation, while heavier oils can only be probed up to 200 μm of thickness, unless a longer wavelength thermal excitation source can be found. In any case, the thermal spectroscopy approach appears as a valid complement to other techniques, such as laser fluorescence (0 to 20 μm of thickness) and microwave radiometry (1 to 4 mm). A limited amount of experimental data could be collected on this second approach, mainly because of the unavailability of proper equipment. Nevertheless, the results obtained with a continuous YAG source and a laboratory monochromator confirmed the expected decrease of the signal magnitude with film thicknesses smaller than the optical penetration depth and provided a better understanding of the optical and thermal interactions in the oil-water medium. Further investigations with more appropriate equipment are recommended.

CONTENTS

1. INTRODUCTION

Canpolar Inc. contacted our institute some time ago for help in the evaluation of laser-based techniques for remote oil film thickness measurement. The intended application is the evaluation of the thickness of crude oil films on ocean water to be performed by airborne instrumentation quickly after an oil spill. Typically, a small aircraft or a helicopter would fly over the spill area within hours from the reported event to monitor the volume, extension and movement of the crude oil film by remotely taking samples of the oil film thickness at periodical intervals.

Two laser-based techniques have been taken into consideration at IMRI for monitoring oil film thickness: a laser-ultrasound approach, which is the object of a separate IMRI report, and an optothermal approach, including a number of possible variations, which is described in this report.

Two optothermal techniques are described in the present report. The first method, time-resolved thermal-wave probing, corresponds to a technology previously developed at IMRI for the evaluation of the thickness of solid coatings on metal. Although its applicability to liquid films was not evident, as mentioned in a previcus letter to Canpolar, it was decided that such an approach was worth a quick laboratory investigation.

The second optothermal technique described in this report, thermally stimulated spectroscopy, was conceived after the results of the thermal-wave method made it clear that the required observation time was impractically long. After consultation with Canpolar, it was thus decided that a preliminary laboratory investigation would have been carried out as well on the thermal spectroscopic method. The results obtained up to now with this approach seem to indicate that such a technique would be convenient for the monitoring of relatively thin films.

2. TIME-RESOLVED THERMAL PROPAGATION APPROACH

2.1 Description of the method

2.1.1 Qualitative introduction

A time-resolved thermal propagation method has been developed a few years ago at IMRI for the thickness evaluation of ceramic coatings on metal (Ref. 1). The

surface of the coating is thermally stimulated by a laser beam creating a thermal front which propagates within the material at a speed which is determined by the thermal diffusivity $a = K/\rho c$ (K being the thermal conductivity, ρ the mass density and c the specific heat) of the material within which the thermal wave propagates. When the thermal front reaches the coating-substrate interface, the thermal flow will be perturbed by an amount depending on the difference between the thermal properties of the coating and substrate materials, and more precisely (see below) on the ratio of their respective effusivities $b = (K\rho c)^{1/2}$.

2.1.2 Analytical modelling

The thermal propagation in the oil-water medium can be monitored by following the temperature evolution of the irradiated surface after application of the laser-heating step by an infrared temperature sensor. The surface temperature vs. time curve (thermogram) in the case of continuous heating of the film surface, starting at the time t = 0, with an absorbed power density P follows the relation (Ref. 2):

$$T(t) = \frac{2P\sqrt{t}}{\sqrt{\pi}\, b_1}\left\{ 1 + 2\sum_{n=1}^{\infty} \Gamma^n \left[\exp\left(-\frac{n^2 z_1^2}{a_1 t}\right) - \sqrt{\pi}\,\frac{nz_1}{\sqrt{a_1 t}}\,\mathrm{erfc}\left(\frac{nz_1}{\sqrt{a_1 t}}\right)\right]\right\} \qquad (1)$$

with $\Gamma = \dfrac{b_2 - b_1}{b_2 + b_1}$

where z_1 is the film thickness and in general the subscripts 1 and 2 refer, respectively, to the coating and the substrate. Because of the arguments of the exp and erfc functions, a discontinuity in the $t^{1/2}$ progression of the surface temperature is expected after a time delay of the order of:

$$t_1 \approx z_1^2/a_1 \qquad (2)$$

which is referred to as the thermal propagation time through a film of thickness z_1 and thermal diffusivity a_1. This is clearly evident from Fig. 2, showing the computed surface temperature increase of a coating on a substrate for different values of the effusivity ratio b_2/b_1. When such a ratio is different from 1, the slope of temperature vs. time curve departs from 1/2 in the log-log scale in the proximity of a value for the adimensional Fourier number $F = t/t_1 = a_1 t/z_1^2 = 1$ corresponding to Eq. (2).

Fig. 2 shows that a first condition for the visibility of the thermal transition at the coating-substrate interface is a difference on their respective thermal effusivities. In our case, the following data have been reported for oil and water (Ref. 3; see previous letter to Canpolar):

THERMAL PARAMETER	OIL	WATER
K (W/mK)	0.14	0.6
ρ (J/KgK)	800	1000
C (Kg/m^3)	1050	4200
$b = (K\rho c)^{1/2}$ (J/m^2Ks^{-1})	340	1600
$a = K/\rho c$ (m^2/s)	$1.7 \cdot 10^{-7}$	$1.4 \cdot 10^{-7}$

The effusivity ratio being nearly equal to 5, we can hope, in theory, to see an inflexion in the thermogram around $t = t_1$ (see Fig. 2). If we can locate such a transition on the thermogram, we can then estimate the film thickness z_1 from Eq. (2) if the thermal diffusivity a_1 of the coating is known.

2.1.3 Finite-difference modelling in the non-ideal case

In reality, other perturbations to the ideal heat propagation curve are expected. A first class of perturbations are related to thermal losses and finite optical penetration in the oil film. Surface losses by radiation and conduction in air above the heated surface, together with 3-D thermal flow losses if the diameter of the irradiated area is finite, tend to saturate the curve to a constant asymptote when the amount of loss becomes comparable to the injected power: see Fig. 3. As to the finite optical penetration in the oil film, both at the laser and at the infrared detector wavelengths, the result is an initial portion of the thermogram (up to a time of the order of the thermal propagation time through the optical depth of penetration) where the slope is closer to 1 than to the nominal value of 1/2.

Even worse are the effects of convection in the liquid. The thermally stimulated convectional flow, whose modelling is difficult (see Appendix of Ref. 4), is strongly dependent on the oil viscosity and thus on ambient temperature and oil type.

Convection produces a radial material flow which stabilizes the surface temperature at levels lower than expected. Moreover, the ocean water movement, particularly under adverse meteorological conditions, is expected to introduce further random fluctuations in the thermogram.

2.2 Experimental Investigation

The analysis presented above shows that the thermogram features of interest for oil film thickness evaluation, i.e. the slope variation around F = 1 (see Fig. 2) for an effusivity ratio of the order of 5, will probably be overshadowed by external perturbations. Nevertheless, a series of laboratory tests were performed at IMRI on oil film of different thickness on water to verify whether some empirical correlation could be established between the shape of the obtained thermograms and the oil film thickness.

2.2.1 Description of the apparatus

The experimental apparatus is represented schematically in Fig. 1. The YAG laser (λ = 1.064 μm) produced a nearly parallel beam of 18 watts, typically 10 mm diameter, which was almost totally absorbed by the oil film. The cryogenically-cooled InSb detector, 1 mm x 1 mm active area, Ge-filtered to be sensitive over the 2 to 5.5 μm spectral range, was imaged on the center of the laser-irradiated area by a 2" diameter, 2" focal length CaF_2 infrared lens with an optical magnification equal to 5 (i.e., lens-to-oil distance equal to 300 mm).

The signal was periodically sampled and displayed logarithmically vs. time after subtraction of the initial signal level before heating. No conversion from the signal (which is proportional to T^n where T is the temperature in degrees Kelvin and n is of the order of 10 in our case, see Ref. 5) to the corresponding temperature was performed. This may introduce some amount of deformation to the curve shape due to the nonlinearity of the signal-to-temperature relation, but such effects are of minor significance at the present stage. The peak oil surface temperature was estimated to be of the order of 80°C during this series of experiments.

The preparation of oil film samples of uniform thickness proved to be more difficult than expected. The oil tended to lump over the water surface and to form a

thick meniscus on the borders of the glass container. With the help of L. Lalumière of Canpolar, we could achieve a certain degree of uniformity by deposing a known volume of oil on the water by a syringe and stirring just before each experimental trial, the oil thickness being evaluated from a knowledge of the injected oil volume and of the water surface. a / 2 a.

2.2.2 Experimental results.

Figs. 4(a) to 4(f) show the thermograms obtained with oil layers of estimated thicknesses from 0.3 to 1.2 mm on water. More than one test was performed on the same sample to verify the repetitivity of the corresponding thermogram. For each thermogram, a 0.5 slope straight line in the log-log scale representing the theoretical $t^{1/2}$ progression (neglecting signal vs. T nonlinearities) is also traced for reference. A full discussion of these results is given in the next section.

For an ideal thermogram, a data inversion can be performed to estimate the thermal properties of the different layers (Ref. 6). For a step thermal excitation, the thermogram T(t) can be inverted to obtain the distribution of the effusivity:

$$b(t) = \frac{2P\, t^{1/2}}{\pi^{1/2}\, T(t)} \qquad (3)$$

where P is the constant laser power density absorbed starting at t = 0. Figs. 5(a) to 5(f) show the results of this deconvolution operated on the data of Figs. 4(a) to 4(f). Because the thermal propagation depth z is linearly related to log t, Figs. 5 can be considered as an estimation of the thermal effusivity vs. depth below the surface of the oil-water sample.

2.2.3 Discussion

The experimental data shown in Figs. 4(a) to (f) have a certain degree of similarity with the theoretical expectations, see Fig. 3. The initial slope is closer to 1 than to 0.5 as expected from the finite optical penetration depth at the laser wavelength and even more in the spectral response region of the InSb detector. Tests were also performed with an HgCdTe detector and the results were similar although more noisy, possibly because of a higher sensitivity to surface flow. The curves tend to

saturate at longer time intervals as predicted by the simulation shown in Fig. 3. The overall results are, however, disappointing for the following reasons:

- The shape of the thermograms obtained for the same sample may present substantial variations from test to test.

- No clearly recognizable features have been observed relating the shape of the curves with the oil film thickness. Although the linear portion of the thermograms shown in Figs. 4(e) and (f) appears to extend to longer time intervals than in the thermograms corresponding to thinner films, the curves corresponding to the same thickness such as Fig. 4(c) present stronger shape variations than curves corresponding to different oil thicknesses.

- The effect of convection in the oil-water samples appears to be of overwhelming importance at these peak temperature levels. Indeed, an actual decrease of the surface temperature during irradiation as observed in Figs. 4(c) or 4(e) can only be explained by convection effects.

Convection was a major source of perturbation of the thermal propagation flow. In certain cases, see Fig. 6, clearly visible liquid flow in the heated oil area produced cyclic fluctuations in the detected signal. The frequency of such pulsations was observed to be relatively constant for a given film thickness, as Fig. 6 shows for two subsequent tests on the same sample. One could explore the possibility to relate such convective phenomena to the oil thickness. However, because of the complexity involved in modelling such flows and of their probable dependence on a variety of hardly predictable parameters such as oil viscosity and surface tension, ambient temperature, power density and beam diameter of the laser, ocean surface turbulence and topography, etc. we chose to orient our priorities toward the spectroscopic approach which is described in the next section.

3. THERMALLY-STIMULATED SPECTROSCOPY APPROACH

3.0 Preliminary considerations

We have seen in the previous section that most of the practical implementation problems encountered with the thermal propagation approach are related to the slow propagation of the thermal front within the oil and water materials, requiring an

observation time of tens of seconds for oil film thicknesses z_1 of the order of 1 mm, the observation time increasing as z^2. During such relatively long periods, thermal losses and the inception of convective flow introduce considerable signal perturbations, not to mention the difficulty for a helicopter to stand still over the ocean surface during the measurement time.

After consultation with Canpolar, we have thus decided to explore an additional approach, based on spectroscopy, which is not dependent on the slow thermal diffusion rate in the material and thus requires much shorter observation times.

The infrared transmission spectra of oil and water (see Figs. 7 and 8) present characteristic absorption bands. Straightforward diffuse-reflectance spectroscopy methods (Ref. 7, Chapt. 8, see in particular Fig. 8-4) would be inappropriate to this application in our opinion: the amount of backscattered light from oil or water impurities is exceedingly small while the specular reflection at the oil-water interface would be overshadowed by the air-oil reflection. Fluorescence techniques have already been considered and are mainly sensitive in the micrometer range of oil film thickness (Ref. 8, Section 10.2.2).

3.1 Description of the method

The approach we have taken into consideration is a modification of the transient infrared emission spectroscopy (TIRES) method which has recently been proposed (Ref. 9) for the analysis of surface properties. In the TIRES method, a laser pulse heats the surface of the sample and the emission spectrum from this surface is quickly recorded. The advantage of this approach vs. conventional emission spectroscopy is that only a shallow depth Δz of the material, corresponding to the thermal propagation depth during the observation time, is effectively probed: self-absorption problems are thus avoided and the obtained spectrum is analogous to a transmittance spectrum through a free-standing film of thickness Δz.

3.1.1 Qualitative description

Our method is also based on laser heating and emission spectroscopy, but the effect of the finite oil layer thickness is now taken into consideration. One possible implementation is shown in Fig. 9. The oil layer on water is heated by laser radiation.

us suppose that the laser penetration depth in oil is much larger than the oil film ness, and that water is transparent to the laser wavelength. The oil layer will thus olume heated almost uniformly, while water remains cool.

The oil layer temperature is probed by two infrared detectors, an InSb sensitive he 4 to 5.5 μm spectral region, and a HgCdTe sensitive in the 8 to 14 μm region. m Fig. 7 we estimate the infrared penetration depth to be of the order of 1 mm (k' = mm^{-1}) for the first detector and of 0.2 mm (k" = 5 mm^{-1}) for the second one.

If the oil film is relatively thick, say thicker than 1 mm, both detectors will probe e same average temperature through the film. If, on the other hand, the film is thin, y 0.2 mm, the HgCdTe will see the same temperature while the InSb, which is obing the average temperature of the oil film and of the portion of cold water within s penetration depth, sees a lower temperature. The ratio of the two detector outputs can thus be used to estimate the oil film thickness.

This method is much faster than the previously investigated thermal wave approach: if we can have enough laser energy within a 1 ms pulse, the measurement can be performed within such a short period, before conduction or convection within the liquid may perturb the data. This approach is different from photothermal spectroscopy (see, e.g., Ref. 11) where a wide-band light source is spectrally scanned and a single infrared temperature sensor is used: such an approach would be inadequate because of the relatively low power of incoherent wide-band light sources, while no powerful laser sources exist in the 3 to 5.5 μm region.

3.1.2 Analytical model

Let us consider an oil film of thickness z_1 on laser-transparent water, with absorption coefficients k, k' and k" and scattering coefficients k_s, k'_s and $k"_s$ respectively at the laser wavelength and over the spectrally sensitive bands of the detectors 1 and 2. The radiation due to laser heating emitted by an oil layer of thickness dz situated at a depth z below the surface (see Fig. 9) and detected by detector 1, with similar expressions for detector 2, can be expressed as:

$$\phi' = C \int_0^{z_1} a \varepsilon \tau \, dz \qquad (4)$$

where C is a constant for the two detectors,

$$a = k \exp(-k - k_s)\, z \tag{5}$$

is the laser absorbance factor (which is proportional to the absorption rate k within dz and to the exponentially-decaying laser power at z),

$$\varepsilon = k' \tag{6}$$

is the emittance of the layer within the spectral band of detector 1, and

$$\tau = \exp(-k' - k_s') \tag{7}$$

is the attenuation of the emitted radiation through the oil.

After integration, the ratio between the radiation detected by the two detectors 1 and 2 becomes, in the absence of scattering and assuming that the temperature elevations are sufficiently small (less than 10°C) to avoid uncompensated nonlinearities for the two detectors:

$$\frac{\phi''}{\phi'} = \frac{k''}{k'} \cdot \frac{k + k'}{k + k''} \left\{ \frac{1 - \exp[-z_1 (k + k'')]}{1 - \exp[-z_1 (k + k')]} \right\} \tag{8}$$

Plots of this ratio vs. the product kz_1 for different detector absorption ratios k"/k' are shown in Fig. 10(a) to (c), respectively for the three cases k'/k = 1, 0.1 and 10. If the values of the three absorption coefficients k, k' and k" are known, a measurement of the signal ratio can thus provide an evaluation of kz_1, and thus of z_1.

3.2 Experimental investigation

3.2.1 Sample characterization

Two oil samples submitted to us by Canpolar were characterized on our FTIR spectrometer. The transmittance spectrum for two oil samples of 200 μm thickness are shown in Figs. 11(a) and (b), respectively for a relatively light oil (type 'A') and for a heavier oil (type 'B'). Apart from the change in the horizontal scale, these spectra are

similar to the ones shown in Fig. 7(b) over the 3 to 17 μm range. From these spectra, we can estimate the oil absorptivity ratio in the 4 to 5.5 μm and in the 8 to 14 μm areas to be of the order of:

$$k''/k' \approx 5 \tag{9}$$

for both kinds of oil.

Below 3 μm, however, the attenuation is quite different for the two oil samples. Apart from the additional band around 2.9 μm, fig. 11(b) shows a depression of the spectral transmittance baseline, which is characteristic of wavelength-dependent attenuation losses due to scattering from local inhomogeneities of size smaller than the light wavelength within the sample (see Ref. 12, Fig. 9). The attenuation is correspondingly different at the 1.064 μm YAG laser wavelength: a direct measurement in transmission through a YAG-irradiated oil sample gave the following estimations:

$$k_A \approx 2\ mm^{-1}\ ; \qquad k_B \approx 10\ mm^{-1} \tag{10}$$

respectively for oil samples A and B (Note: the attenuation coefficients given in Eq. (10) were measured with a detector angular aperture of 0.1 rad and thus include a strong scattering component which is slightly overevaluated with respect to the hemispheric scattering coefficient k_S in Eq. (5)).

From Eq. (10) and the spectra of Fig. 11 one can estimate the ratios:

$$k'/k_A \approx 0.4\ ; \qquad k'/k_B \approx 0.1 \tag{11}$$

respectively for the two samples. We can now refer back to the theoretical curves shown in Figs. 10(a) and (b): for $k''/k' = 5$ (Eq. 9) and from Eqs. (10) and (11), we obtain the following nearly linear theoretical ranges for the signal ratio of the two detectors:

Table 1:
Theoretical oil film thickness range with thermally-stimulated spectroscopy.

SAMPLE TYPE	LOWER LIMIT		UPPER LIMIT	
	ϕ''/ϕ' value	film thickness z_1	ϕ''/ϕ' value	film thickness z_1
A	0.9	50 μm	0.5	1 mm
B	0.96	20 μm	0.78	200 μm

Out of these ranges, the expected variations of the ϕ''/ϕ' value with the film thickness become vanishingly small. We can thus conclude that because of the relatively high attenuation at the YAG wavelength, heavy oil films can be evaluated only up to a few hundred micrometers of thickness.

3.2.2 Experimental setup

A few compromises had to be made owing to the unavailability of a few equipment components at the present time. Pulsed YAG lasers being not available to us when the experiments were made, we opted for the 18W continuous laser used in the previous part of this investigation. As to the detectors, although both an InSb and a HgCdTe detector were available, their unfiltered spectral response extended, respectively, from 2 to 5.5 μm and from approximately 4 to 14 μm. Tests were made with such detectors using a configuration of the kind shown in Fig. 9, but the results were partially inconsistent due, we believe, to the excessively wide spectral bands of these detectors.

We thus opted for a small grating monochromator, see Fig. 12, which could unfortunately operate only in the 1 to 6 μm range, hoping to find some correlation with the spectral absorbance distribution of oil for thin films. To evaluate the thickness of thin films of poor uniformity, we used a near-visible fiber optic illuminator and a Si detector (spectral range 0.5 to 1 μm) to measure the near-visible transmittance of the

film in the probed position: typical transmittances for the oil type 'A' used in our tests were of the order of 30% for a 200 μm-thick film and 2% for a 1 mm film. Because of the small throughput of the spectrometer, we had to integrate the signal over typically 12 seconds, during which conduction and convection effects are expected to play a significant role in the liquid.

3.2.3 Experimental results

A series of spectra obtained with the setup shown in Fig. 12 is shown in Fig. 13. The curves correspond to oil films with different near-visible transmittances (see above), i.e. of different thickness, from a transmittance of 0% (very thick oil film) to 100% (pure water). The horizontal scale, in seconds, corresponds to the grating scanning time: the corresponding wavelength values are shown on the top of the graph. The strong 4.3 μm negative peak is a spectrometer artifact. The lack of signal in the 1.4 to 3.3 μm area is mainly due to the low blackbody radiation at low wavelengths.

The following observations can be made from the data of Fig. 13:

- The average radiated intensity is an increasing function of the oil thickness for thin films: we can easily distinguish between pure water (100% transmittance) and oil film of nearly 100 μm (60%), 250 μm (23%) etc. in thickness, on the basis of the average spectral intensity alone.

- For thicker films, near 2% transmittance, there appears to be an inversion of this tendency, the intensity decreasing from the 2% to the 0% transmittance films.

- In certain cases, in particular for the 2% transmittance or nearly 1 mm-thick films, the spectral radiation in the 3.3 to 4 μm region appears to be enhanced.

3.3 Discussion

The interpretation of the results shown in Fig. 13 is complicated by a number of factors, of which many are more related to the limitations of our experimental apparatus than to the theoretical expectations.

3.3.1 Conduction and convection effects

Because we had to integrate through more than 10 seconds, conductive thermal propagation takes place between the heated oil and the water, which can no longer be considered cold. The thermal propagation depth within water during 10 s can be estimated at nearly 1 mm, resulting in heat removal from thin films and possibly in convective flow.

3.3.2 Emitted radiation from water

The boundary water layer which is heated by conduction is a good emitter of radiation: fig. 8 shows that the infrared penetration depth in water in the 2.5 to 6 μm spectral region is of the order of or smaller than 25 μm: the emittance of a 1 mm-thick heated water layer is thus close to unity. In the 4 to 6 μm window (see Fig. 11a) the water-emitted radiation is well transmitted by the oil layer.

3.3.3 Qualitative interpretation of the results

The experimental results of Fig. 13 may tentatively be interpreted as follows. The radiation in the 3 to 6 μm area (limited by the low blackbody emittance at near-ambient temperature on the low side and by the spectrometer response on the high side) is due to both the emittance of the laser-heated oil and of the conduction-heated water for thin films.

As the film thickness increases (from 0% to 23% transmittance) the equilibrium temperature of the oil film increases because the stored heat increases while the conduction losses are nearly constant. The average radiated intensity increases correspondingly.

As the film thickness exceeds 1 mm, the oil layer acts as a thermal barrier for the water which stays cool. The emittance of the heated layer of oil is smaller than unity if the scattering-limited penetration depth for the YAG laser is shorter than the infrared penetration depth in the 4 to 6 μm area. The lower radiation level of the pure oil (0% transmittance) sample may thus be interpreted as due to the lower emittance of oil as compared to water.

In the 3 to 4 μm region we have an absorption band for oil (see Fig. 11a). This absorption stops the water-emitted radiation for thin films, depressing the relative emittance in this region (see Figs. 14(a) and (b) showing the normalized spectra for 64% and 23% transmittance). For thicker films (see Figs. 14(c) to (e)) the higher emittance of oil between 3 and 4 μm shows up well against the lower oil emittance in the 4 to 6 μm area.

3.3.4 A possible alternative

The considerations above concerning the emittance of water suggest a possible variant, see Fig. 15. If one can, as suggested by Fig. 14.2 of a previous Canpolar proposal, heat the water surface through the oil by a microwave pulse, the spectral distribution of the detected infrared radiation will be similar to a transmittance spectrum through a free-standing oil film. By using the 4 to 5.5 μm and the 8 to 14 μm spectral bands to evaluate the oil thickness we would then have the advantages of:

- a wider thickness range, from nearly 20 μm to 2 mm, because the strong scattering at the YAG wavelength is avoided, and
- a better reliability because the different types of oil appear to have similar attenuation ratios in these bands, see Eq. (9).

The viability of such an approach is, however, strongly conditional to the availability of sufficiently powerful microwave pulses as well as to the validity of our assumptions concerning the absorbance properties of water and oil in the microwave region, a technology in which we are not specialists.

3.4 Conclusion and suggestions

An optothermal approach has been taken into consideration for a possible application to oil film thickness monitoring in case of oil spills. Two optothermal methods, thermal propagation and thermally stimulated spectroscopy, have been theoretically and experimentally analyzed.

The first technique is based on the observation of the thermal propagation of a laser-generated heat pulse through the oil-water medium. Although theoretically

feasible, due to the different thermal properties of oil and water, such an approach revealed to be strongly perturbed by thermal losses, finite optical penetration effects and convective flow in the liquid, even in a quiet laboratory environment. Most of the problems arise because of the relatively long observation time, several tens of seconds for film thicknesses of 1 mm, which is required to follow the diffusion of the thermal wave through the oil film and into the water. Because of these problems, we do not advise to pursue this line of investigations at the present time.

The second technique, thermally stimulated spectroscopy, is based on the spectral emittance properties of the laser-heated oil layer. A model indicates that, if a YAG laser is used for the thermal excitation, the range of oil thicknesses which may be probed with this method are of the order of 50 μm to 1 mm in the case of light oils and of 20 μm to 200 μm for heavier, YAG light scattering oils. A wider range, up to 2 mm, could be obtained if a radiation which is exempt from scattering in the oil, such as microwave radiation, could be used for the thermal excitation. This approach thus appears to be useful at least as a complement of the laser fluorescence (0 to 20 μm) and of the microwave (1 to 4 mm thickness) techniques.

An experimental investigation of the thermal spectroscopic approach could be performed only partially due to the unavailability of proper equipment, such as suitably filtered detectors and a pulsed laser. A test performed with a monochromator to cover a reduced portion of the spectrum of interest confirmed the expected reduction of emittance in the 4 to 6 μm spectral region due to the translucency of oil both in this spectral region and at the YAG wavelength. Other effects which are due, in our opinion, to emittance from water conduction-heated through contact with the oil film resulted in a better understanding of the complex optical and thermal interactions in the oil-water medium.

Although quite preliminary, the results obtained with the thermal spectroscopy approach are sufficiently encouraging to suggest further investigations in the following directions:

1. Suitable filters should be designed to limit the response of the InSb and of the HgCdTe to the appropriate spectral bands. A filter responsive to the 3.3 to 3.5 μm region could also be used to evaluate film thicknesses in the 0 to 20 μm range.

2. Pulsed (~ 1 ms) laser irradiation should be tested in order to overcome both problems of convection effects and of fast airborne applicability of the spectral technique. Short-term (less than 1 s) time-resolved effects due to heat propagation from oil to water should nevertheless be investigated to see if the appearance of water spectral features could help in the data interpretation.

3. Laboratory tests should be carried out to fully characterize different oils at various temperatures and to better understand the relevant physical phenomena. For example, tests could be performed on oil films laying on a smooth, laser reflecting metal surface to obtain data which are less affected by film nonuniformities and liquid convection in order to help interpreting the oil-water tests.

4. Evaluate the signal-to-noise ratio obtainable on a remotely heated spot a few tens of meters away, to simulate the airborne operation. Although such a configuration would result in a decrease of the viewing aperture by nearly a factor of 10, and thus of the signal by a factor of 100, the detectivity levels reached by thermovision cameras indicate that the signal-to-noise ratio should still be adequate in this case.

5. Explore other sources of radiation, such as microwaves or far-IR lasers as alternative heating mechanisms.

REFERENCES

1. P. Cielo and S. Dallaire, "Optothermal NDE of thermal-barrier coatings", J. Mater. Eng. 9, 71 (1987).

2. H.S. Carslaw and J.C. Jaeger, "Conduction of Heat in Solids", Chapt. 10, Oxford University Press, 1959.

3. Y.S. Touloukian et al. "Thermophysical Properties of Matter" IFI/Plenum, 1970.

4. J.P. Boillot, P. Cielo et al., "Adaptive welding by fiber-optic thermographic sensing: an analysis of thermal and instrumental considerations" Welding Journ. 64, 209-s (1985).

5. P. Cielo, "Pulsed photothermal evaluation of layered materials" J. Appl. Phys. 56, 230 (1984).

6. D.L. Balageas, J.C. Krapez and P. Cielo, "Pulsed photothermal modelling of layered materials", J. Appl. Phys. 59, 348 (1986).

7. P. Cielo, "Optical techniques for Industrial Inspection", Academic Press, 1988.

8. R.M. Measures, "Laser Remote Sensing", Wiley-Interscience, 1984.

9. R.W. Jones and J.F. McClelland, "Transient infrared emission spectroscopy" Anal. Chem. 61, 650 (1989).

10. P. Cielo and K. Cole. "Laboratory investigation on the evaluation of crude oil concentration by spectroscopic methods", Report IGM 88-404-06, IMRI, May 30, 1986.

11. A. Mandelis, "FM time delay photoacoustic and photothermal wave spectroscopies" Rev. Sci. Instrum. 57, 617 (1986).

12. P. Cielo, K. Cole and B.D. Favis, in: "Instrumentation and Automation in the Paper, Rubber, Plastics and Polymerization Industries", A. Kaya and T.J. Williams Eds., p. 161. IFAC/Pergamon Press, 1986.

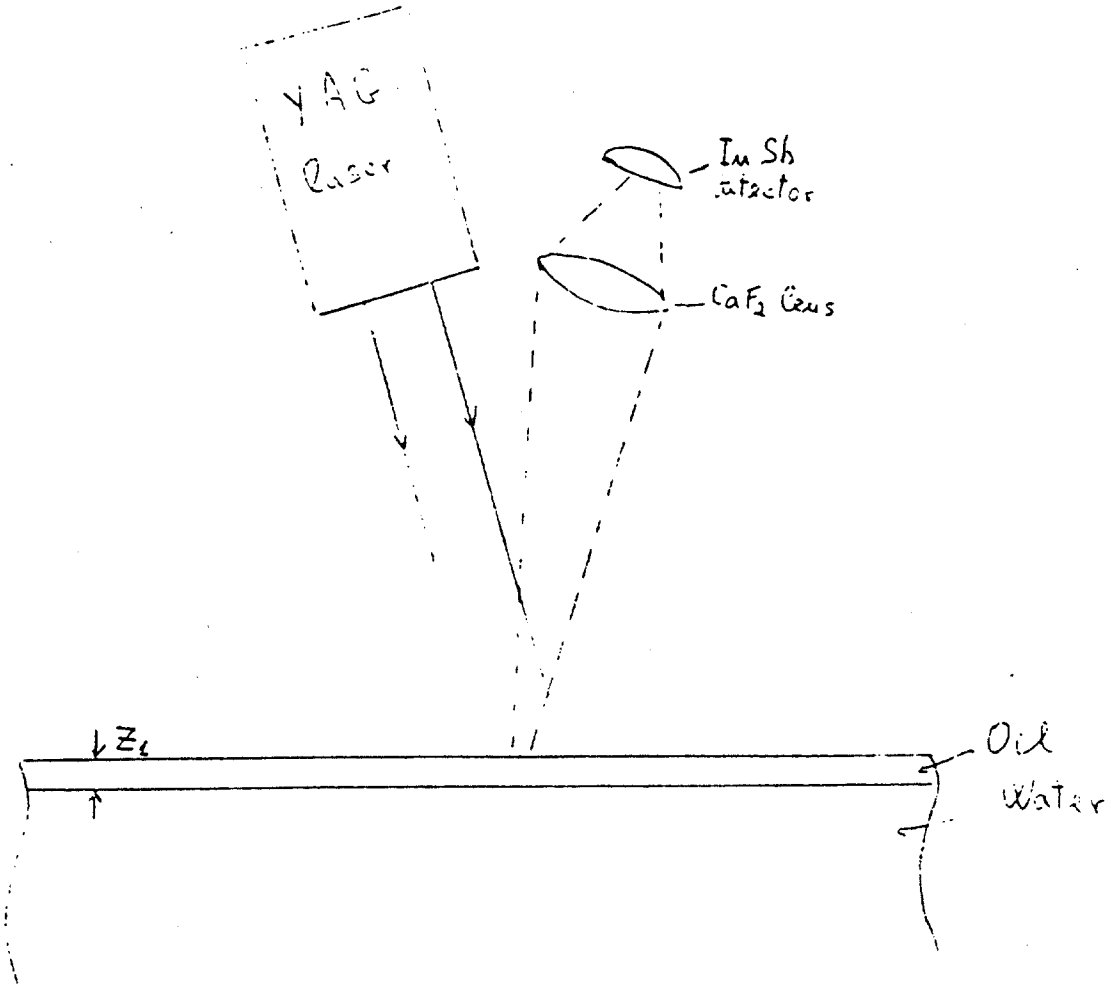

Fig. 1 Experimental setup for the thermal-wave tests.

Fig. 2

Temperature history for various effusivity ratios of the two layers

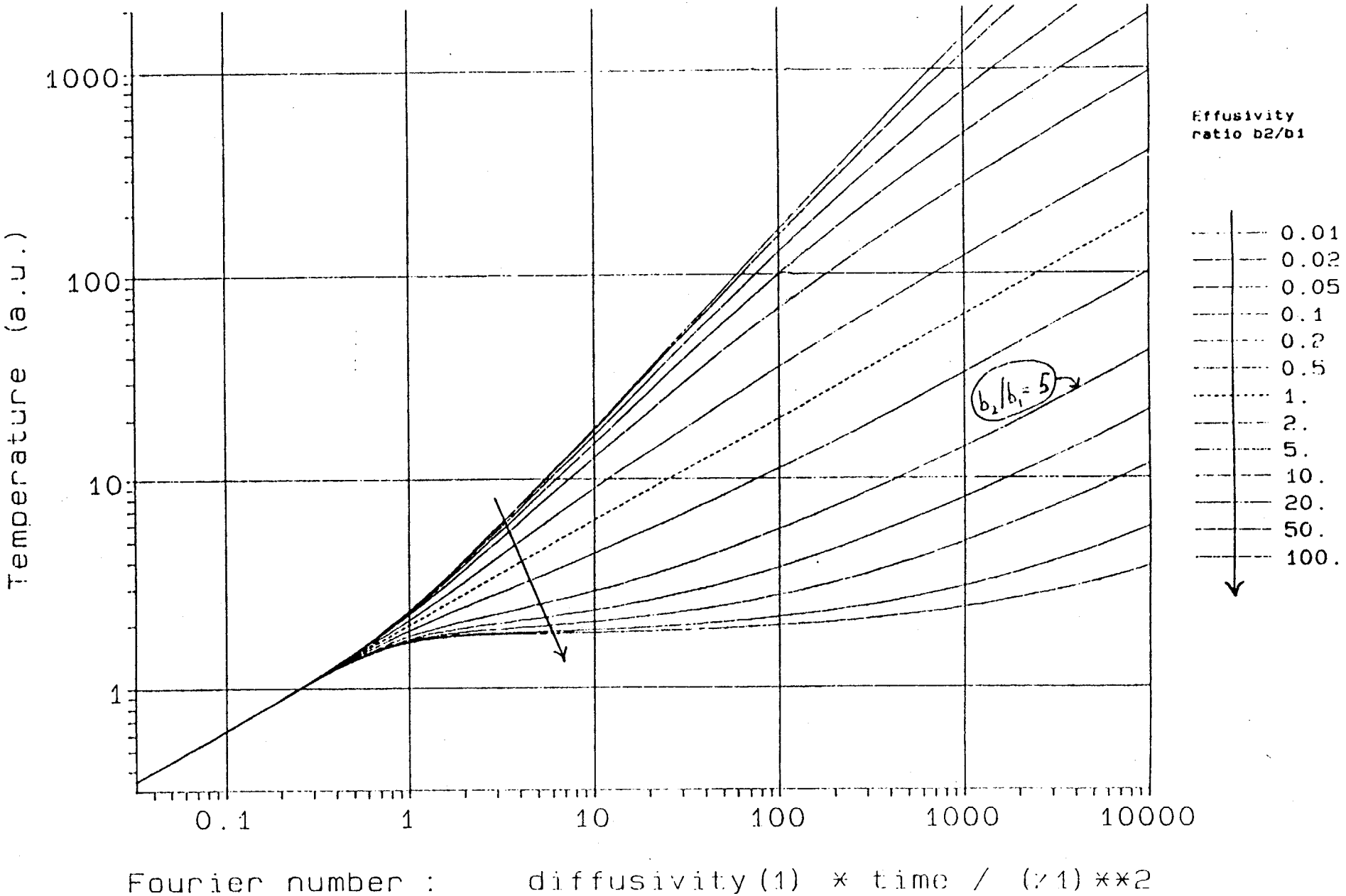

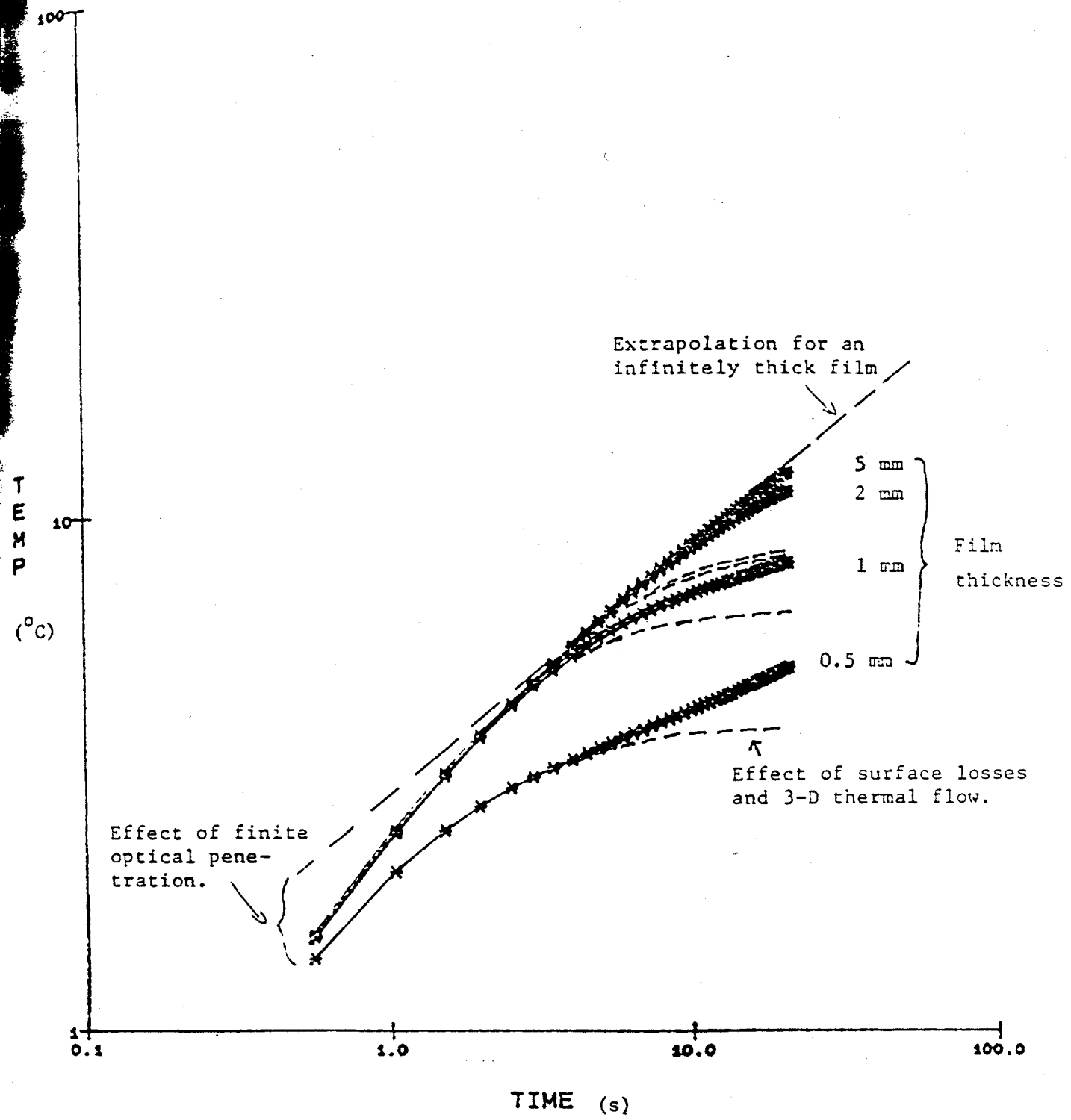

Figure 3: Finite-difference simulation of the surface temperature evolution of an oil film on water under step laser irradiation.

Temperature for a 320 microns estimated oil layer thickness

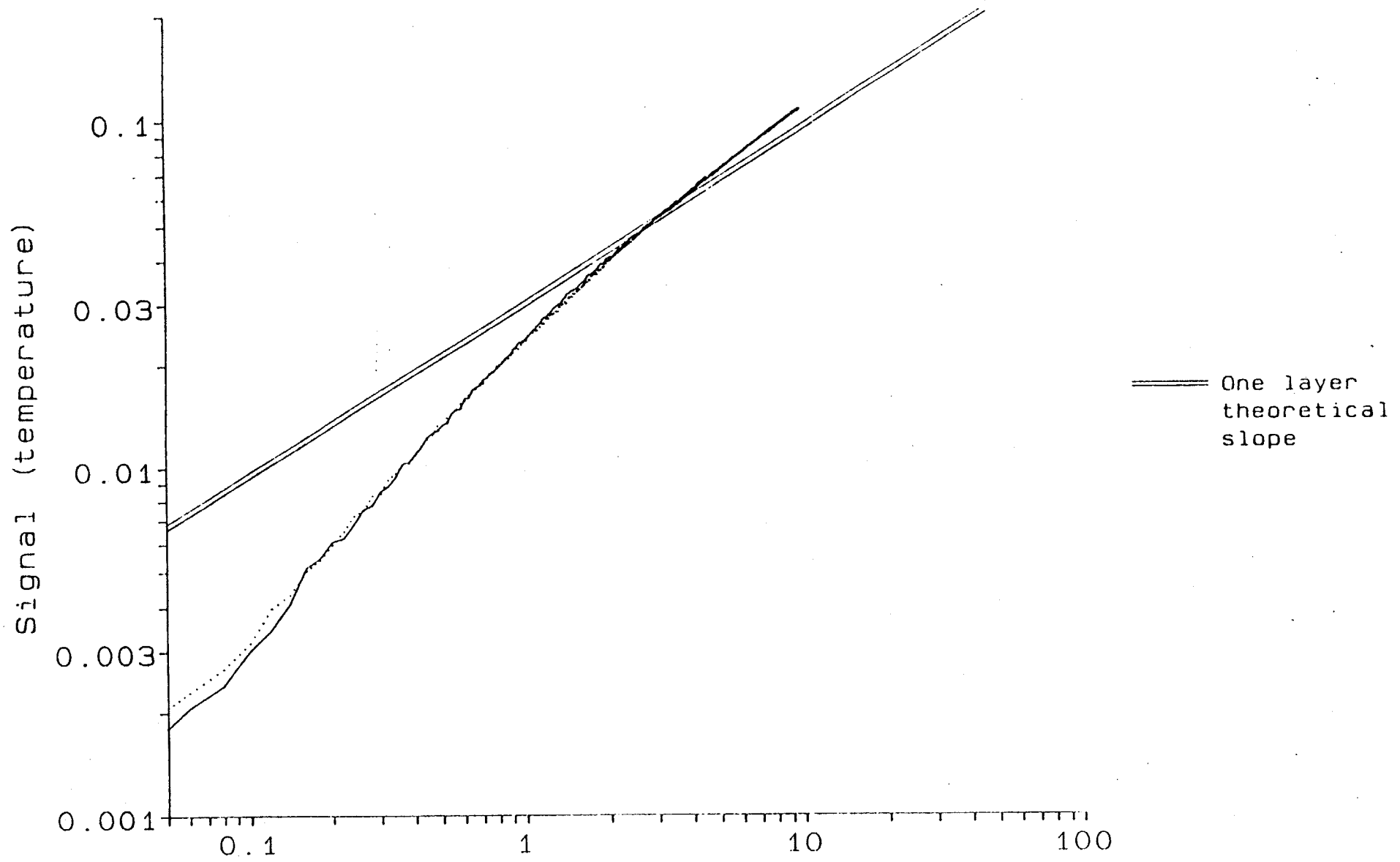

Fig 4(a) 320μm

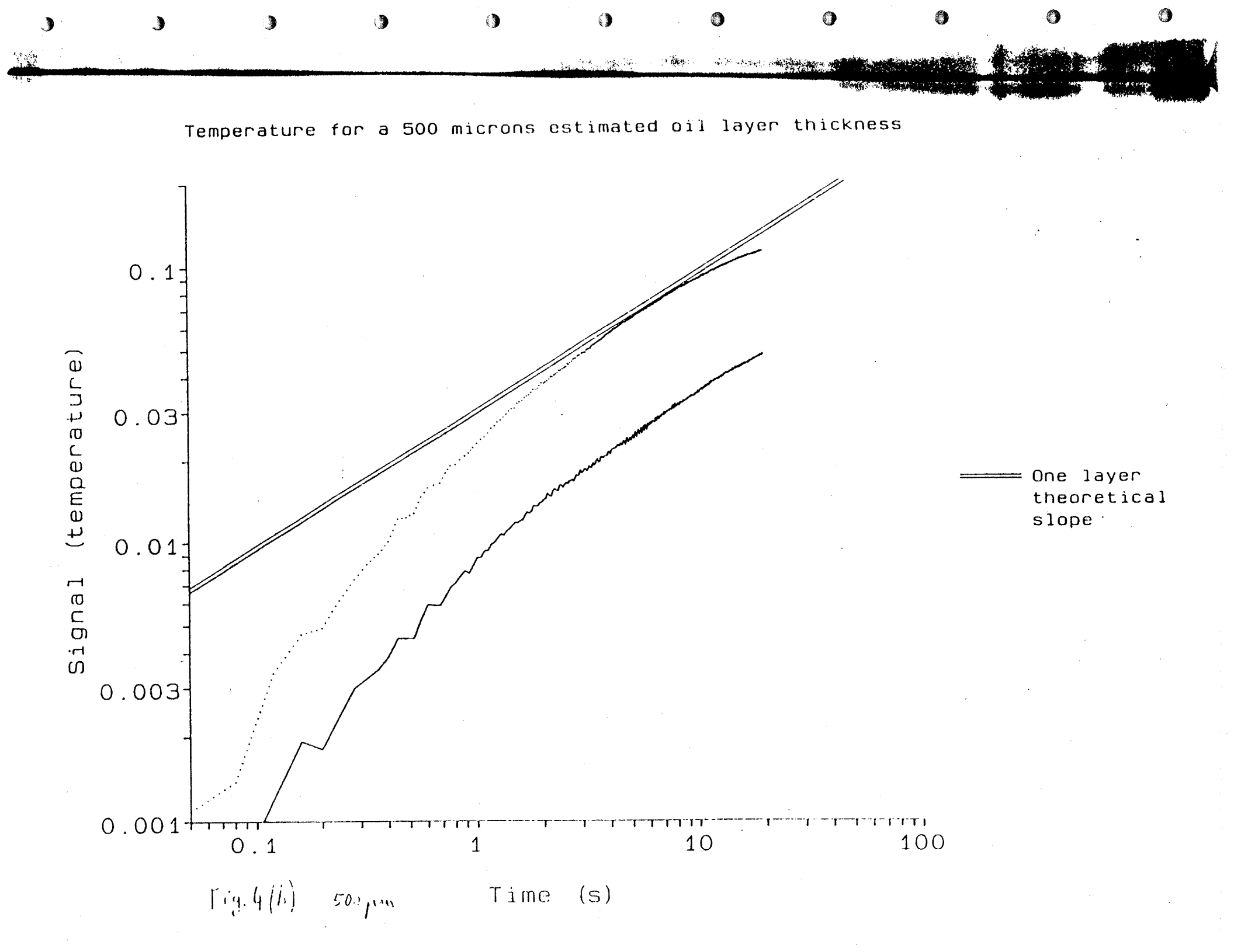
Temperature for a 500 microns estimated oil layer thickness
Signal (temperature)
0.1
0.03
0.01
0.003
0.001
0.1
1
10
100
Time (s)
One layer
theoretical
slope

Fig. 4 (b) 500 μm

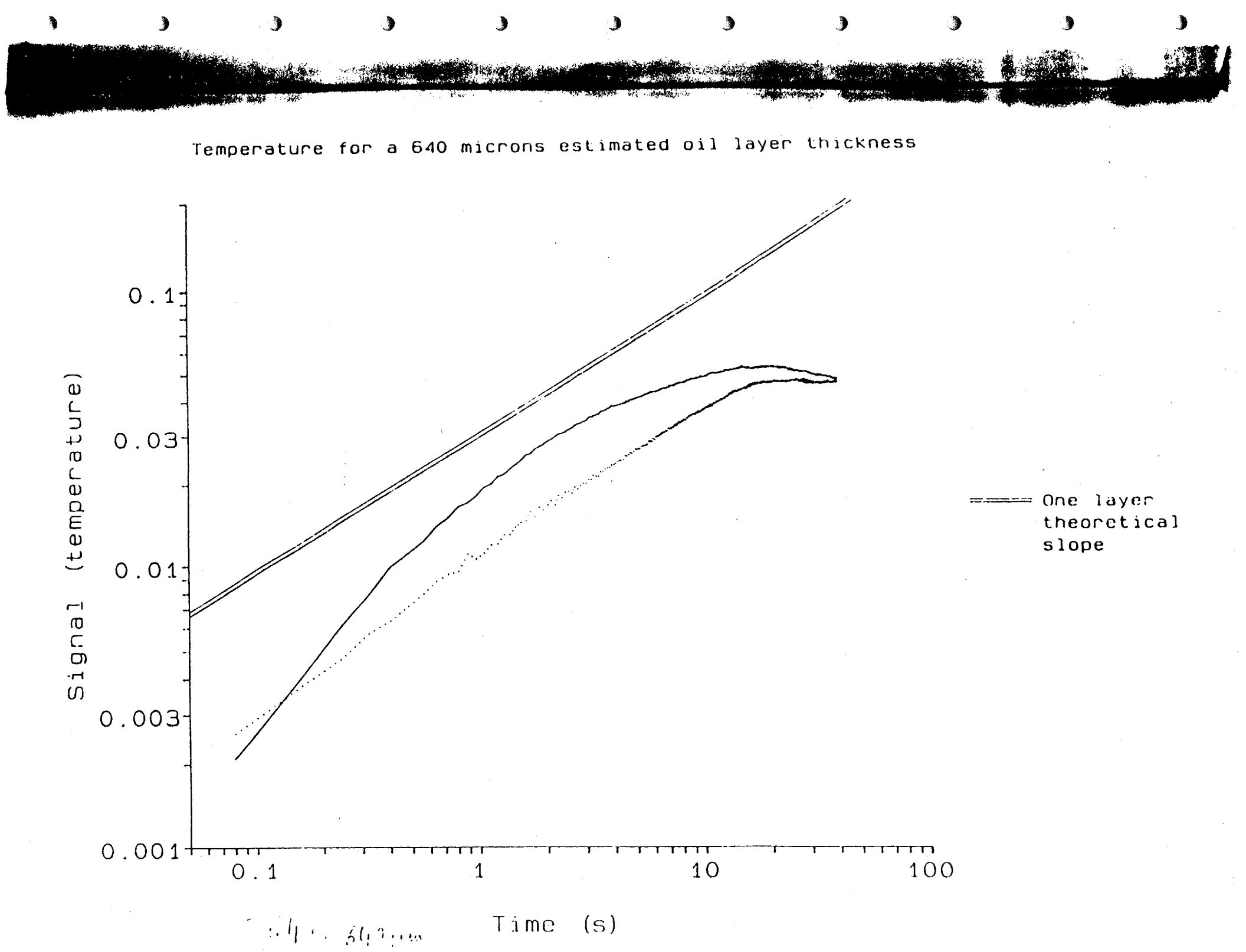
Temperature for a 640 microns estimated oil layer thickness
Signal (temperature)
0.1
0.03
0.01
0.003
0.001
0.1
1
10
100
Time (s)
One layer
theoretical
slope

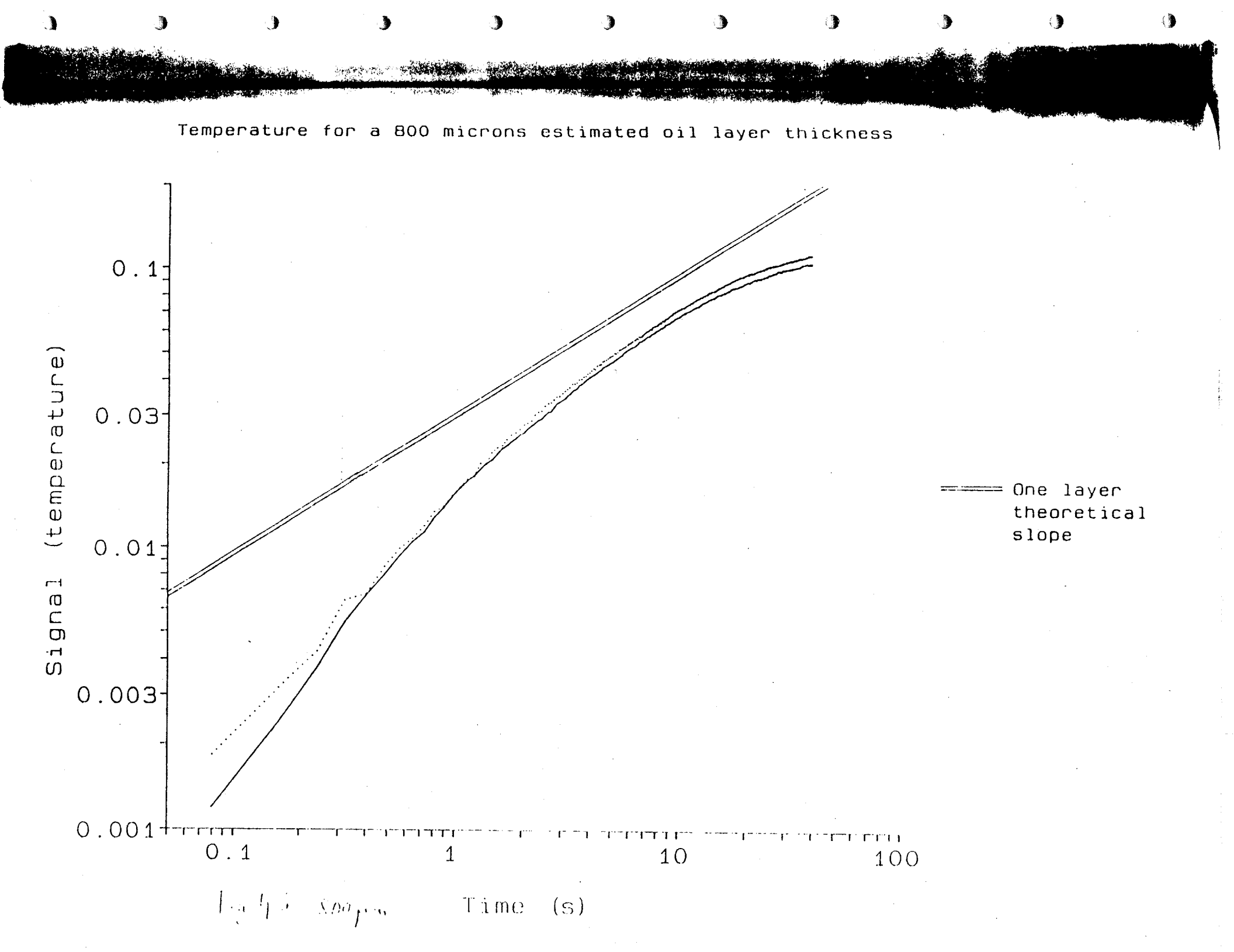
Temperature for a 800 microns estimated oil layer thickness
Signal (temperature)
0.1
0.03
0.01
0.003
0.001
0.1
1
10
100
Time (s)
One layer
theoretical
slope

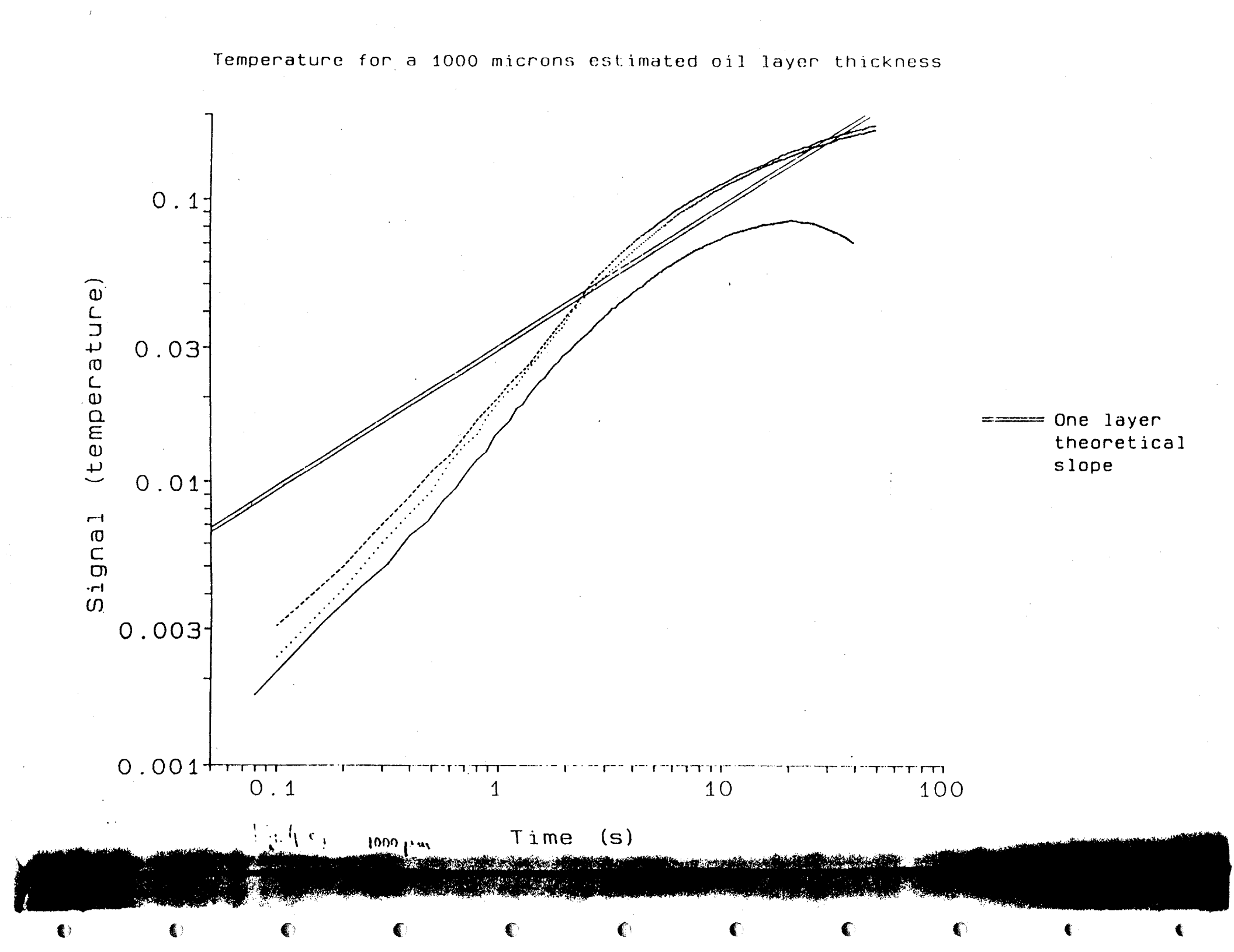
Temperature for a 1000 microns estimated oil layer thickness
Signal (temperature)
0.1
0.03
0.01
0.003
0.001
0.1
1
10
100
Time (s)
One layer
theoretical
slope

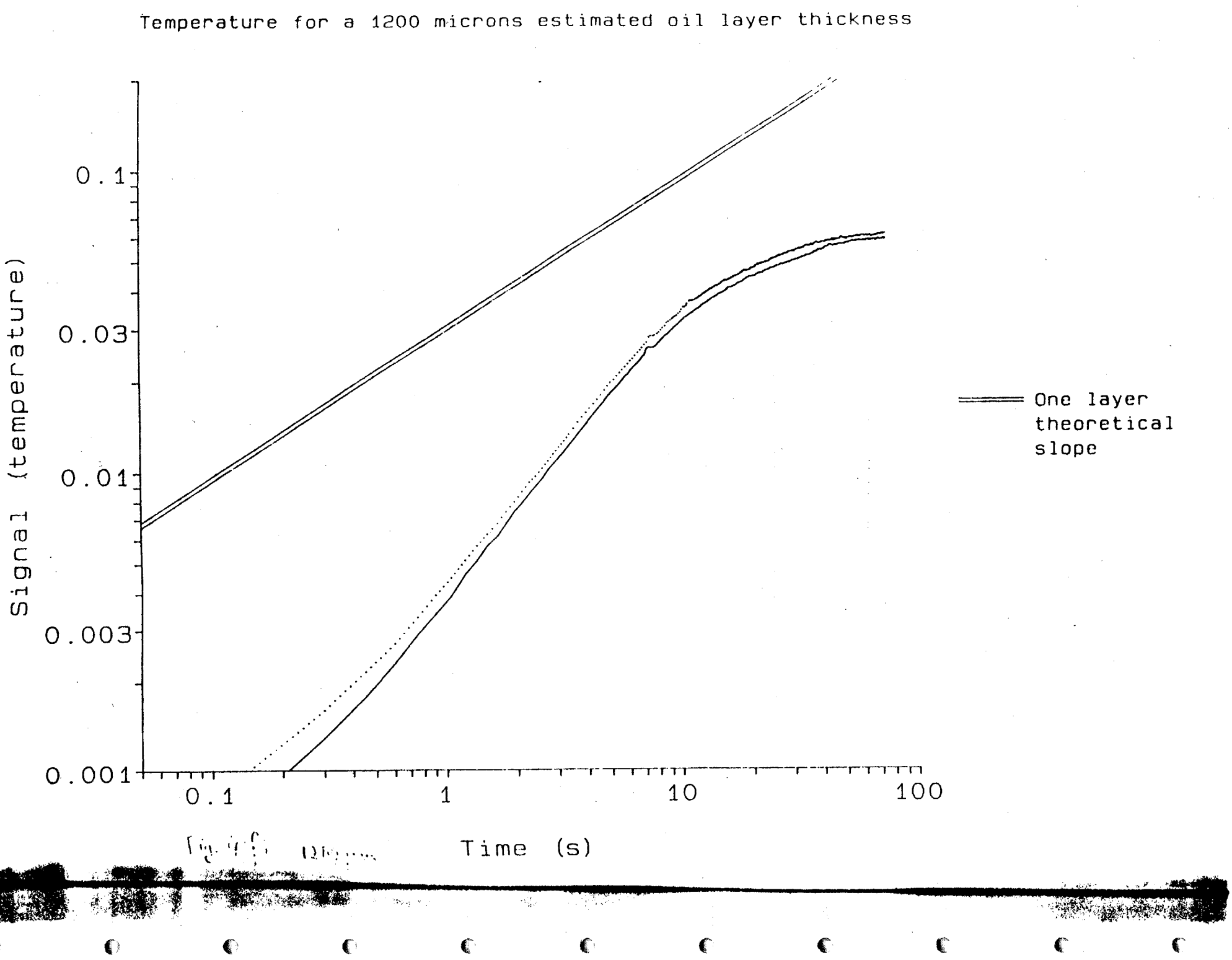
Temperature for a 1200 microns estimated oil layer thickness
Signal (temperature)
0.1
0.03
0.01
0.003
0.001
0.1
1
10
100
Time (s)
One layer
theoretical
slope

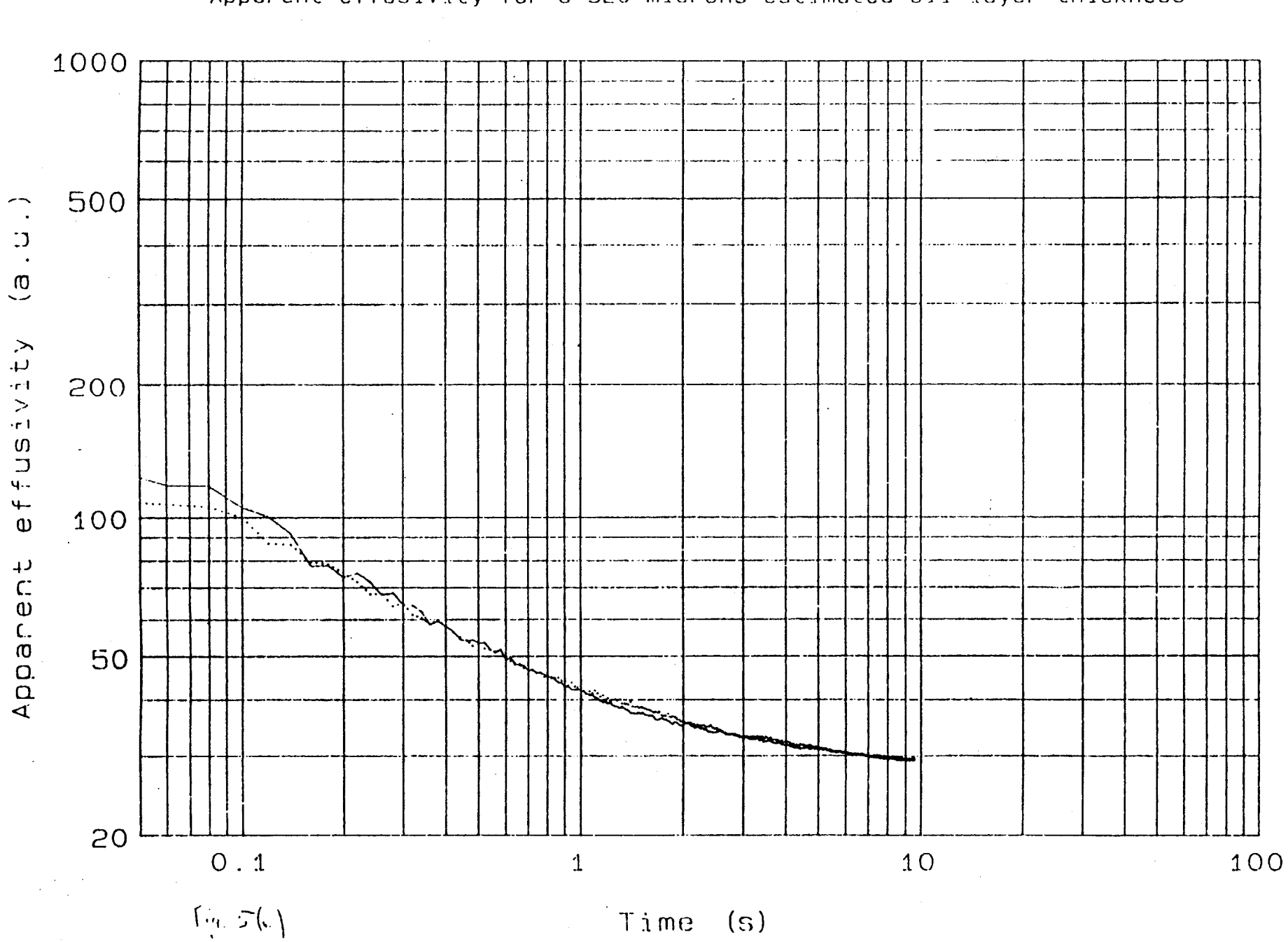
Apparent effusivity for a 320 microns estimated oil layer thickness
1000
500
200
100
50
20
Apparent effusivity (a.u.)
0.1
1
10
100
Time (s)

Fig 5(a)

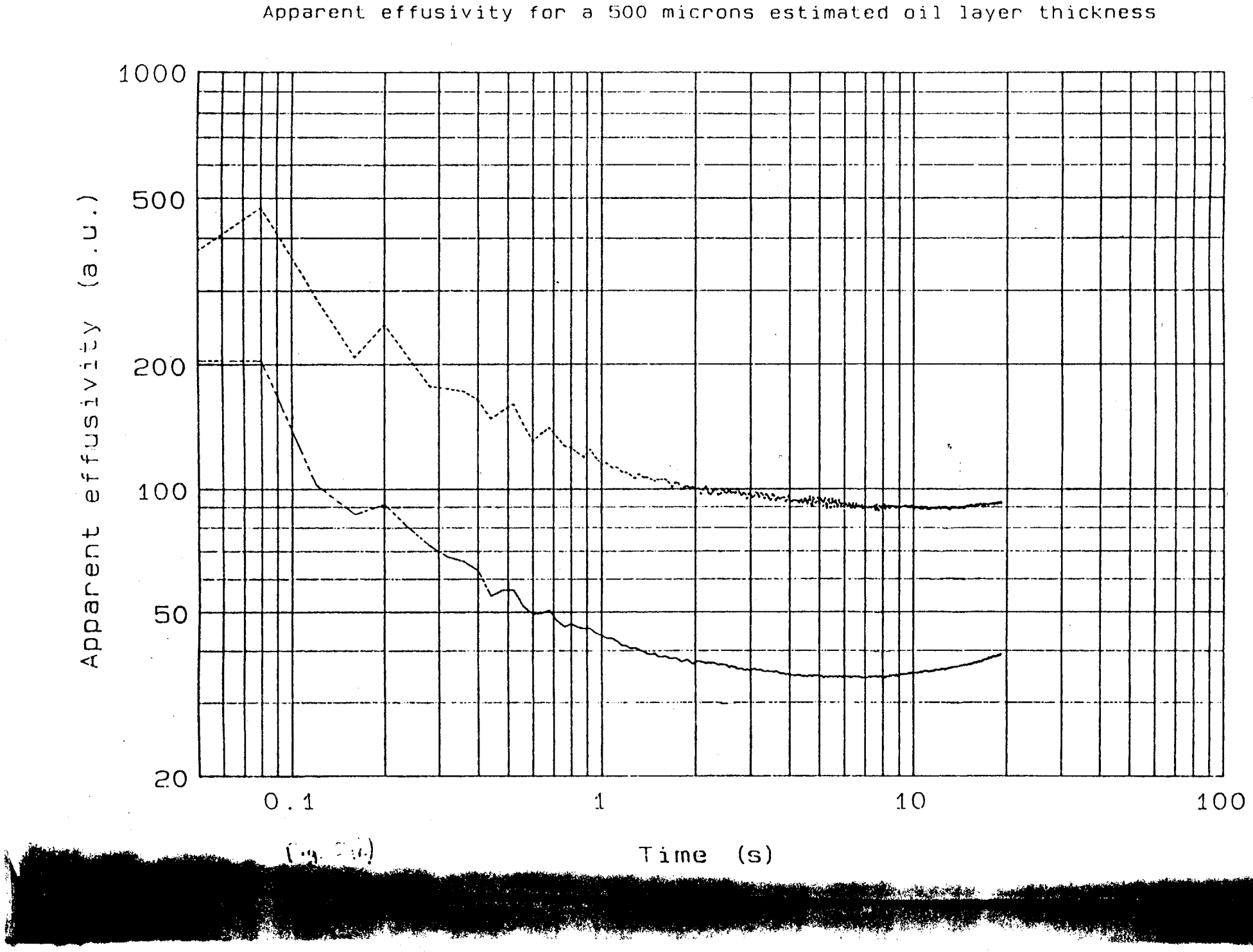
Apparent effusivity for a 500 microns estimated oil layer thickness
1000
500
200
100
50
20
Apparent effusivity (a.u.)
0.1
1
10
100
Time (s)

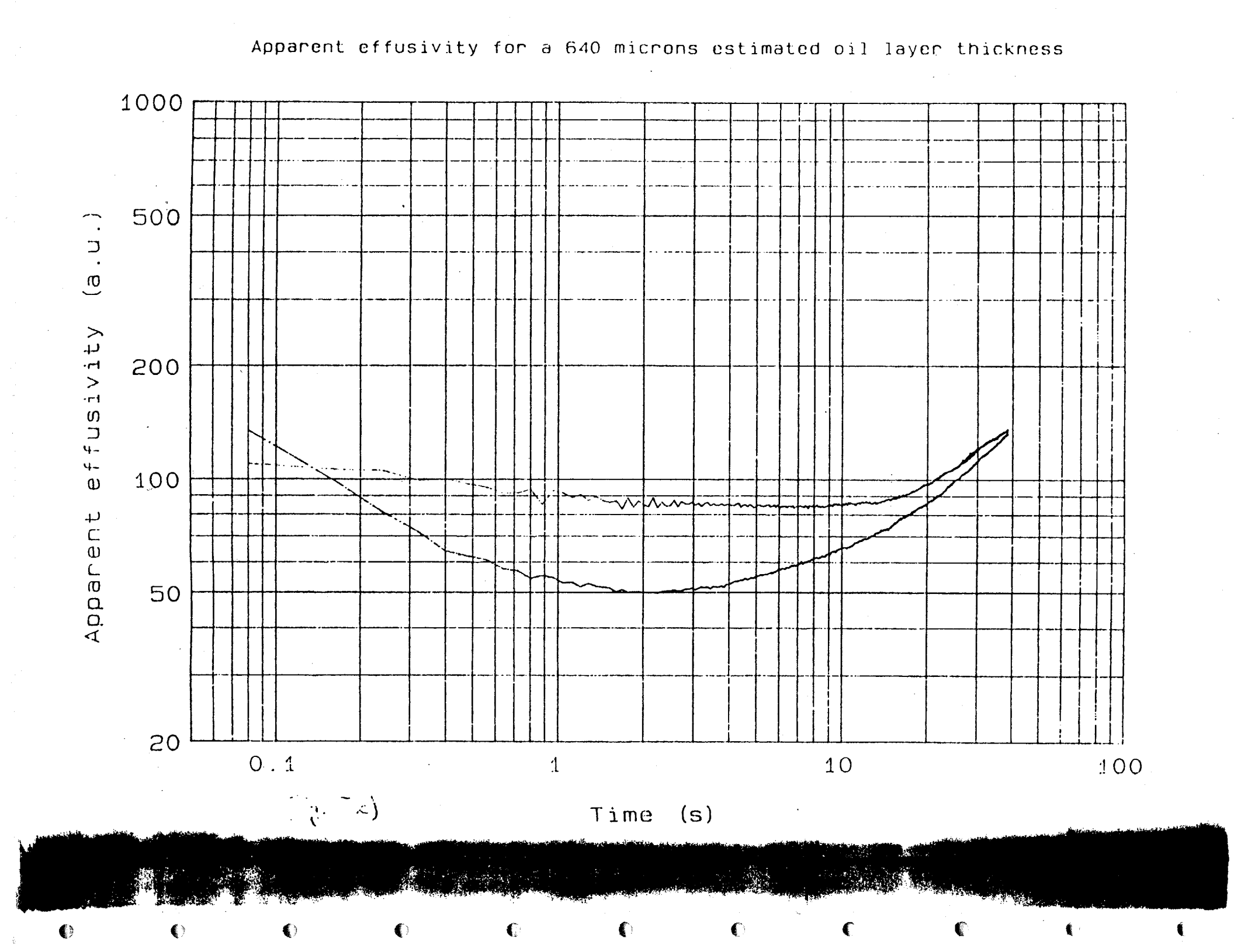
Apparent effusivity for a 640 microns estimated oil layer thickness
1000
500
200
100
50
20
Apparent effusivity (a.u.)
0.1
1
10
100
Time (s)

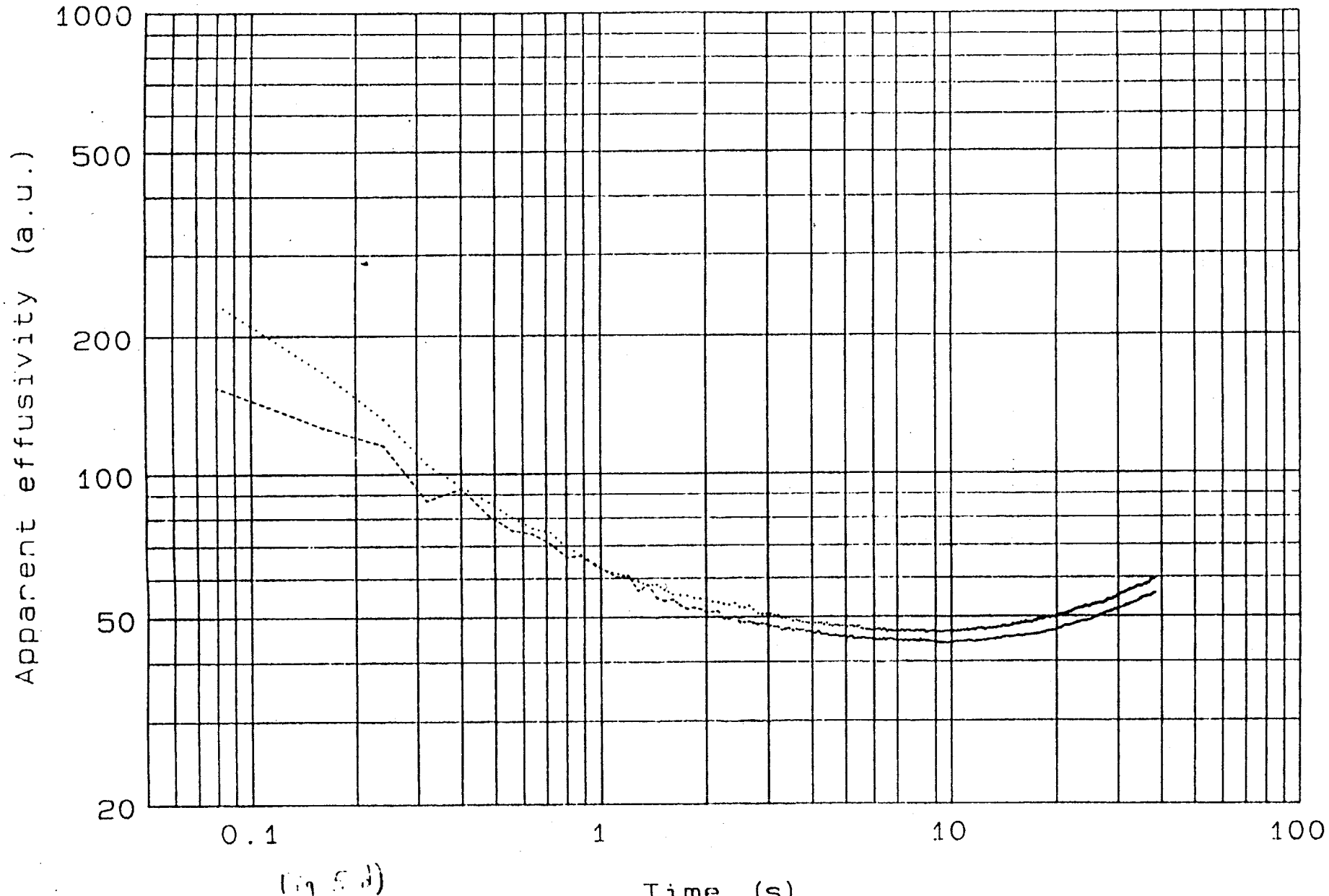
Apparent effusivity for a 800 microns estimated oil layer thickness
1000
500
200
100
50
20
Apparent effusivity (a.u.)
0.1
1
10
100
Time (s)

(Fig 5 d)

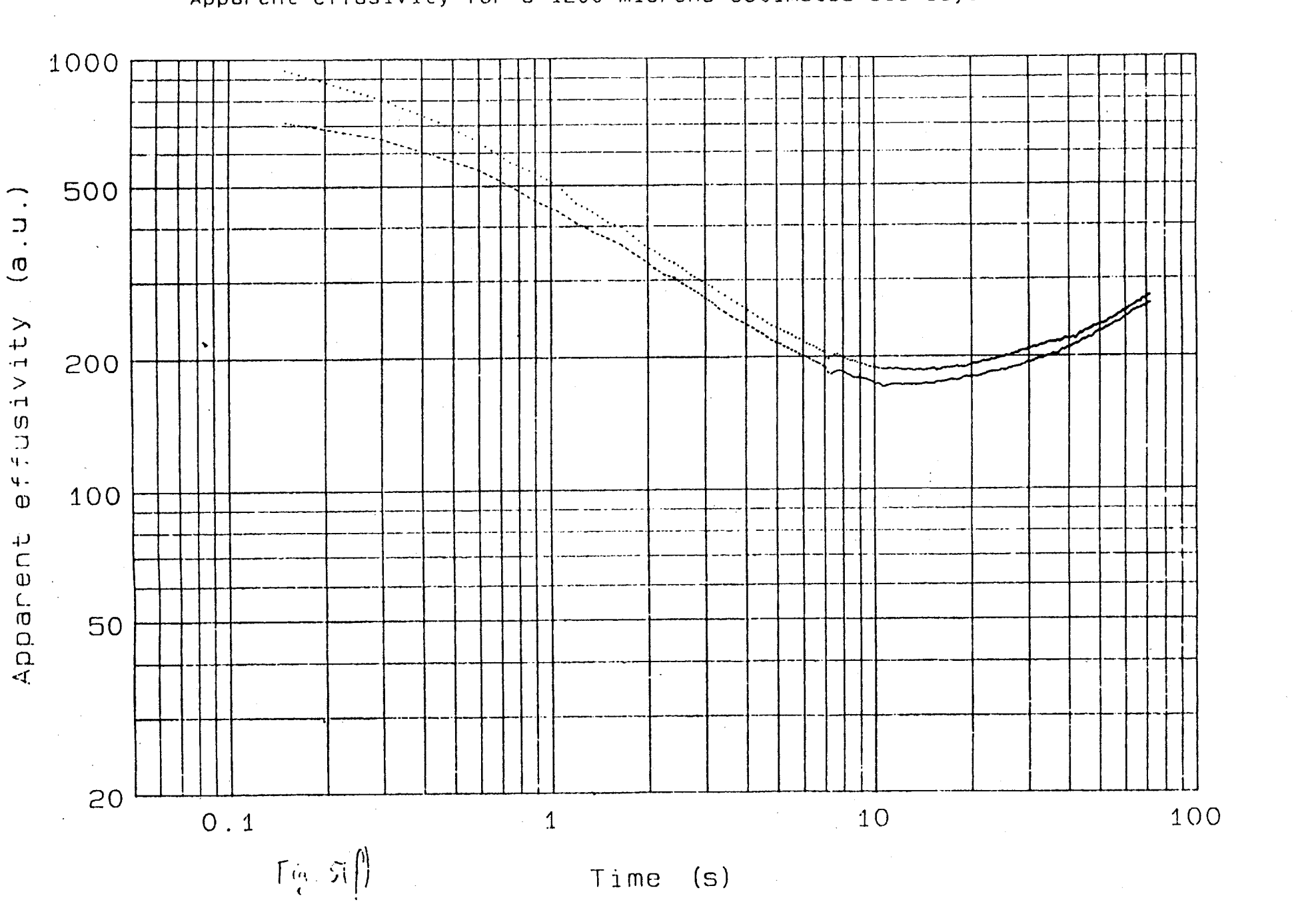
Apparent effusivity for a 1200 microns estimated oil layer thickness
1000
500
200
100
50
20
Apparent effusivity (a.u.)
0.1
1
10
100
Time (s)

Fig 5(f)

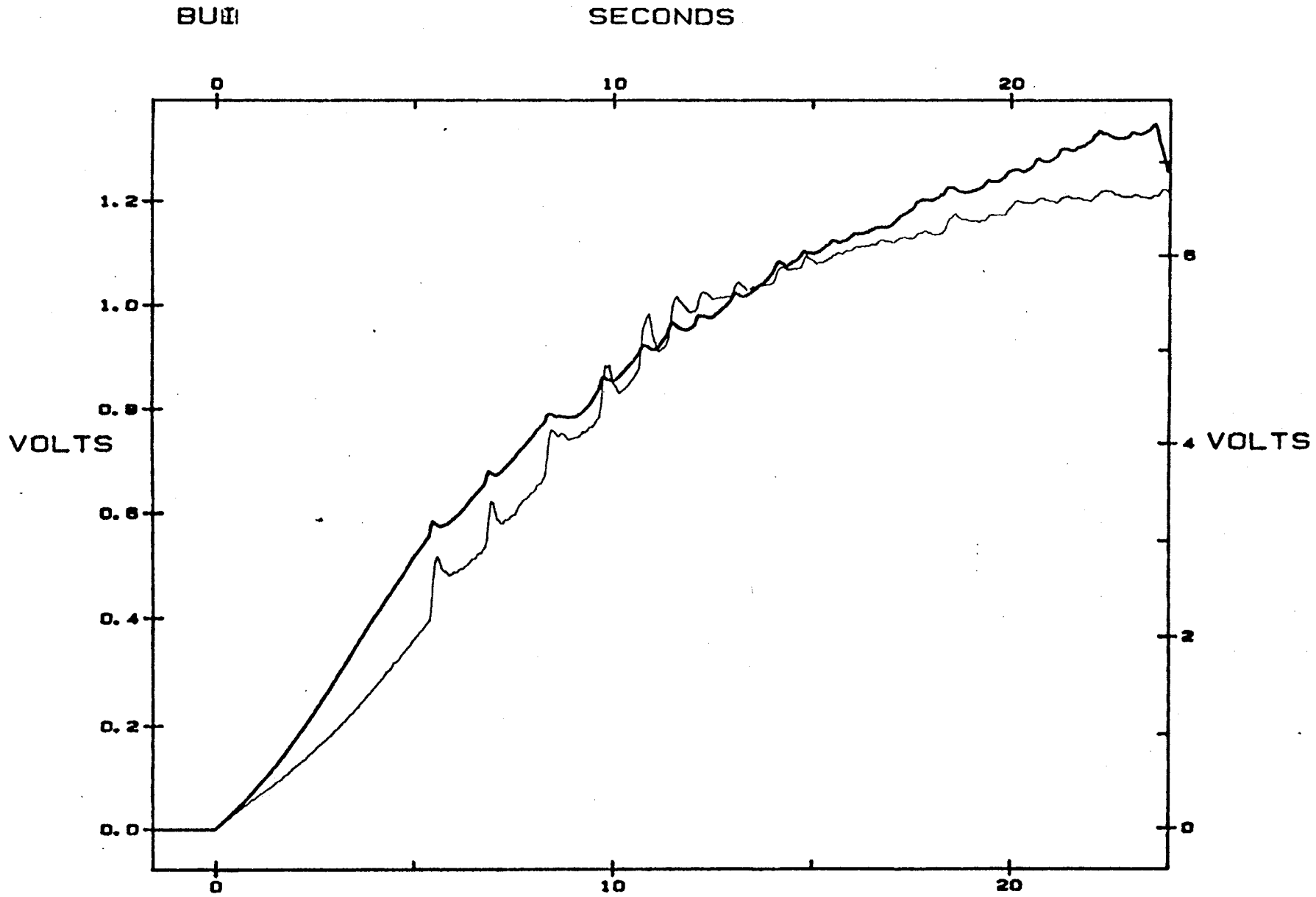
BUII
SECONDS
0
10
20
1.2
1.0
0.8
VOLTS
0.6
0.4
0.2
0.0
6
4 VOLTS
2
0
0
10
20
SECONDS

Fig. 7(a) Infrared transmission spectrum of a 30 μm-thick oil film (from Ref. 10)

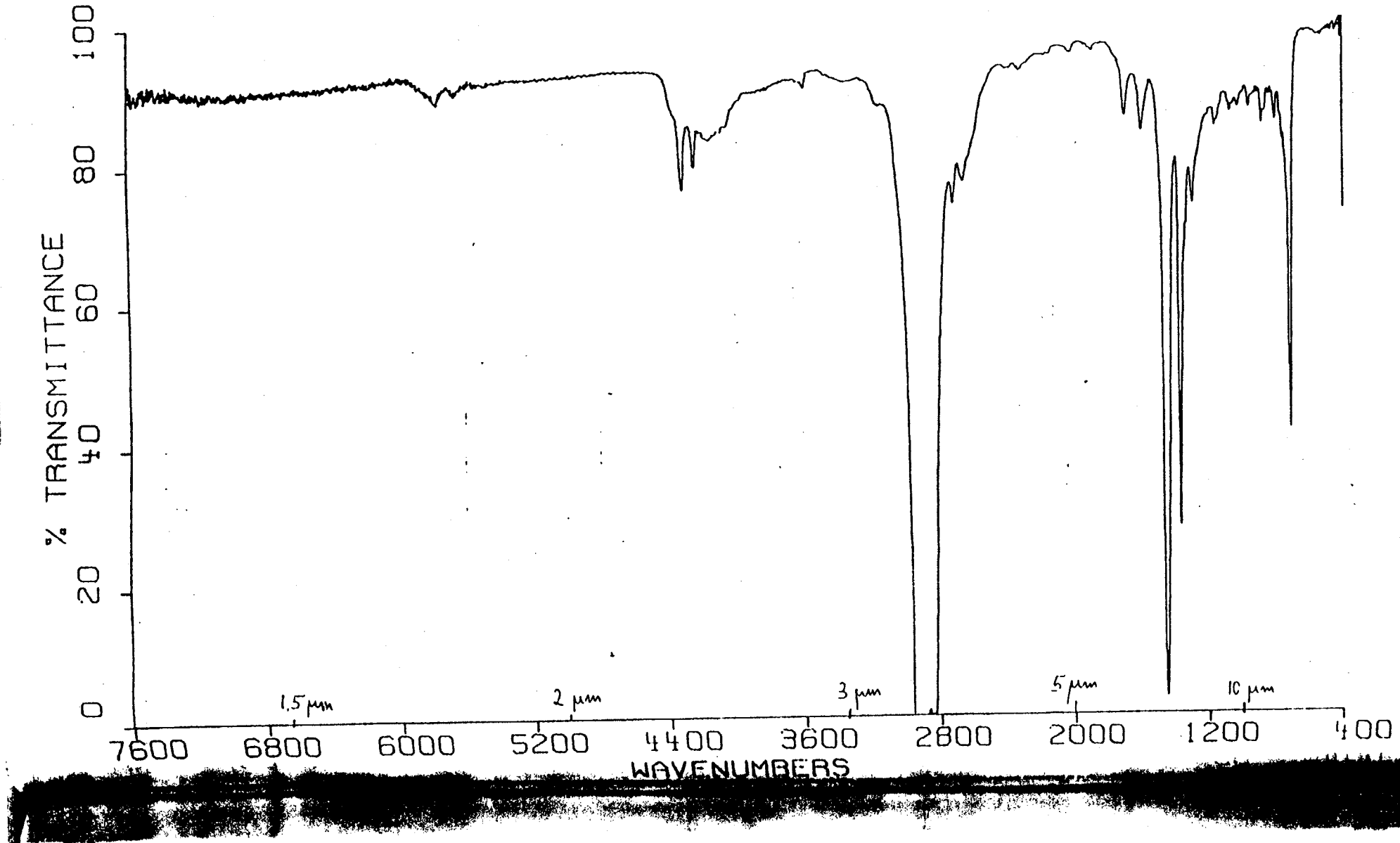

Fig. 7(b) Some oil as in Fig. 7(a), but 200 μm-thick film.

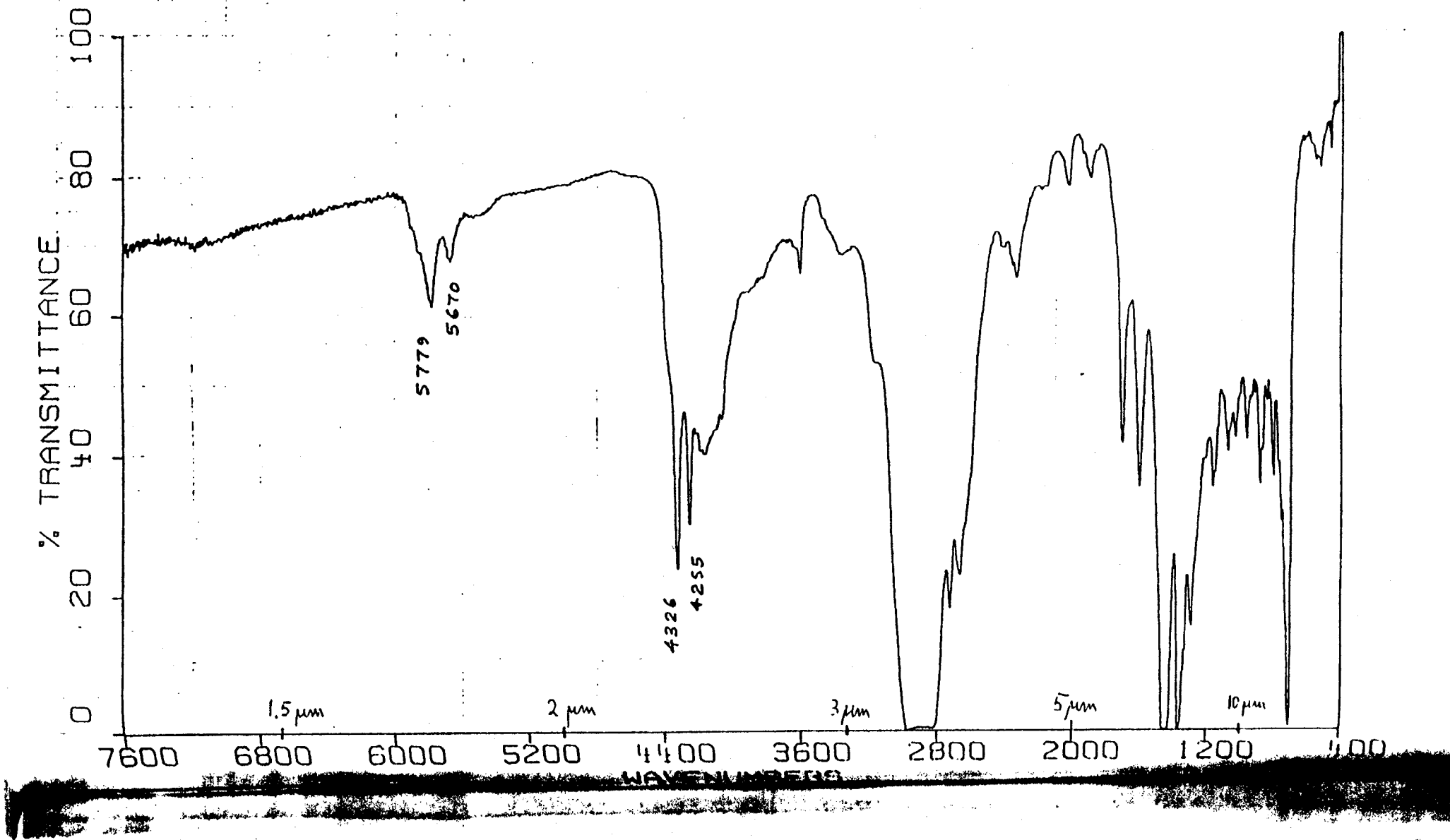

FIG. 8 Spectrum of a nearly 25 μm-thick water sample.

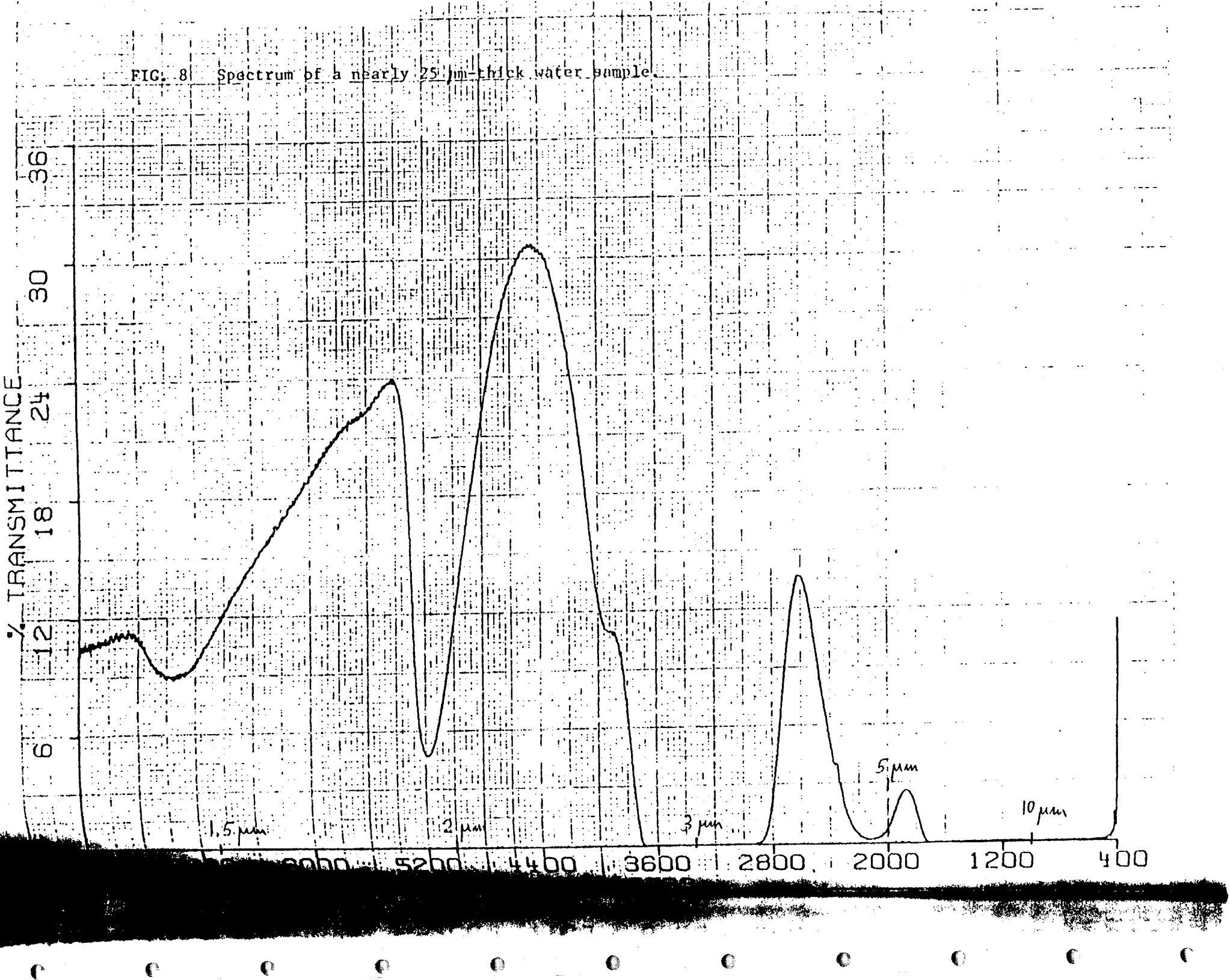

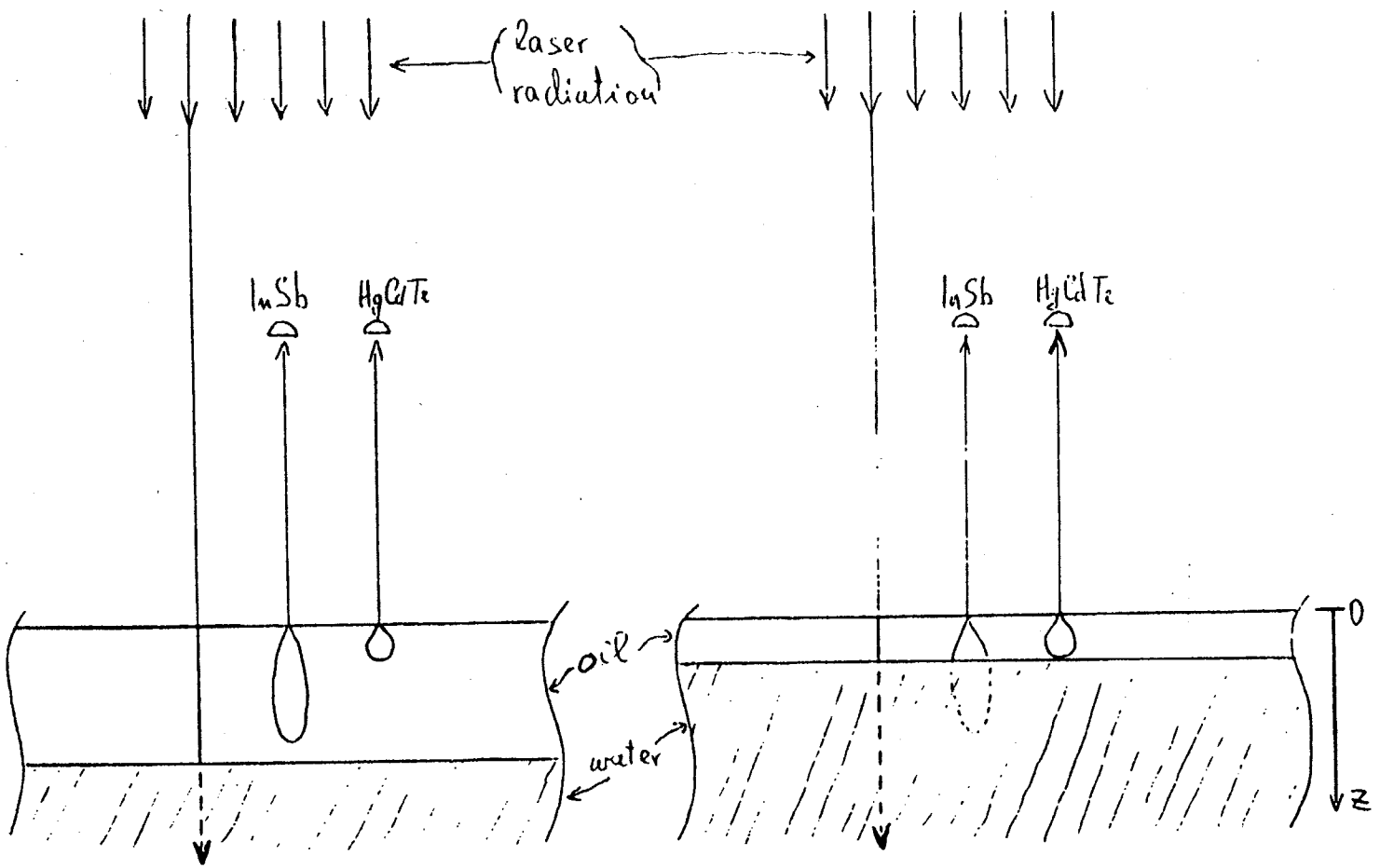

Fig. 9: Thermally-stimulated spectroscopy of a thicker (left) or thinner (right) translucent film.

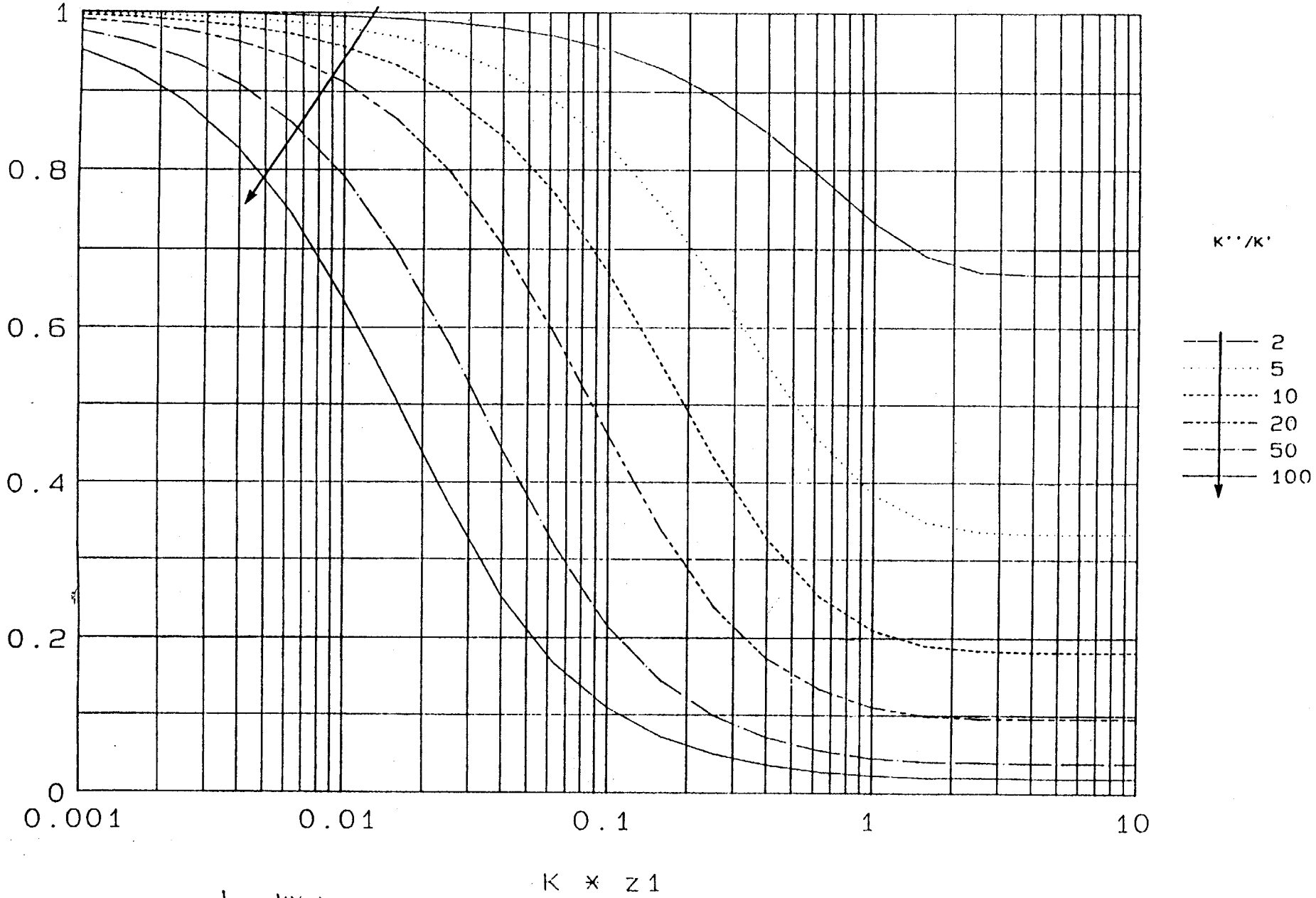
Signal ratio curves for K''/K = 1
1
0.8
0.6
0.4
0.2
0
0.001
0.01
0.1
1
10
K * z1
K''/K'
2
5
10
20
50
100

Signal ratio curves for K''/K = 10

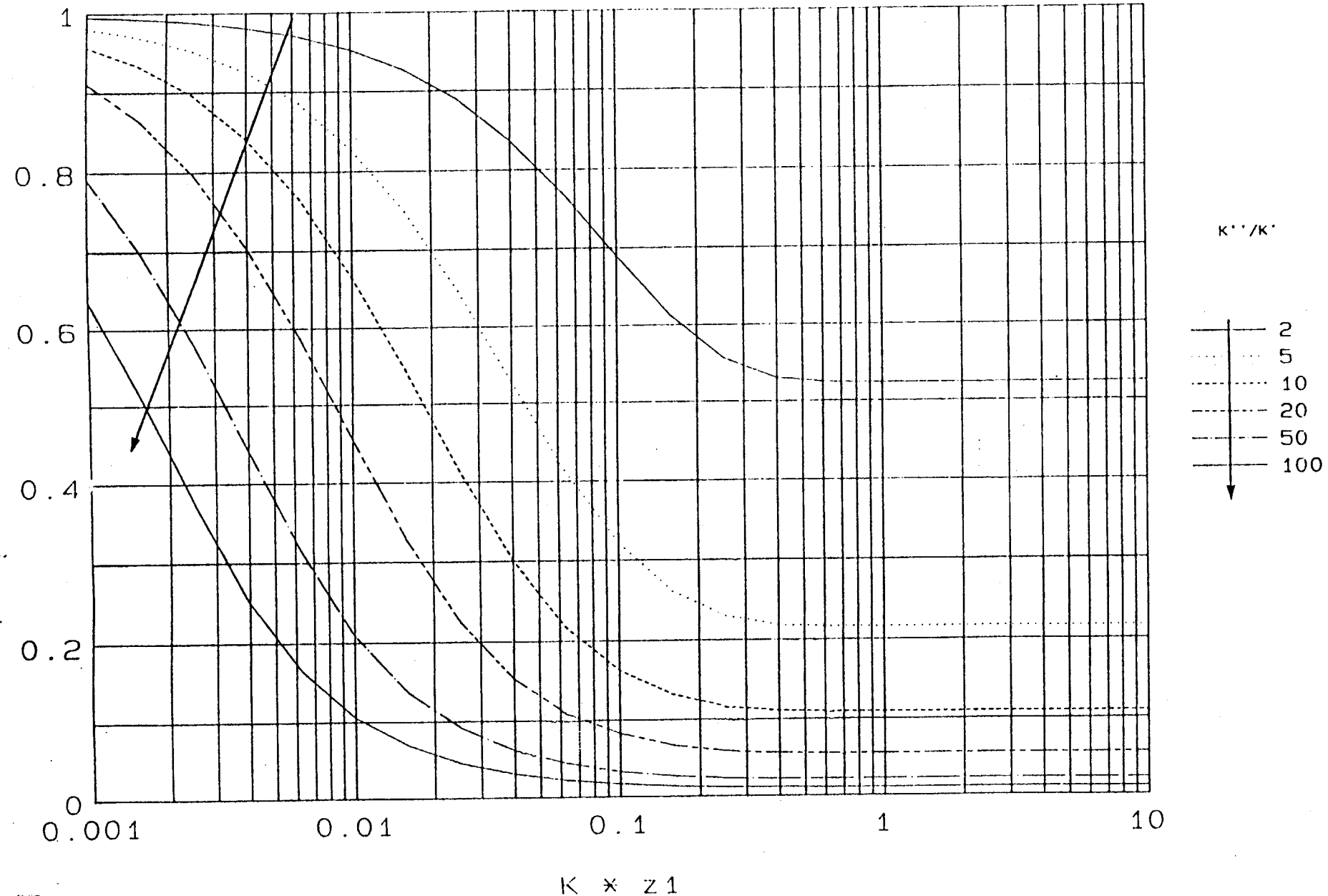

Fig. 11(a) Transmittance spectrum of Canpolar oil sample type 'A', 200 μm-thick.

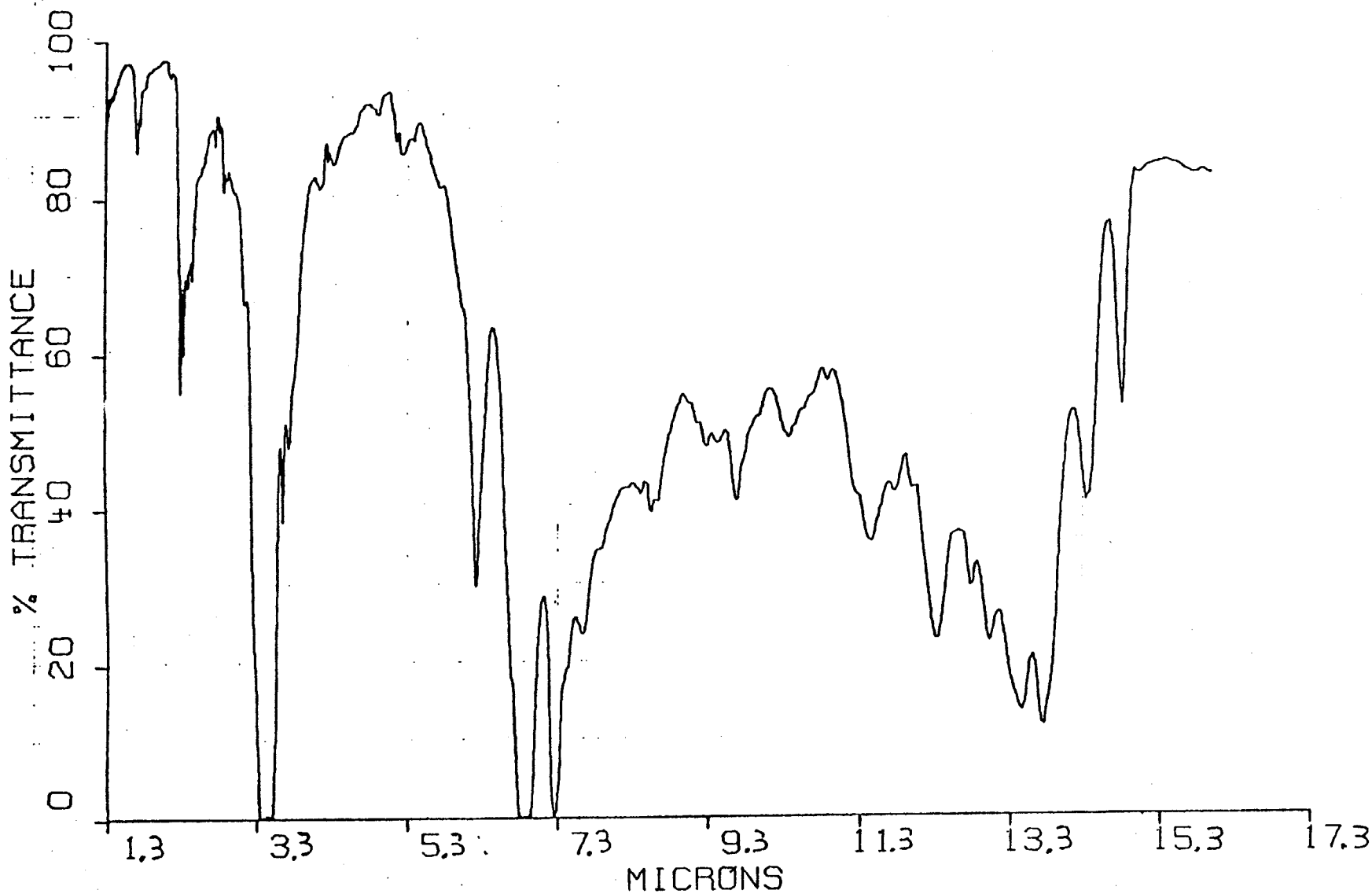

Fig. 11(b) Same as Fig. 11(a), but with sample type 'B'.

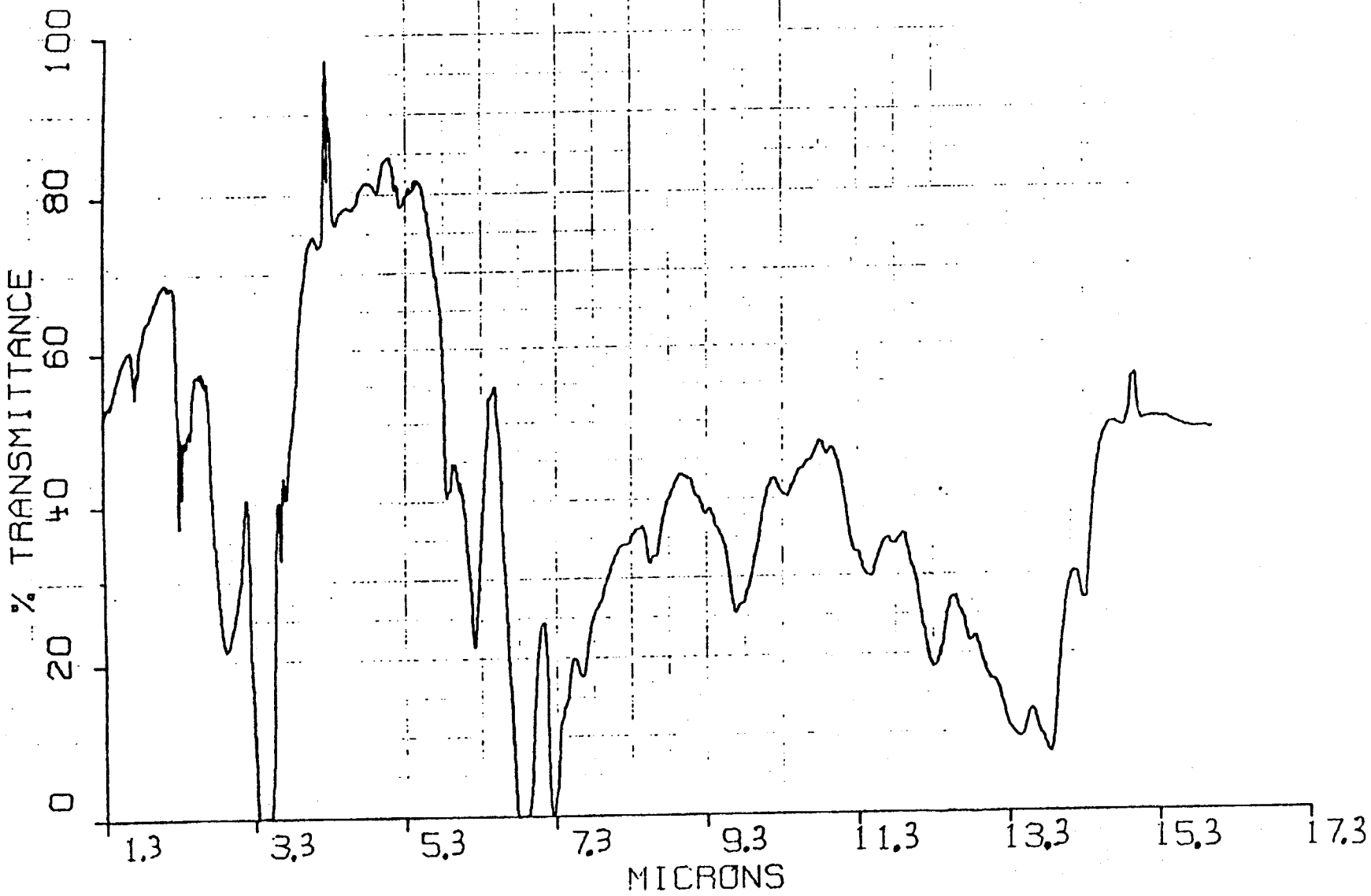

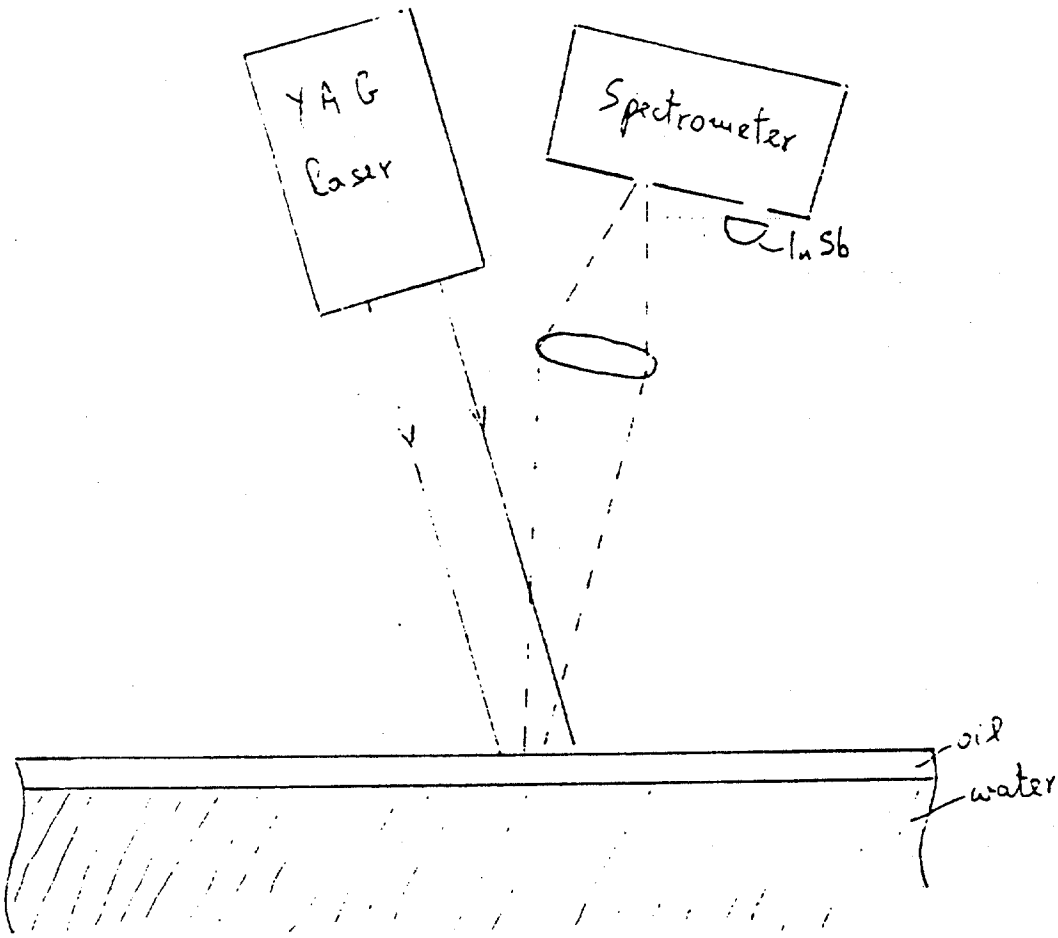

Fig. 12 Spectrometric setup used in the experimental investigations.

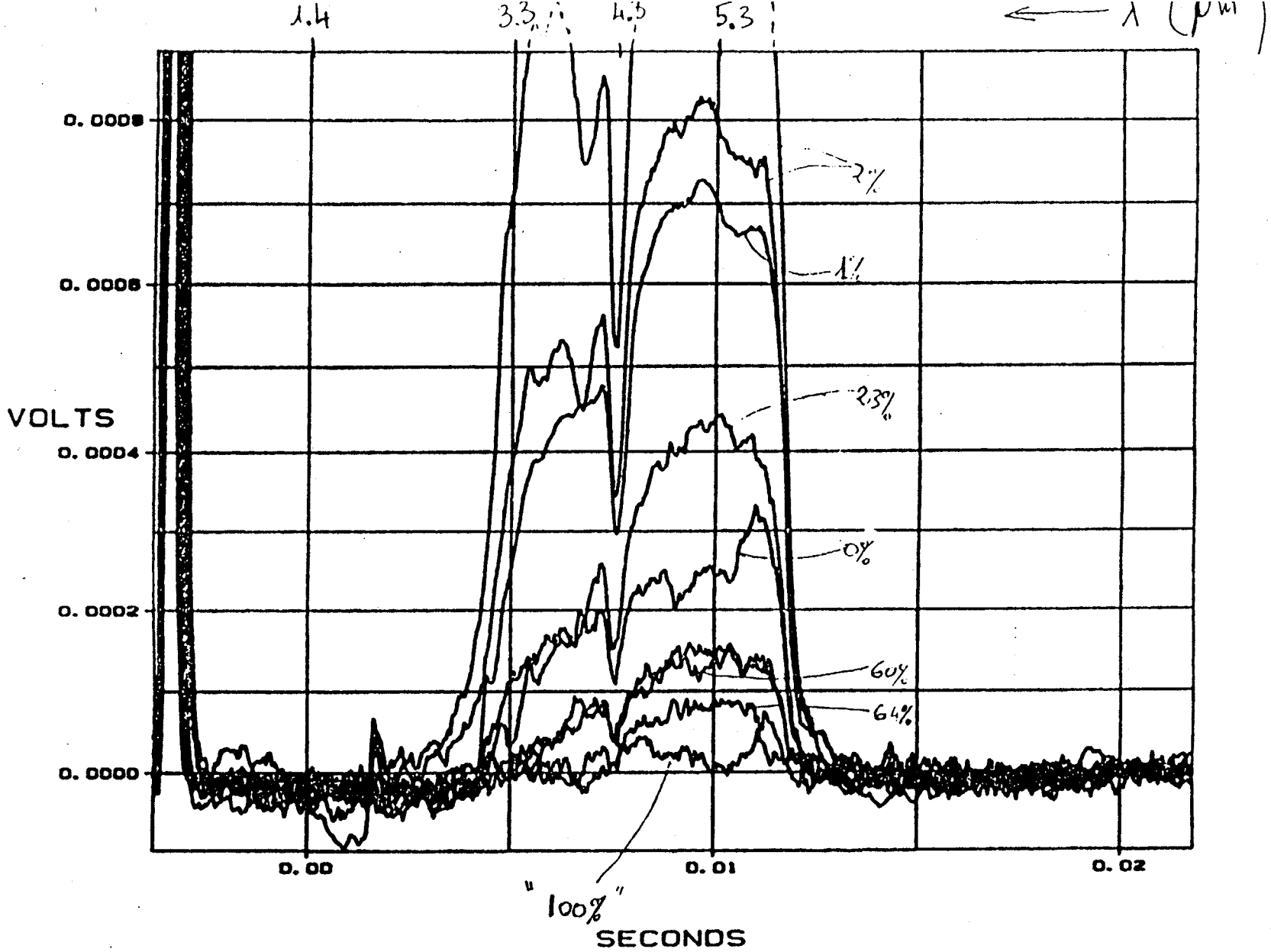

Fig. 13: Spectra of type 'A' oil films of different near-visible percent transmittance, i.e. different thickness (smaller transmittances correspond to thicker films).

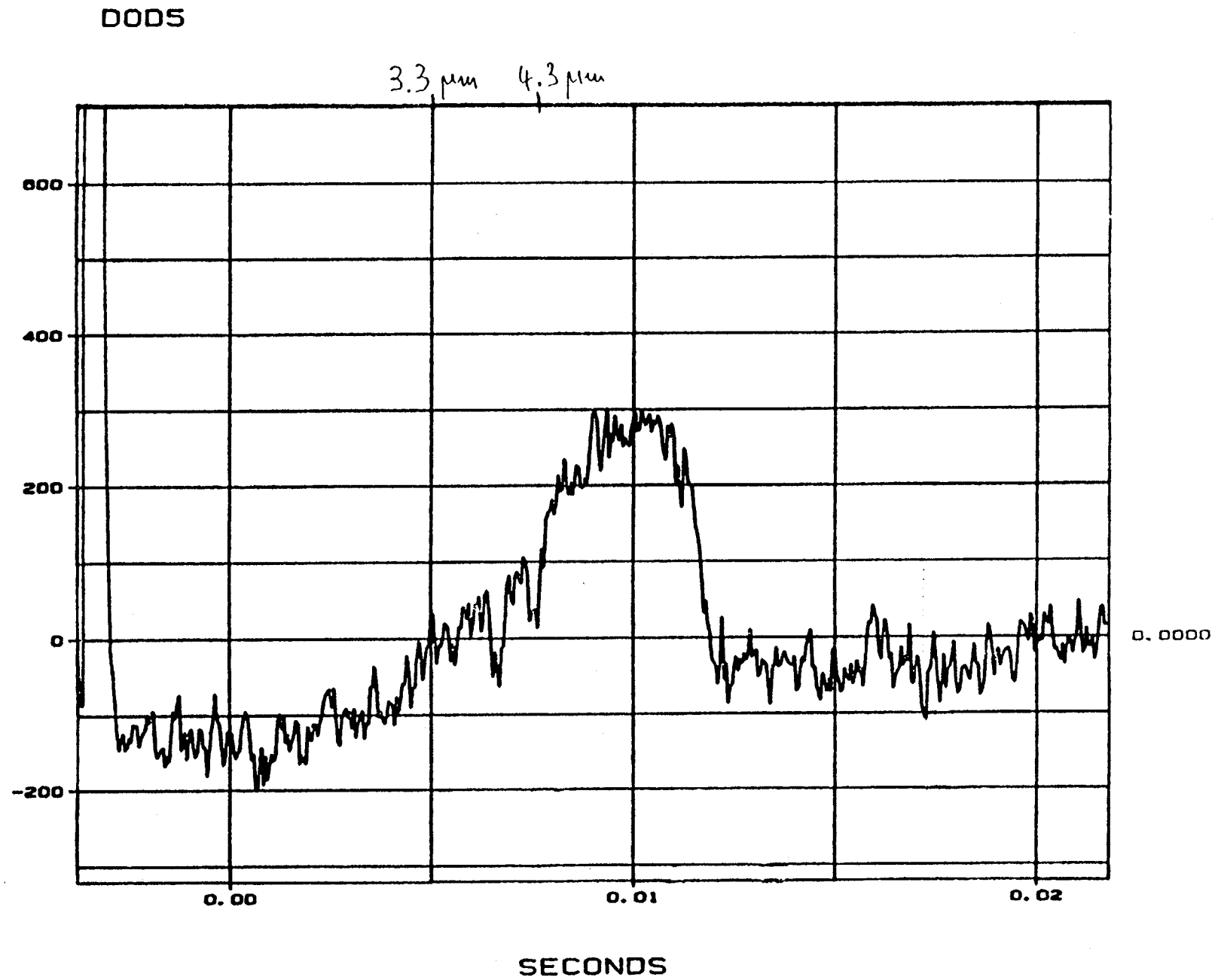

(S3) T = 64%

Fig. 14(a)

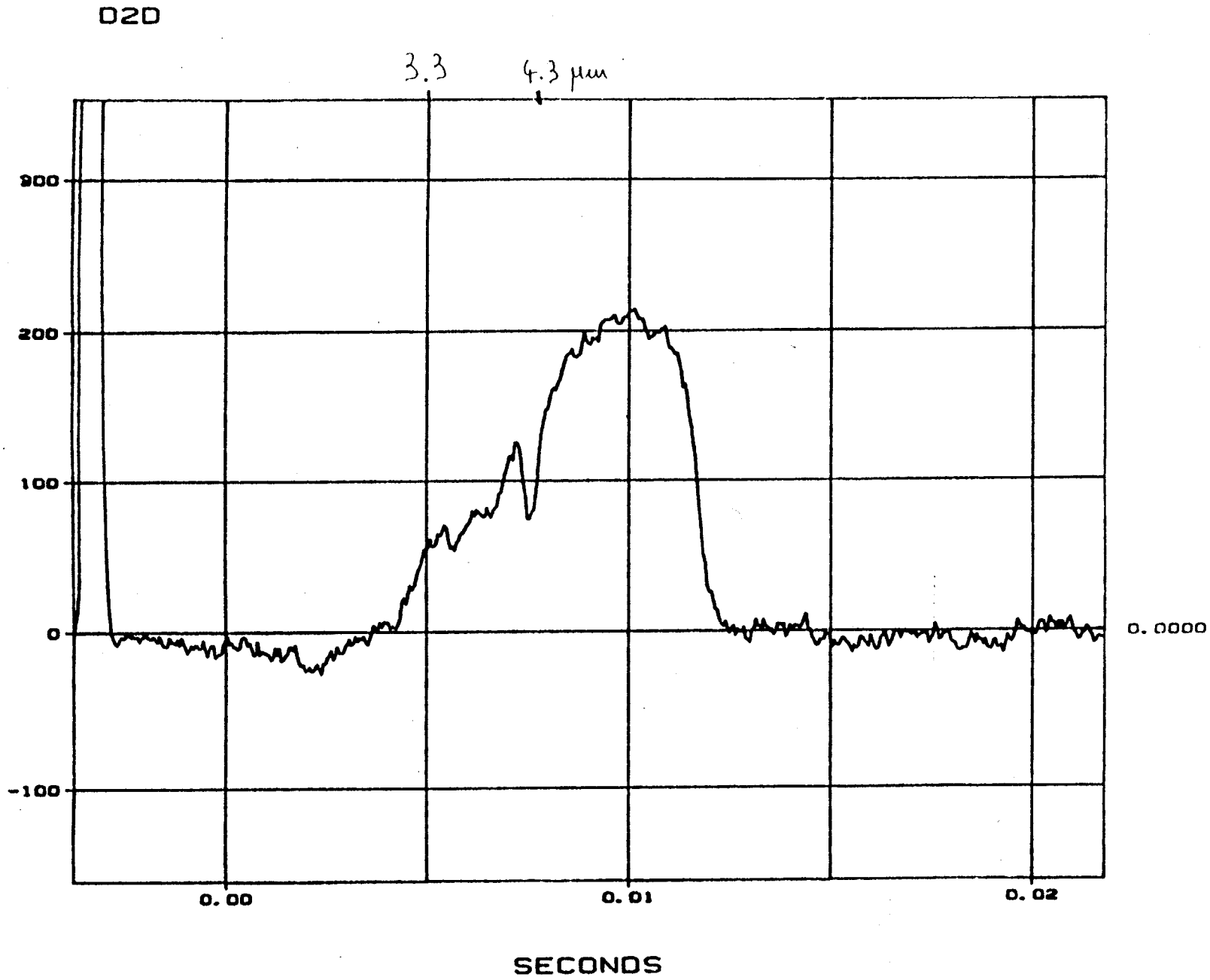

(55) T = 23%

Fig. 14(b)

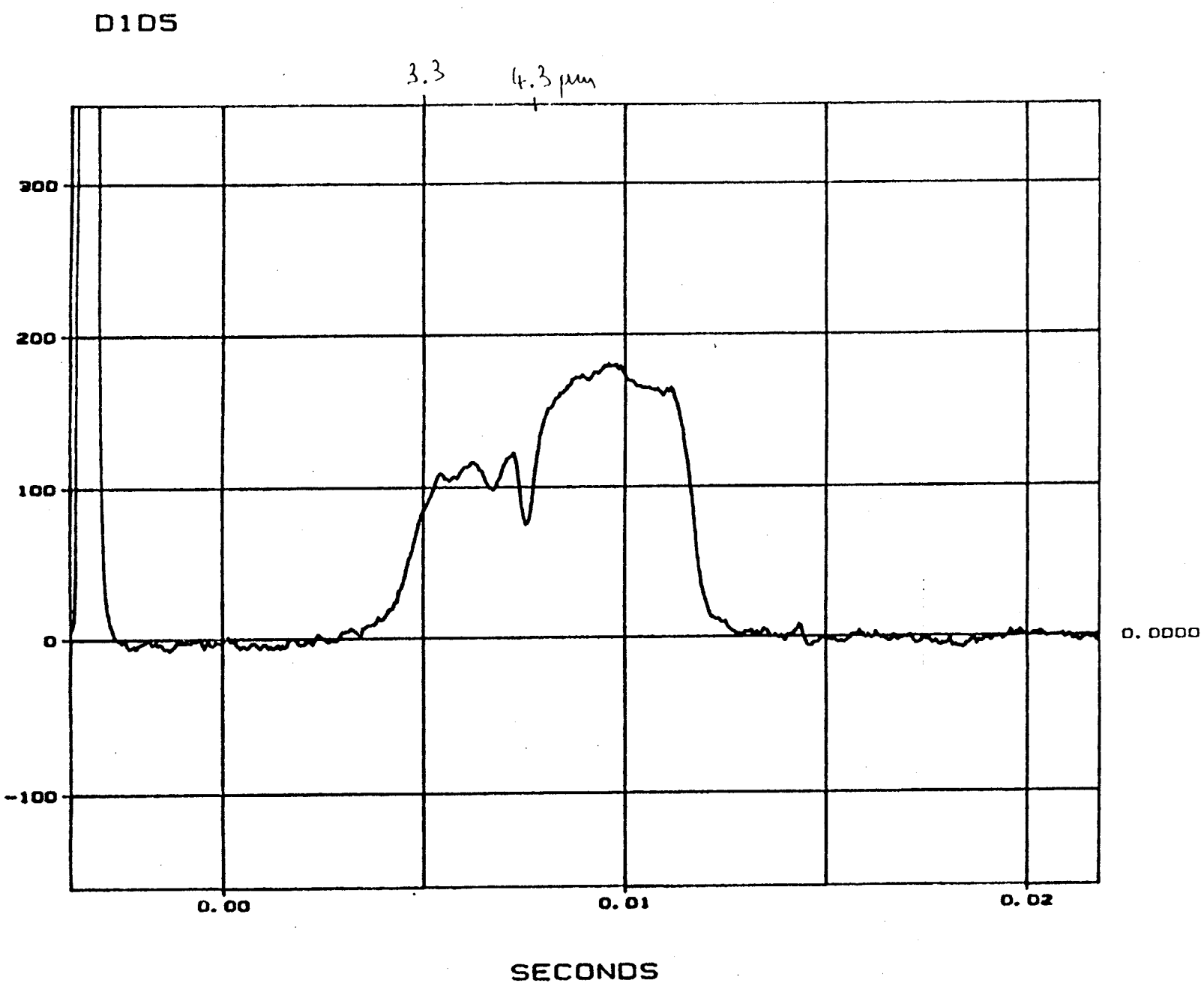

(57) T = 2%

Fig. 14(c)

D2D5

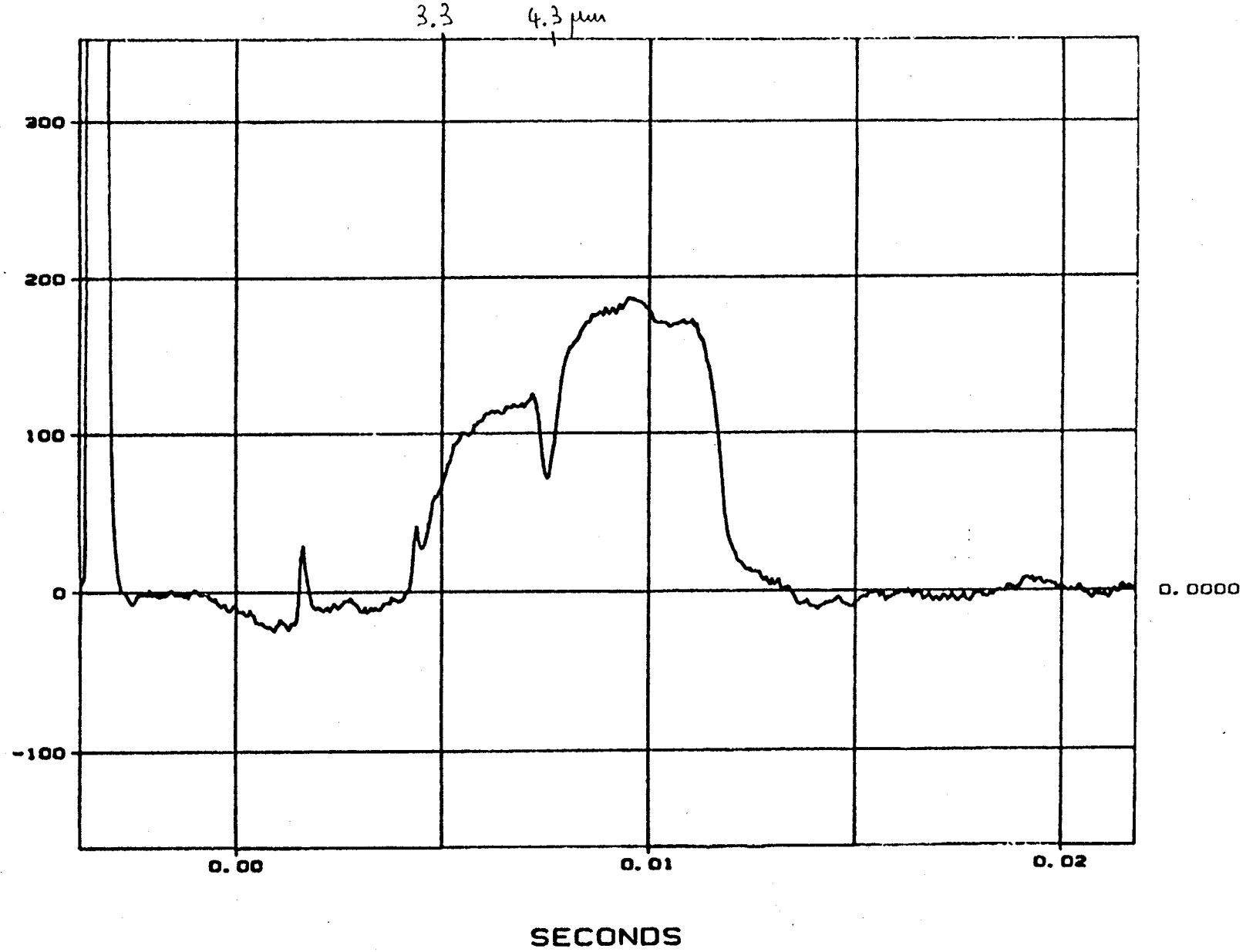

(S8) T = 1% Fig 14(d)

PROGRESS REPORT NO. 1

July 1st, 1990

Remote measurement of oil thickness on water

1. Thermal approach

Various optical filters have been ordered and we expect to work on this approach very soon.

2. Modeling of thermoelastic generation of ultrasound

During the first stage of this project, we have developed a model to calculate the thermo-elastic displacement on a two-layer system produced by the absorption of a laser pulse. By using an integral transform we derived the transfer function of the problem. This means that we can now use in the simulation any laser pulse shape. This model was implemented, in a first step, on a VAX mini-computer. The calculated surface displacement for a 500 μm oil film on water system is shown in figure 1 for a pulse shape of the form $\tau \exp(-t/\tau)$. We notice the echo of the interface oil-water arriving at the surface at t = 0.9 μsec.

We have also developed a computer model for calculating the signal response of a confocal Fabry-Pérot which detects the displacement of the surface. This calculation was simply done by summing the different waves arriving at the optical detector after being delayed by multiple reflections within the Fabry-Pérot. This approach may limit the time scale of the model but permits a rapid computation of the signal, which is necessary for the implementation of the program on a micro-computer.

Combining the thermo-elastic generation model with the Fabry-Pérot response computer program, we were able to calculate the theoretical signal for a given thickness and a given confocal Fabry-Pérot. Figure 2 shows the signal obtained for the displacement of figure 1 with a Fabry-Pérot in the transmission

mode. The goal of this modeling effort is to determine the optimum configuration of the Fabry-Pérot for detecting a thin film of oil (thickness < 1 mm). Preliminary results shown in figure 3 indicate that sensitivity increases by using a Fabry-Pérot in a reflection mode with a high reflectivity for the back mirror (i.e. high finesse). This investigation will be continued until the optimal configuration for the detection of thin oil films is clearly established.

We are now going to implement this computer program on a PC computer. This will permit a direct comparison to the actual measured data, which is also acquired with a PC. Since we have used a numerical integral transform for calculating the theoretical signal, it will be readily possible to integrate the actual laser pulse shape which will be measured into the model. This work is scheduled to be completed early August.

3. Physical studies using laser-ultrasonsic

Not yet started.

4. Pool-size experiments with laser-ultrasonics

An optical configuration for generation and detection in our large scale laboratory has been determined. Various optical and mechanical components for the focalization of the pump laser beam and for the collection of the reflected probe beam have been ordered. Further planification tasks (pool purchase, laser safety, mechanical design ...) are going to be continued.

Theoretical surface displacement of oil-water.

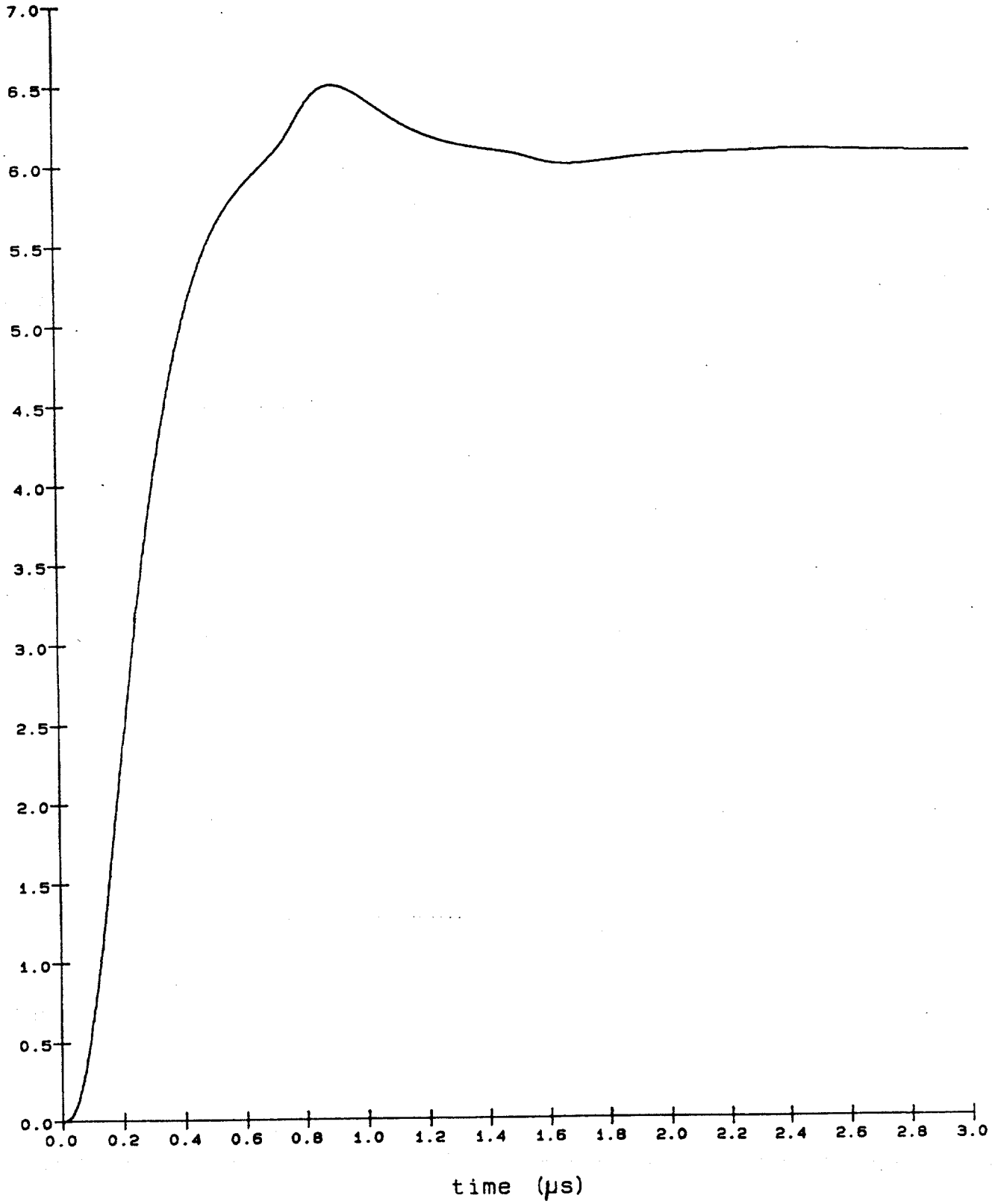

pulse rise time : 100 nsec, oil thickness = 500 um.

figure 1

Fabry-Perot signal in transmission mode.

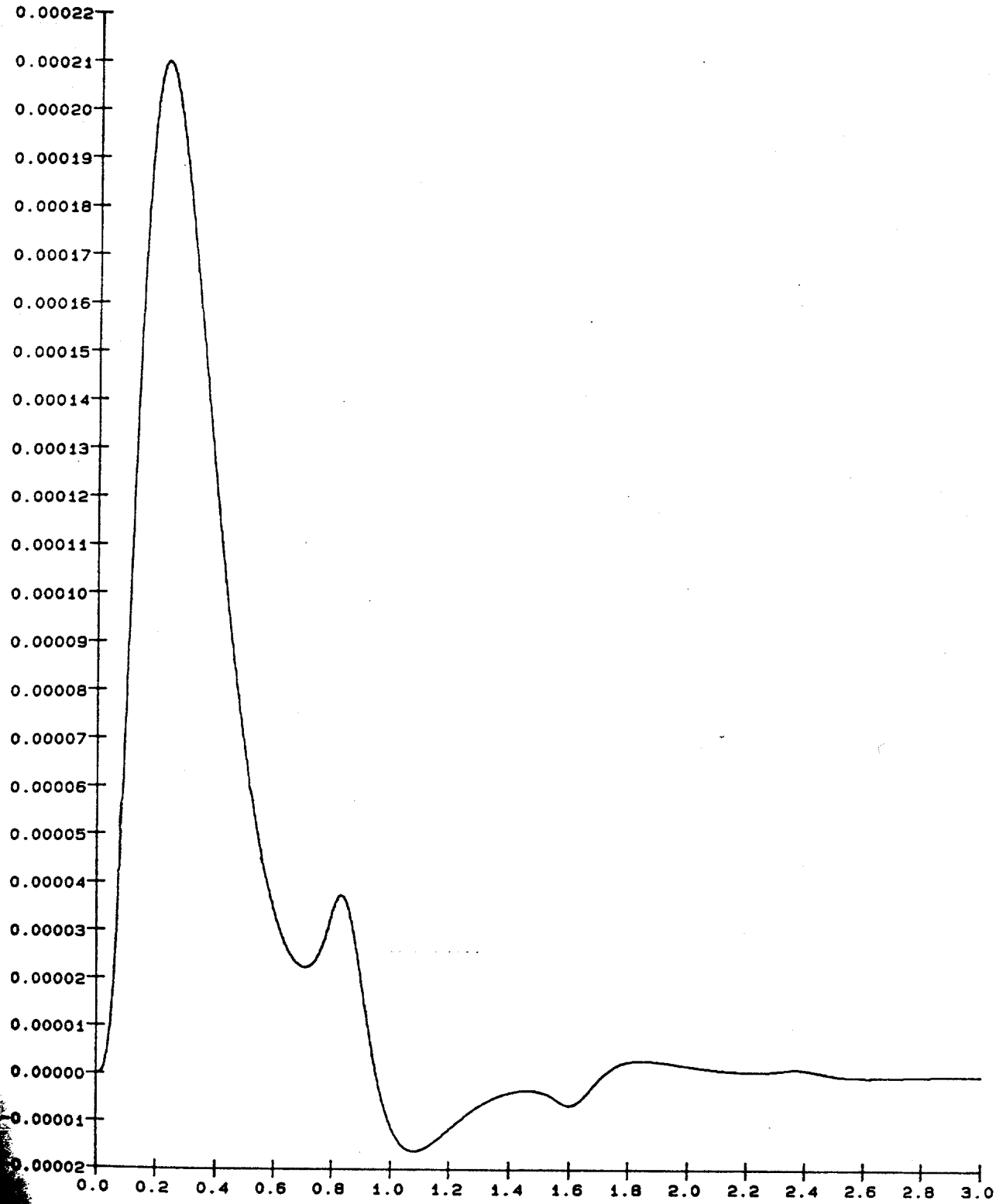

se rise time : 100 nsec. oil thickness : 500 um.

Figure 2

Theoretical signal of the Fabry-Perot

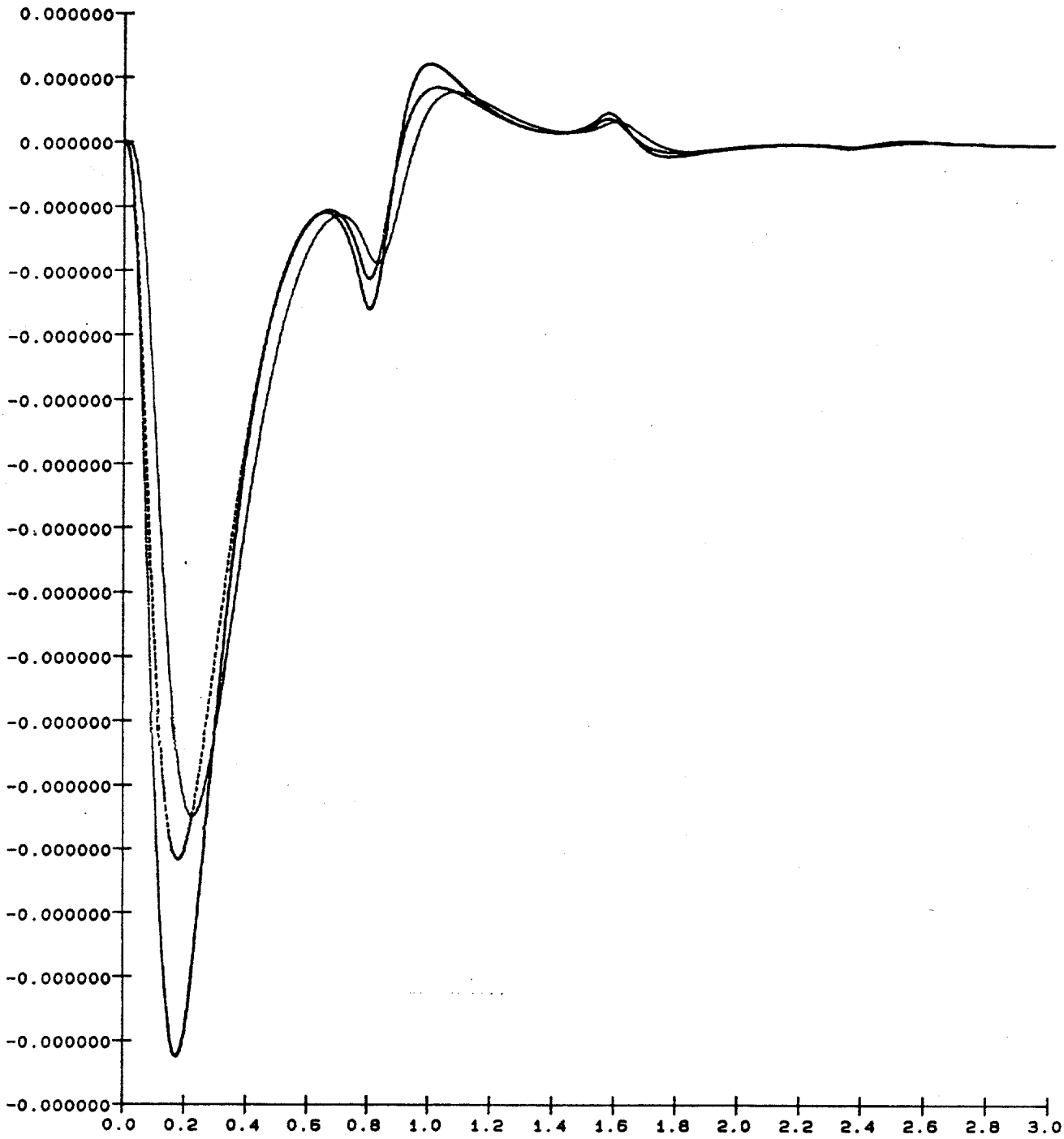

pulse rise time : 100 nsec, oil thickness : 500 um

figure 3.